Failure Prediction of Spatial Wood Structures: Geometric and Material Nonlinear Finite Element Analysis

by

Samruam Tongtoe

Dissertation submitted to the Faculty of the

Virginia Polytechnic Institute and State University

in partial fulfillment of the requirements for the degree of

Doctor of Philosophy

in

Civil Engineering

APPROVED:

S. M. Holzer, Chairman

D. A. Garst

J. R. Loferski

R. H. Plaut

S. Thangjitham

April 1997

Blacksburg, Virginia

Keywords: Glulam, Wood, Nonlinear, Finite Element, Dome

Failure Prediction of Spatial Wood Structures:
Geometric and Material Nonlinear Finite Element Analysis

by

Samruam Tongtoe

Committee Chairman: Dr. S. M. Holzer

Civil Engineering

(ABSTRACT)

The purpose of this study is to investigate spatial wood structures, trace their response on equilibrium paths, identify failure modes, and predict the ultimate load. The finite element models of this study are based on the Crafts Pavilion dome (Triax) in Raleigh, North Carolina, and the Church of the Nazarene dome (Varax) in Corvallis, Oregon. Modeling considerations include 3-d beam finite elements, transverse isotropy, torsional warping, beam-decking connectors, beam-beam connectors, geometric and material nonlinearities, and the discretization of pressure loads.

The primary objective of this study is to test the hypothesis that the beam-decking connectors (B-D connectors) form the weakest link of the dome. The beam-decking connectors are represented by nonlinear springs which model the load slip behavior of nails between the beam and the decking.

The secondary objective of this study is to develop models that are sufficiently simple to use in engineering practice.

Acknowledgments

I would like to express my sincere appreciation to my Committee Chairman, Dr. S. M. Holzer, for his guidance, teaching, patience, encouragement, and continued support. I also feel indebted to Dr. J. R. Loferski for his teaching and guidance in Wood Structures. Thanks are due to Professor D. A. Garst for his generosity and participation in the committee. I would also like to express my appreciation to Dr. R. H. Plaut and Dr. S. Thangjitham for their assistance, suggestions, and review of this dissertation.

Special thanks are extended to my beloved parents. Thanks are also extended to Mr. and Mrs. J. B. Reeves for their love and support. I also thank Mrs. Marlai Saisuttivong, Mr. Chalermsak and Mrs. Ponpen Tongthammachart for their love and generous support.

I would also like to sincerely thank Dr. A. A. Trani, Dr. J. R. Martin, Dr. Jacem Tissaoui, and Raul Andruet for their friendship and support.

I would like to thank the Royal Thai Air Force for the financial support throughout my studies in the United States.

Finally, I would like to dedicate this dissertation to my wife, Supunnika Tongtoe, and my son, Benya Tongtoe, for their patience, encouragement, and continuous support throughout my studies.

Table of Contents

List of Figures

List of Tables

Chapter 1

Introduction

1.1 General

The purpose of this study is to investigate the behavior of spatial wood structures: trace their response on equilibrium paths, identify failure modes, and predict the ultimate load. The term "spatial" signifies that the structures are designed to possess a three-dimensional load-carrying mechanism (Holzer et al., 1990). Spatial wood structures include lattice shells, radial rib domes, grid domes, Triax (Neal, 1973), and Varax (Eshelby and Evans, 1988) domes. Although this study is confined only to Triax and Varax glued-laminated timber (glulam) domes, the modeling and analysis techniques can be applied to spatial wood structures in general. The finite element models of this study are based on the Crafts Pavilion dome (Triax) in Raleigh, North Carolina, and the Church of the Nazarene dome (Varax) in Corvallis, Oregon. A full description of Triax and Varax domes is presented in Chapter 4 and Chapter 5, respectively.

This study is a continuation of experimental and numerical investigations of spatial wood structures (Davalos, 1989; Holzer et al., 1990; Davalos et al., 1991; Holzer et al., 1992; Kavi, 1993; Holzer et al., 1994; Holzer and Tongtoe, 1995). Holzer and Loferski (1987) provide the most valuable background information for research on glulam lattice domes. Davalos (1989) first developed a nonlinear finite element program to investigate the stability of glulam space frames. ABAQUS, a commercial finite element program, was later selected as a tool to experiment with a variety of models. It was chosen because of its extensive library of elements and its nonlinear analysis capabilities. It also allows the user to create subroutines to define elements and constitutive laws that are not available in its library. The Integrated Design Engineering Analysis Software package (I-DEAS) was also selected as a pre- and post-processor (Broyles, 1990).

1.2 Objectives

The objectives of this study are as follows:

1. To develop finite element models of Triax and Varax domes to predict their behavior and failure modes. Both geometric and material nonlinearities are considered.

2. To study the effect of tongue-and-groove decking on the overall stability of the domes and to test the hypothesis that the beam-decking connectors form the weakest link of the domes. The connector elements are represented by nonlinear springs that model the behavior of the nails joining the decking to the top of the beams.

3. To provide a summary of major modeling assumptions and their reasons.

4. To study the effects of variations in the joint stiffness. The main difference between the Varax and Triax domes is the design of joints (steel hubs). The Varax joint has rotational stiffness (Eshelby and Evans, 1988). The Triax joint is a pin joint.

5. To develop models that are sufficiently simple to use in engineering practice.

Chapter 2

Literature Review

2.1 Introduction

In this chapter, background information on methods of finite element stability analysis of spatial wood structures is presented. It includes a summary of linear, nonlinear, and combined linear/nonlinear analyses. Some examples of spatial wood structures for which stability investigations are performed with finite element methods are also included.

2.2 Finite Element Stability Analysis of Spatial Wood Structures

For an n-degree-of-freedom system, the nonlinear equations of equilibrium can be written in vector form as (Bathe, 1982)

$$R - F = 0 \tag{2.1}$$

where R is the externally applied nodal force vector, and F is the internal nodal force vector that equilibrates a configuration defined by the nodal displacement vector. Three methods of finite element stability analysis have been used for spatial wood structures: linear analysis, nonlinear analysis, and combined linear and nonlinear analysis (Holzer et al., 1990).

2.2.1 Linear Analysis

In linear analysis, it is assumed that the displacements of a structure are small, the material is linearly elastic, and the boundary conditions remain unchanged during a load application (Bathe, 1982). The displacement response, the applied load, and the stiffness matrix are related by the standard linear equation

$$Ku = R \tag{2.2}$$

where K is a constant matrix and the displacement vector u is a linear function of the load vector R. The linear buckling analysis can be summarized as follows (Holzer et al., 1990):

1. A reference load ${}^{r}R$ is applied to the structure, the standard linear equation

$$K_o\,{}^{r}u = {}^{r}R \tag{2.3}$$

   is solved for the nodal displacements, ${}^{r}u$, and the resulting finite element stresses are computed. K_o is the linear elastic stiffness matrix.

2. For proportional loading, the load vector can be expressed as

$$R = \lambda\,{}^{r}R \tag{2.4}$$

   where λ is the load parameter (the load proportionality factor) and the reference load ${}^{r}R$ is a constant vector.

3. The stiffness matrix corresponding to the load vector is defined by

$$K = K_o + \lambda\,\Delta K \tag{2.5}$$

where ΔK is the incremental stiffness matrix.

4. At the critical load, the stiffness matrix

$$K = K_o + \lambda_{cr} \Delta K \tag{2.6}$$

is singular, i.e., the determinant of K is 0.

5. The corresponding buckling load can be written as

$$R_{cr} = \lambda_{cr} \, {}^{r}R \tag{2.8}$$

6. The determination of the critical state is equivalent to the eigenvalue problem

$$(K_o + \lambda \Delta K)\phi = 0 \tag{2.9}$$

where λ is an eigenvalue and ϕ is the corresponding buckling mode shape.

2.2.2 Nonlinear Analysis

In structural mechanics, a problem is considered to be nonlinear if the stiffness matrix or the load vector depends on displacements (Cook et al., 1989, p.501). Nonlinearities in a structure can be classified as material nonlinearity or as geometric nonlinearity. Material nonlinearity is related to changes in material properties, as in a nonlinear stress-strain relationship. Geometric nonlinearity is related to changes in configuration, where the strain-displacement relationship is nonlinear and equilibrium is satisfied for the deformed state of the structure.

Nonlinear analysis is used to trace the equilibrium path up to and beyond the first critical point, at which the structure becomes unstable. There are two algorithms commonly used in the incremental iterative solution of nonlinear problems: the Newton-Raphson method and the Riks method. The Newton-Raphson method and its modifications can be used to trace nonlinear prebuckling paths through bifurcation before reaching a limit (turning) point. The Riks method can be used to trace the nonlinear equilibrium paths through bifurcation and limit points along the curve.

2.2.2.1 Newton-Raphson Method (N/R Method)

The Newton-Raphson method starts with a known equilibrium point (Holzer, Watson, and Vu, p.4), and then uses iterative procedures to find the next equilibrium point at an increment of load. This procedure is repeated again and again until the load approaches the limit point. For a single degree-of-freedom (DOF) system, the process starts with a known equilibrium position (q^0) as shown in Figure 2.1. The specified load and the corresponding equilibrium position are denoted by Q^N and q^N, respectively. It can be seen that the internal resistance of the structure, F^0, falls short of equilibrating the applied load, Q^N, by a residual amount, R^0, an unbalanced force. The structure must deform in order to develop the internal resistance necessary to equilibrate Q^N. This deformation is found through successive iterations. For a given trial configuration, the N/R procedure is as follows:

1. Establish the tangent stiffness matrix $K_T{}^0$

2. Evaluate the equilibrium nodal force F^0

3. Compute the vector of unbalanced nodal force R^0

$$R^0 = Q^N - F^0 \tag{2.10}$$

4. Solve the linearized equation for Δq^1:

$$K_T^0 \Delta q^1 = R^0 \tag{2.11}$$

5. Update the vector of nodal displacements:

$$q^1 = q^0 + \Delta q^1 \quad (2.12)$$

6. Formulate K_T^1 and compute R^1. The procedure is repeated until the residual is within a preset tolerance of the original load increment (Bathe, 1982).

In the Newton-Raphson method, the stiffness matrix is updated after each iteration. This can result in high computational cost. The modified Newton-Raphson method is developed to reduce the expensive repetitions of forming the tangent-stiffness matrix. This method is the same as the N/R method, except the tangent-stiffness matrix is not updated or is updated infrequently as shown in Figure 2.2.

2.2.2.2 Modified Riks-Wempner Method

The modified Riks-Wempner method was found to be most effective in tracing nonlinear equilibrium paths through bifurcation and limit points along the curve (Holzer et al., 1990).
In the N/R algorithm, the Δq^k term is the unknown quantity for which the equation is solved. In the Riks method (Figure 2.3), a generalized arc length, Δs, is the independent variable which controls progress along the equilibrium path (Holzer, Watson, and Vu, pp.4-5). The length Δs of the tangent to the current equilibrium point is prescribed, and the new equilibrium position is at the intersection of a normal plane to Δs with the equilibrium path.

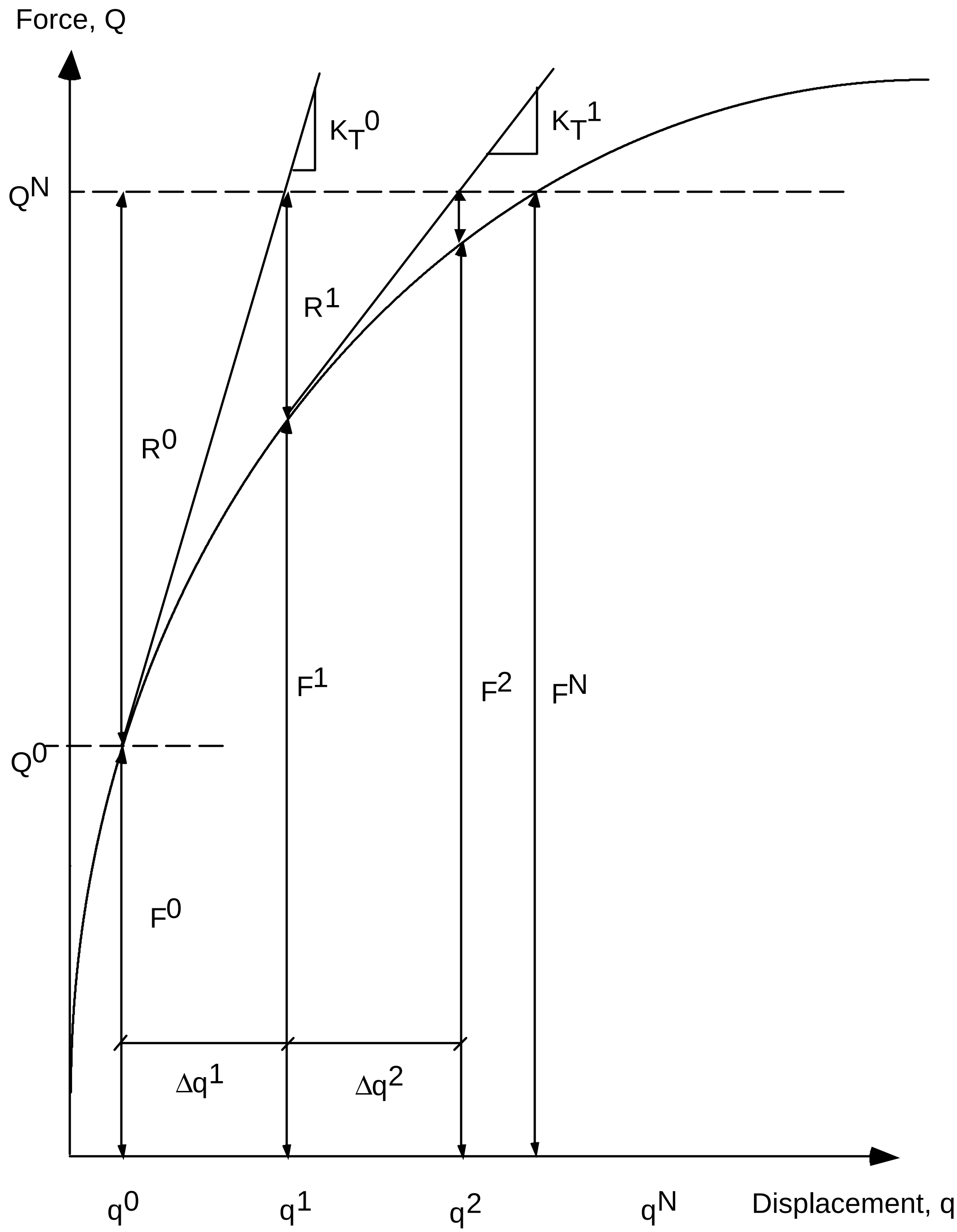

Figure 2.1 Newton-Raphson Method

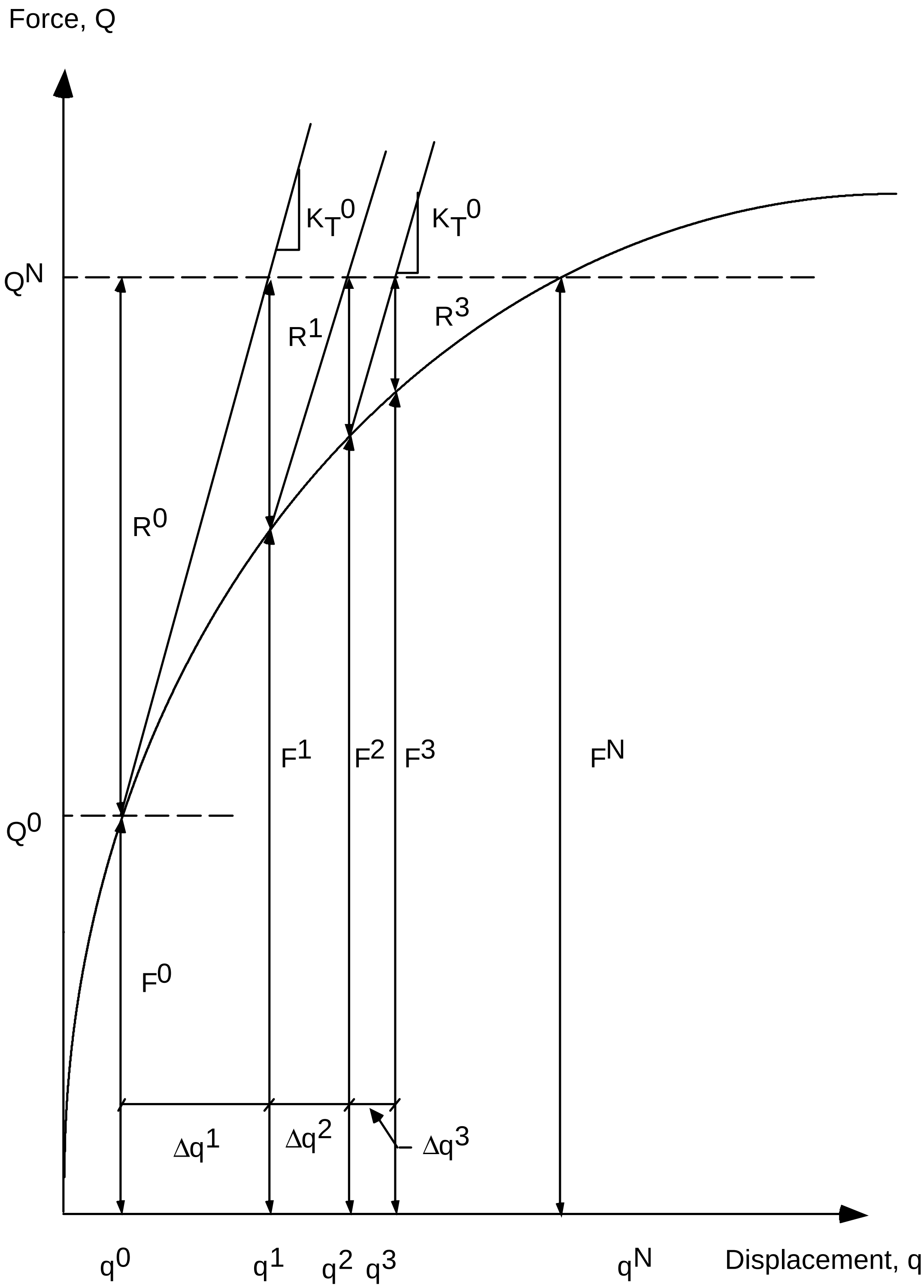

Figure 2.2 Modified Newton-Raphson Method

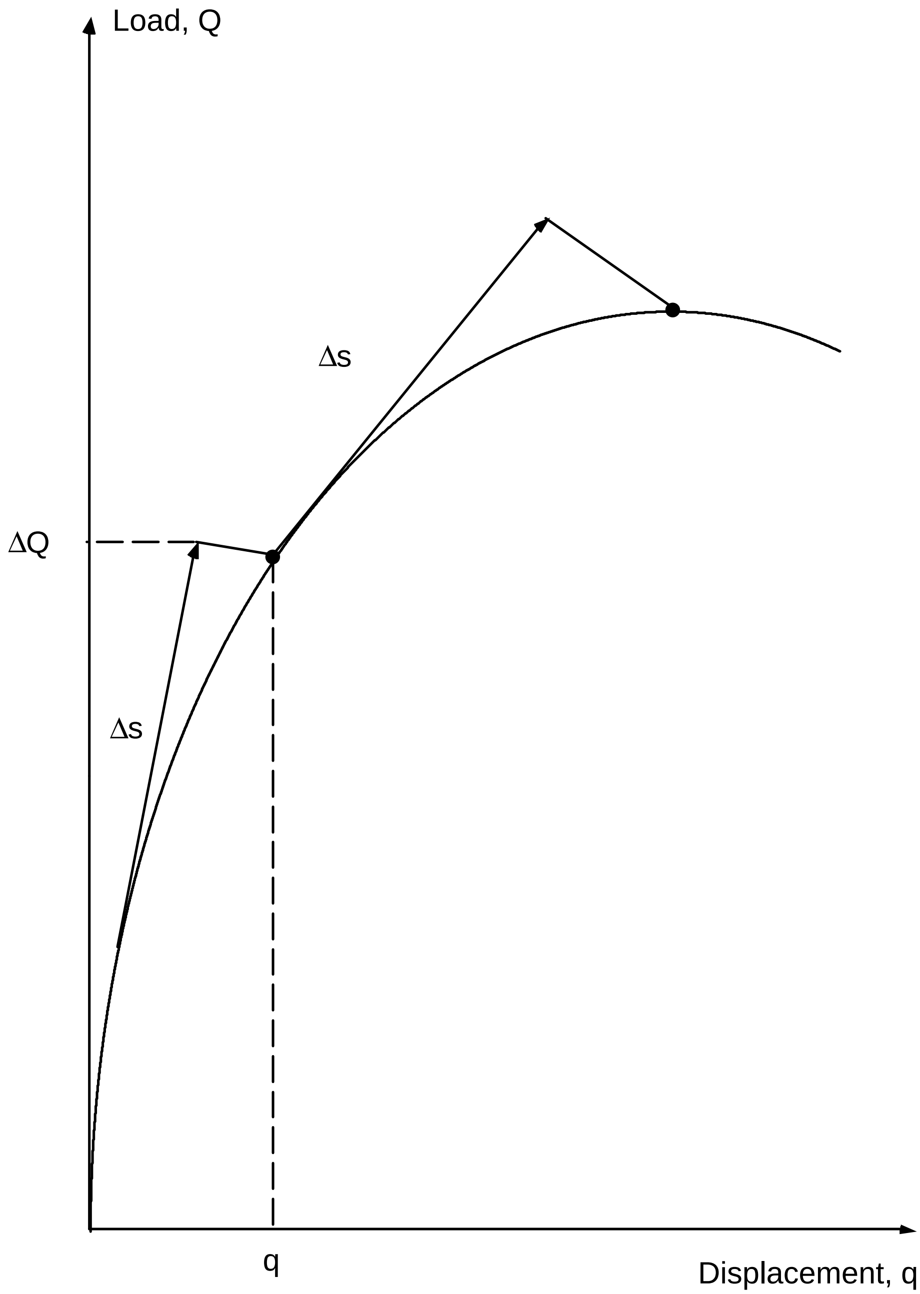

Figure 2.3 Modified Riks-Wempner Method

2.2.3 Combined Linear/Nonlinear Analysis

A combined linear and nonlinear stability analysis, which incorporates the efficiency of linear buckling prediction and the accuracy of nonlinear analysis, is recommended by Brendel (1979), Brendel and Ramm (1980), Brendel, Kempen, and Ramm (1982), and Chang and Chen (1986). The combined linear and nonlinear analysis can be used to determine the critical loads of most types of structures through simple linear interpolation/extrapolation of a few values obtained from the analysis (Chang and Chen, 1986, p.845). The combined analysis is also considered to be an improvement over linear analysis because it can account for large prebuckling deformations (Holzer et al., 1990). The combined analysis proceeds as follows (Holzer et al. 1992):

1. A base pressure ${}^{b}p$ is applied and a nonlinear analysis is performed to obtain the corresponding tangent stiffness matrix ${}^{b}K$. The base load can be expressed as

$$ {}^{b}p = p_D + {}^{b}\lambda\, p_L \tag{2.13} $$

   where p_D is the dead load, p_L is the live load, and ${}^{b}\lambda$ is a multiple of the live load (a scalar load parameter).

2. A 'small' live load increment is applied to define a reference pressure ${}^{r}p$ for which the tangent stiffness matrix ${}^{r}K$ is computed. The change in the stiffness between the base and reference loads

$$ \Delta K = {}^{r}K - {}^{b}K \tag{2.14} $$

   represents an approximation for the differential stiffness at the base load.

3. According to the linear buckling theory, it is assumed that the change in the stiffness is proportional to the change in the load. If

$$p \quad = \quad {}^{b}p + \Delta\lambda p_L \tag{2.15}$$

then

$$K \quad = \quad {}^{b}K + \Delta\lambda \, \Delta K \tag{2.16}$$

At critical load, the stiffness matrix **K** is singular, i.e., the determinant of K = 0, which corresponds to the eigenvalue problem:

$$({}^{b}K + \Delta\lambda\Delta K)\,\Delta u \quad = \quad 0 \tag{2.17}$$

where $\Delta\lambda$ and Δu denote the eigenvalues and the eigenvectors (the buckling mode shapes). Let $\Delta\lambda_{cr}$ be the smallest eigenvalue; then the predicted buckling load is expressed as

$$p_{cr} \quad = \quad {}^{b}p + \Delta\lambda_{cr} p_L \tag{2.18}$$

or, by equations 2.13 and 2.18,

$$p_{cr} \quad = \quad p_D + {}^{b}\lambda_{cr} p_L \tag{2.19}$$

where

$${}^{b}\lambda_{cr} \quad = \quad {}^{b}\lambda + \Delta\lambda_{cr} \tag{2.20}$$

2.2.4 Critical Load Predictions

The results of the combined linear and nonlinear stability analysis are presented as a critical load prediction curve. The curve is constructed by performing the combined analysis for increasing values of ${}^{b}\lambda$, a scalar load parameter at the base load, to obtain the corresponding eigenvalues $\Delta\lambda_{cr}$. The critical load parameter λ_{cr} of the structure can be predicted at the intersection of the critical load prediction curve and the 45^0 line ($\lambda = {}^{b}\lambda$) as shown in Figure 2.4. According to Eq. 2.19, the critical load can be computed as

$$p_{cr} \quad = \quad p_D + \lambda_{cr} p_L \tag{2.21}$$

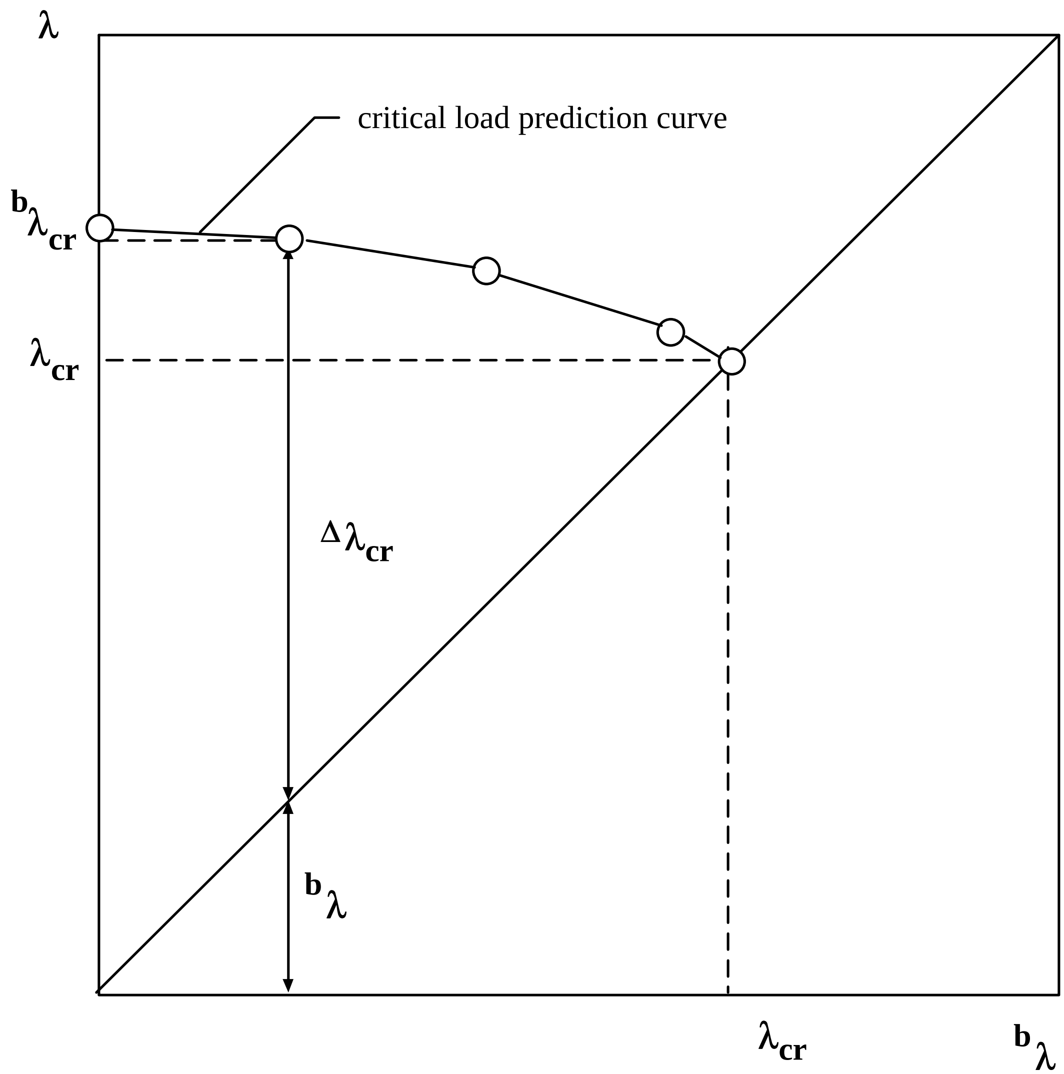

Figure 2.4 Critical Load Prediction Curve

2.3 Spatial Wood Structures

This section is concerned with the status of current stability investigations of spatial wood structures in which stability investigations are performed with the finite element method. The structures surveyed include wooden lattice domes and shells.

2.3.1 Crafts Pavilion Triax Dome in Raleigh, North Carolina (1975)

The dome is a 3-way grid dome (Tsuboi, et al., 1984) whose design is based on the Crafts Pavilion dome in Raleigh, N.C. The dome has a span of 133 ft (40.5 m), a rise of 18 ft (5.5 m), and a radius of 133.3 ft (40.6 m). It consists of a triangulated network of curved glulam beams, a tongue-and-groove decking supported by curved purlins, and a steel tension ring. The glulam beams are joined by patented steel hubs, and the decking is nailed to the beams and purlins.

The geometry of the dome, which is characteristic of Triax (Neal, 1973) and Varax (Eshelby and Evans, 1988) domes, is obtained by projecting a plane network of equilateral triangles onto the spherical surface of the dome. The projection is defined by rays that originate at the center of the sphere. Thus, all members lie in great circle planes and have the same radius of curvature. The dome is composed of six identical sectors.

This dome was chosen by Davalos (1989) to conduct a study on the behavior of the structure because its relatively small size permits a refined finite element analysis. Finite element models with various features have been constructed to represent the behavior of the glulam dome (Holzer, et al., 1992; Holzer, et al., 1994). Finite element models of the network of curved glulam beams include: curved 3-noded Timoshenko beams and straight, 2-noded Bernoulli/Euler beams; the assumption of transverse isotropy (Davalos, et al., 1991); torsional deformation with and without warping (Kavi, 1993); geometric and material nonlinearities (Telang, 1992); rigid and flexible joints. The current study centers on the effect of the beam-decking connectors on the dome behavior. The connector elements are nonlinear springs that model the behavior of the nails joining the top of the beams with the decking. The dome is subjected to the dead load pressure of

16 psf (766 Pa) and the live load pressure of 20 psf (958 Pa) resulting from snow load over the entire dome or over half of the dome. The dome was modeled, analyzed, and post-processed with the commercial finite element programs I-DEAS and ABAQUS. The study showed that the decking contributes significantly to the ultimate load capacity of the dome, and beam-decking connector failures seem to trigger failure of the dome. In addition, nonlinear material behavior is linked with the failure mode for snow over half of the dome.

2.3.2 Sports Building at Northern Arizona University, Flagstaff (1978)

This spherical dome has a span of 502 ft (153 m) and a rise of 92.4 ft (28.2 m). The dome consists of a triangulated network of curved glulam beams, a tongue-and-groove decking supported by curved purlins, and a post-stressed reinforced concrete ring. The structural members consist of glued-laminated (glulam) southern yellow pine interconnected at their joints with bolted steel connectors. The grid members are 27 in. (68.6 cm) deep and have a width of 5.25 in. (13.3 cm) The perimeter members are 27 in. (68.6 cm) deep and have a width of 8.75 in. (22.2 cm). The dome is cyclically symmetric and composed of six identical spherical triangle sectors. The dome is supported by 36 reinforced concrete buttresses. These buttresses are connected by a post-stressed reinforced concrete ring that resists the tension created by the dome.

The analysis of the dome was performed with the GENSAP program (Melaragno, 1991). The loading conditions are composed of 40 psf (1915 Pa) for snow load, 30 psf (1436 Pa) for horizontal wind load, and 17.4 psf (833 Pa) for dead load. The dome was designed by Rossman and Partners Architects and by John K. Parsons & Associates (Melaragno, 1991).

2.3.3 Tacoma Dome, Tacoma, Washington (1983)

The Tacoma Dome is one of the world's largest-diameter wooden domes (Faherty and Williamson, 1995). The dome has a span of 530 ft (162 m), a rise of 100 ft (30 m), and is supported by a post-tensioned reinforced concrete ring. The main skeleton wooden framework consists of 414 curved glulam beams. The grid members are 30 in. (76 cm) deep and have a width of 6.75 or 8.75 in. (17 or 22 cm). The joists are 5 1/8 in. (13 cm) wide and vary in depth from 9 to 18 in. (23 to 46 cm).

The design and analysis of the dome are presented by Eshelby and Evans (1988). The analysis of the dome is performed by the DOME program (Eshelby and Evans, 1988). The grid members are modeled as curved beams, with axial, bending, and shear stiffness. The flexible joints are represented by rotational springs. The effect of the decking is reflected by the constraint that grid members deform only in their great circle planes. Linear analysis and classical eigenvalue buckling analysis are performed. The loading conditions considered include various combinations of dead, snow, wind, and seismic loads. The critical design conditions were unsymmetrical snow loads and wind loads.

2.3.4 Earle A. Chiles Center, University of Portland, Oregon (1984)

This wooden dome has a span of 305 ft (93 m) and a rise of 62 ft (19 m). The dome consists of a primary frame made of glulam Douglas-fir beams which are interconnected at the joints by means of patented steel connectors (Varax hubs). The main skeleton framework consists of 756 curved glulam beams. These beams have a constant cross-section with depth of 24 in. (61 cm) but variable lengths. The dome was designed by RSG Architects, Phoenix, Arizona, and engineered and built by Western Wood Structures of Tualatin, Oregon.

2.3.5 Lattice Wood Shells, Nara, Japan (1988)

Three wood shells were built for the 1988 Nara Silk Road Exposition in Japan near Osaka. The three shells are the Nara Pavilion, the Theme Pavilion, and the Information Office. The Theme Pavilion is 343 ft (104.5 m) in length. The Nara Pavilion is 205 ft (62.5 m) in length. The Information Office is 130 ft (39.5 m) in length. The structures consist of wood members prebent to follow the contour of the shell, with a minimum radius of 33 ft (10 m). The curved wood members have a cross-section of 2.8 in. (7 cm) in width and 1.6 in. (4 cm) in depth. The members are made out of cryptomeria, a Japanese type of cedar. These structures were designed and constructed by T. Maeno, M. Wada, T. Nagase, and T. Hisatok (Melargano, 1991).

2.3.6 Sport Training Complex, University of Northern Michigan, Marquette (1990)

This dome is one of the largest wooden dome in the world (Melargano, 1991). The dome has a span of 533.5 ft (163 m) and a rise of 126.25 ft (39 m). The geometry of the dome is defined as part of a sphere with a radius of 344.5 ft (105 m). The laminated arched beams have a constant cross-section of 37.5 in. (95 cm) in depth and 8.75 in. (22 cm) in width but variable lengths. The glulam beams are interconnected at the joints by means of patented steel connectors (Varax hubs). The structures are made up of glued laminated Douglas-fir beams and a tongue-and-groove decking supported by curved purlins. The dome is supported by 40 concrete buttresses. These buttresses are connected at their bases by a prestressed concrete ring 30 in. (76 cm) deep and 60 in. (152 cm) wide. The dome is composed of five identical spherical sectors.

The dome was designed by T.M.P. Associates, Inc., Bloomfield Hills, Michigan, and engineered and built by Western Wood Structures of Tualatin, Oregon. The dome was designed for a dead load of 20 psf (958 Pa), a live load of 60 psf (2,873 Pa), and a wind load of 80 mph (129 kmh).

2.4 Summary

Finite element stability investigations of spatial wood structures are divided into three groups: linear analysis, nonlinear analysis, and combined linear and nonlinear analysis. Linear analysis is a simplified version of nonlinear analysis. As a result, nonlinear analysis can be a much more expensive for large structures. There are two types of nonlinear analyses commonly used: the Newton-Raphson method and the Riks method. Both methods can be used to trace the equilibrium path of a structure to the first critical point. However, the Newton-Raphson method can trace the equilibrium path of a structure only up to a limit point while the Riks method can trace it through a limit point.

The combined linear and nonlinear stability analysis is considered to be a practical tool for the stability investigation of complex structures (Holzer et al., 1992). It combines the accuracy of nonlinear analysis with the efficiency of linear buckling predictions.

The status of current stability investigations of existing spatial wood structures was presented in this chapter. Some examples of spatial wood structures in which stability investigations are performed with finite element methods were also presented.

Chapter 3

Beam-Decking Connector Elements

3.1 Introduction

In this chapter, background information on the beam element formulation and beam decking connector (BDC) stiffness matrix formulation is presented. Davalos (1989) modeled the Triax dome with curved, three-node beam elements based on the Timoshenko beam theory. ABAQUS designates these beam elements as B32, where B stands for beam, 3 for space, and 2 for quadratic interpolation. Wu (1991) modeled the dome with two-node beam elements (B33) based on the Bernoulli-Euler beam theory. The B33 elements have cubic interpolation. He concluded that the choice of the beam finite elements is not crucial in the construction of the dome model. In this study, the dome model is constructed with B33 elements because the B33 element contains one less node than the B32 element. Using B33 elements greatly reduces the number of nodes in the assembly of the dome model.

Beam decking connector elements are used to simulate the effect of the decking on the behavior of the dome (Tsang, 1991; Kavi, 1992). The beam decking connector element is a nonlinear springs. Each connector element shares the same nodes as the beams through interpolation. Hence, the introduction of the connector elements does not add degrees of freedom to the assembly. This modeling technique is based on the method used by Dolan (1989). A full description of the formulation of the beam decking connector element is presented in this chapter.

3.2 Beam Formulations

A review of beam formulations based on Timoshenko and Bernoulli-Euler theories is presented in sections 3.2.1 and 3.2.2, respectively. A typical beam element and two coordinate systems are shown in Figure 3.1.

3.2.1 Mindlin-Timoshenko Beam Theory

Figure 3.2a shows a normal to the mid-surface (neutral axis). A plane initially normal to the middle surface of the beam remains plane but not necessarily normal. The Mindlin-Timoshenko beam theory allows shear deformation. From Figure 3.1b, the displacements can be defined as

$$v(x,y) = v(x,0) \tag{3.1}$$

$$u(x,y) = u(x,0) - y\,\theta \tag{3.2}$$

where θ represents a small angle of rotation of the normal to surface of the beam. Axial normal strain and transverse shear strain are defined as

$$\varepsilon(x,y) = \frac{\partial}{\partial x}\, u(x,y) \tag{3.3}$$

$$\gamma(x,y) = \frac{\partial}{\partial x}\, v(x,y) + \frac{\partial}{\partial y}\, u(x,y) \tag{3.4}$$

Let

$$u = u(x,0) \tag{3.5}$$

$$v = v(x,0) \tag{3.6}$$

The strain-displacement relations can be written as

$$\varepsilon(x,y) = \frac{\partial u}{\partial x} - y\frac{\partial \theta}{\partial x} \tag{3.7}$$

$$\gamma(x,y) = \frac{\partial v}{\partial x} - \theta \tag{3.8}$$

Equation (3.8) indicates that the transverse shear strain is constant over the depth of the beam because it does not vary with y.

The stress-strain relations for the Mindlin-Timoshenko beam element can be written as

$$\sigma = E\,\varepsilon \tag{3.9}$$

$$\tau = \frac{1}{\kappa}\,G\,\gamma \tag{3.10}$$

where E = elastic modulus
G = shear modulus
σ = normal stress
ε = normal strain
τ = shear stress
γ = shear strain
κ = shear correction factor

For a rectangular cross section, a correction factor of 1.2 is used (Bathe, 1982 and Cook, 1989). This factor accounts for the inconsistency of a parabolic distribution of the shear stress τ and a constant distribution of the shear strain γ.

3.2.2 Bernoulli-Euler Beam Theory

In Bernoulli-Euler beam theory, normals remain straight, undeformed, and normal to the neutral axis of the beam as shown in Figure 3.2b. Since there is no shear deformation in this model, Eq. (3.8) becomes

$$\gamma(x,y) \quad = \quad \frac{\partial v}{\partial x} - \theta = \quad 0 \qquad (3.11)$$

which yields

$$\theta \quad = \quad \frac{dv}{dx}$$

(3.12)

If the middle surface of the beam is unstrained, i.e., $\frac{du}{dx} = 0$, the strain-displacement relations for the Bernoulli-Euler beam element can be expressed from Eqs. 3.7 and 3.12 as

$$\varepsilon(x,y) \quad = \quad -y\frac{d\theta}{dx} \quad = \quad -y\frac{d^2v}{dx^2} \qquad (3.13)$$

The stress-strain relations for the Bernoulli-Euler beam element can be expressed as

$$\sigma \quad = \quad E\,\varepsilon \qquad (3.14)$$

The geometry of the beam element is defined with linear interpolation functions as

$$x \quad = \quad \sum_{i=1}^{2} \hat{N}_i\, x_i \qquad (3.15)$$

where x_i = x-coordinate of node i

$$\hat{N}_i \quad = \quad \text{interpolation function of coordinate } x_i$$

The linear interpolation functions for coordinates are given as

$$\hat{N}_1 = 1-\xi, \quad \hat{N}_2 = \xi, \quad \xi = \frac{x}{L} \tag{3.16}$$

The configuration of the beam element is defined with cubic interpolation functions as

$$v = \sum_{i=1}^{4} N_i \, d_i = Nd \tag{3.17}$$

where

$$\begin{aligned} N_1(\xi) &= 1 - 3\xi^2 + 2\xi^3 \\ N_2(\xi) &= (\xi - 2\xi^2 + \xi^3)L \\ N_3(\xi) &= 3\xi^2 - 2\xi^3 \\ N_4(\xi) &= (-\xi^2 + \xi^3)L \\ \xi &= x/L \end{aligned} \tag{3.18}$$

From Eqs. (3.13) and (3.15) the compatibility condition can be written as

$$\begin{aligned} \varepsilon(x,y) &= -y\frac{d^2v}{dx^2} = -\frac{4y}{L^2}\frac{d^2v}{d\xi^2} \\ &= \left[-\frac{4y}{L^2}N''\right]d = \left[-\frac{4y}{L^2}\bar{B}\right]d \\ &= Bd \end{aligned} \tag{3.19}$$

where $$B = -\frac{4y}{L^2} N'' = -\frac{4y}{L^2} \bar{B}$$

$$\bar{B} = N'' = \left[N_1'' \middle| N_2'' \middle| N_3'' \middle| N_4'' \right]$$

$$\bar{B} = \left[6(2\xi - 1) \middle| 2L(3\xi - 2) \middle| 6(-2\xi + 1) \middle| 2L(3\xi - 1) \right]$$

The stiffness matrix of the beam element is defined as (Cook et al., 1989)

$$\begin{aligned} k &= \iiint_{Vol} B^T E B \, dA \, dx \\ &= \frac{16}{L^4} E \int_{x1}^{x2} \left(\iint_{Area} y^2 \, dA \right) \bar{B}^T \bar{B} \, dx \\ &= 8\left(\frac{EI}{L^3}\right) \int_{-1}^{1} \bar{B}^T \bar{B} \, d\xi \\ &= 8\alpha \int_{-1}^{1} \bar{B}_i \bar{B}j \, d\xi \end{aligned}$$

where Vol denotes the volume of the element and Area denotes cross-sectional area. The moment of inertia of cross-sectional area is I = $\iint_{Area} y^2 \, dA$. The element stiffness matrix can be written as

$$k = \alpha \begin{bmatrix} 12 & 6L & -12 & 6L \\ 6L & 4L^2 & -6L & 2L^2 \\ -12 & -6L & 12 & -6L \\ 6L & 2L^2 & -6L & -4L^2 \end{bmatrix} \qquad (3.20)$$

where $$\alpha = \frac{EI}{L^3}$$

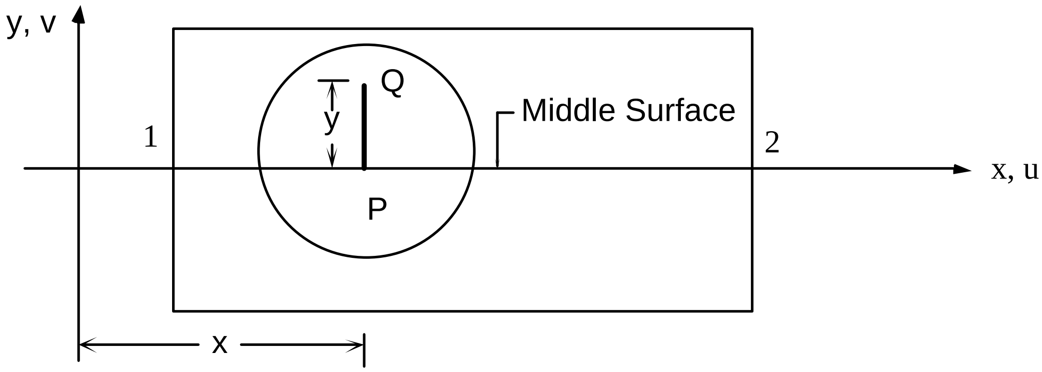

(a) Beam

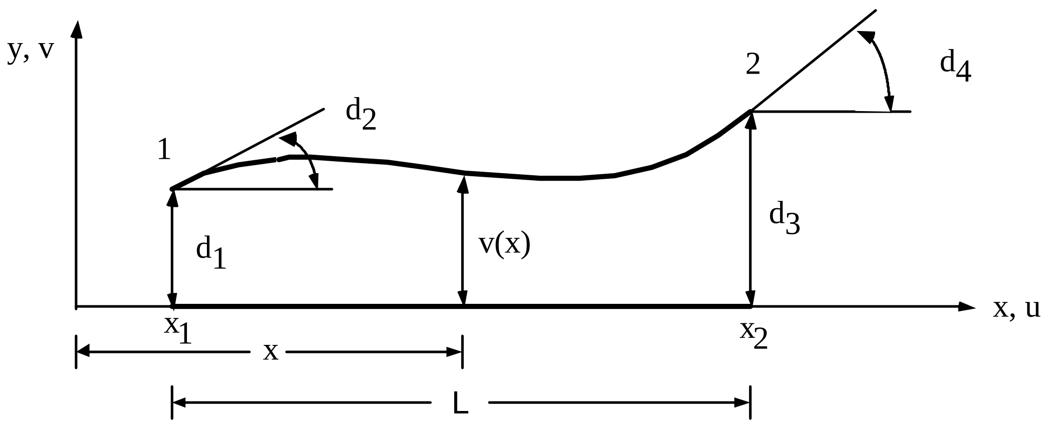

(b) Global Coordinate System

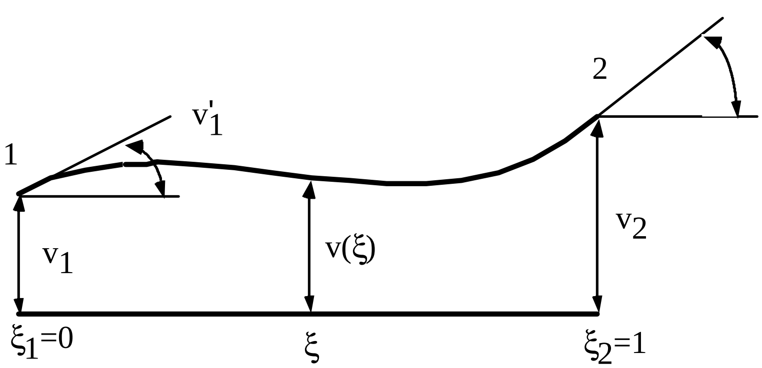

(c) Local (Parent) Coordinate System

Figure 3.1 Beam Finite Element

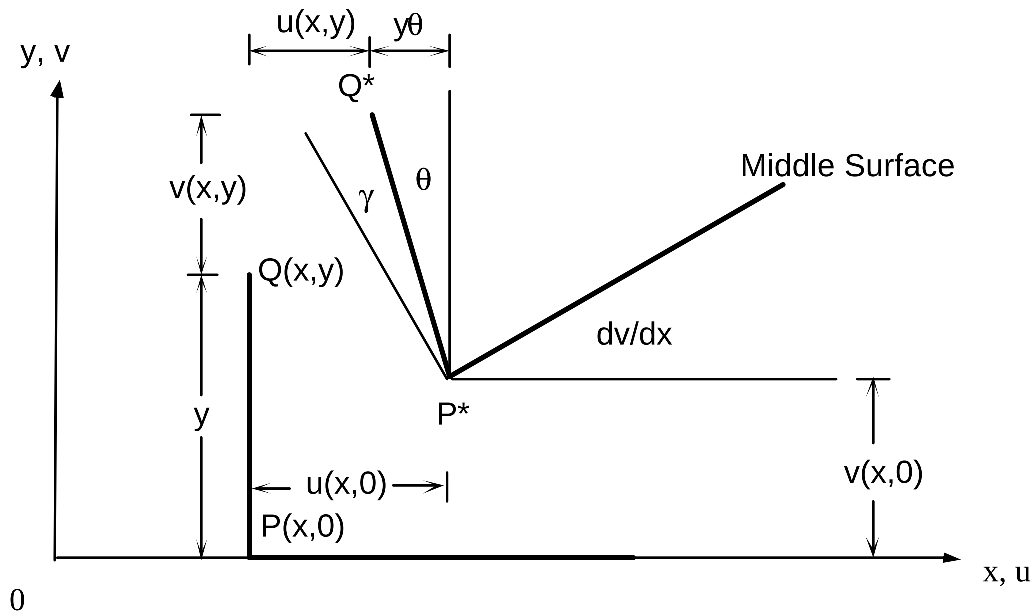

(a)

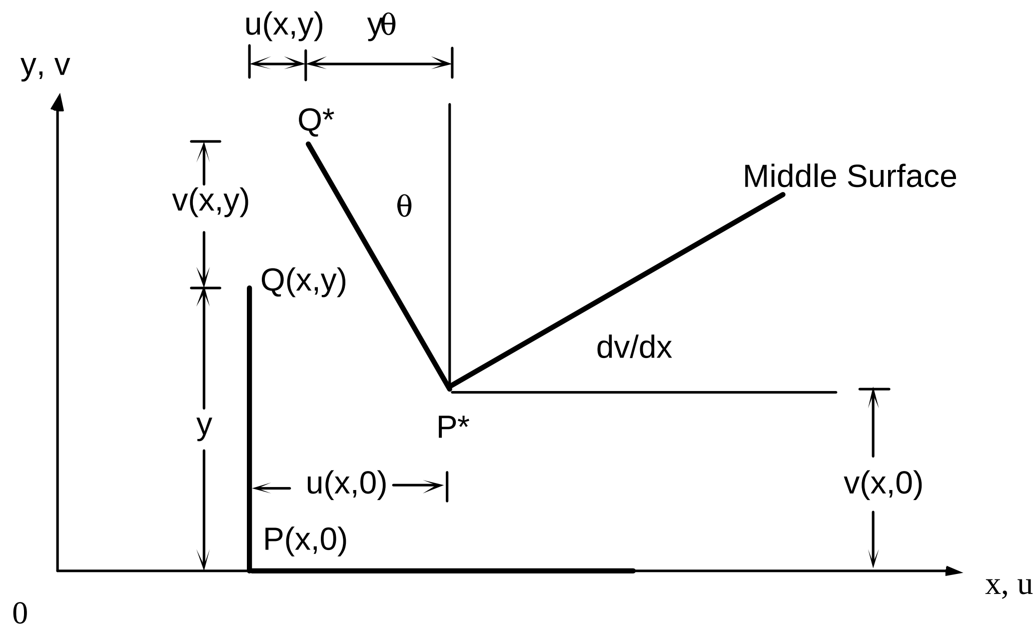

(b)

Figure 3.2 Kinematics: (a) Mindlin-Timoshenko Beam Element;
(b) Bernoulli Beam Element

3.3 Beam-Decking Connector Element (BDC)

The behavior of the nails joining the top of the beams with the decking is represented by the beam-decking connector elements (Dolan, 1989; Holzer, 1991; Tsang, 1992; and Kavi 1993). The decking is nailed to each glulam beam at 16 locations. The connector elements are composed of 16 nonlinear springs that provide lateral support for each beam. Each spring is connected at one end to a rigid link which is connected the centroidal axis of the beam and the other end to a fixed support (Fig. 3.3). The fixed support is used because the membrane deflections of the decking are neglected. The load-deflection curve (slip) for a linear spring and a 16-d common nail are shown in Figure 3.4 (Kavi, 1993). When the elongation of a spring reaches 1 in., the spring is disconnected. In this chapter, the formulation of the BDC element is explained. The two-dimensional and three-dimensional beam decking connector stiffness matrices are formulated in Section 3.3.1 and Section 3.3.2, respectively.

3.3.1 Formulation of 2-D BDC Stiffness Matrix

A spring connected to a plane beam element is shown in Figure 3.5 (a). The beam has four degrees of freedom, d_1-d_4. The elongation of the spring can be determined through interpolation functions from the nodal displacements of the beam element. Thus, the spring does not add degrees of freedom to the beam assembly. The parent element for the beam is shown in Figure 3.5 (b). The connector element is a nonlinear spring with stiffness $\gamma(v_s)$, where v_s is the deflection of the spring. Since the curve is bilinear, a constant spring stiffness value can be used up to 0.056 in. as shown in Figure 3.4b. For a constant stiffness of γ, the spring energy can be written as (Figure 3.4a)

$$U_s = \frac{1}{2}\gamma v_s^2 = \frac{1}{2} v_s^T \gamma v_s \tag{3.21}$$

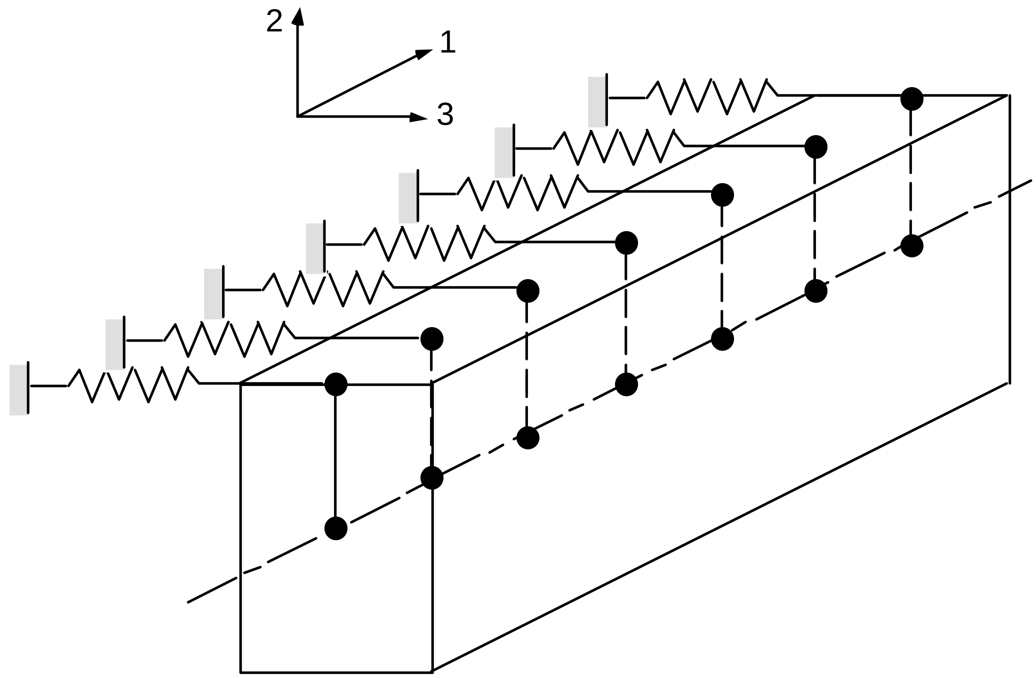

Figure 3.3 Beam-Decking Connector Element (BDC)

Since the connector element and the beam element share the same degrees of freedom, the spring deflection can be obtained from the beam interpolation functions (Holzer, 1985, p.8) as follows:

$$v_s(\xi) = N_1(\xi)d_1 + N_2(\xi)d_2 + N_3(\xi)d_3 + N_4(\xi)d_4 \quad = \quad N_s d \tag{3.22}$$

where

$$\begin{aligned} N_1(\xi) &= 1 - 3\xi^2 + 2\xi^3 \\ N_2(\xi) &= (\xi - 2\xi^2 + \xi^3)L \\ N_3(\xi) &= 3\xi^2 - 2\xi^3 \\ N_4(\xi) &= (-\xi^2 + \xi^3)L \\ \xi &= x/L \end{aligned} \tag{3.23}$$

and

$$N_S = [N_1 \;\; N_2 \;\; N_3 \;\; N_4]$$

$$d = \begin{bmatrix} d_1 \\ d_2 \\ d_3 \\ d_4 \end{bmatrix}$$

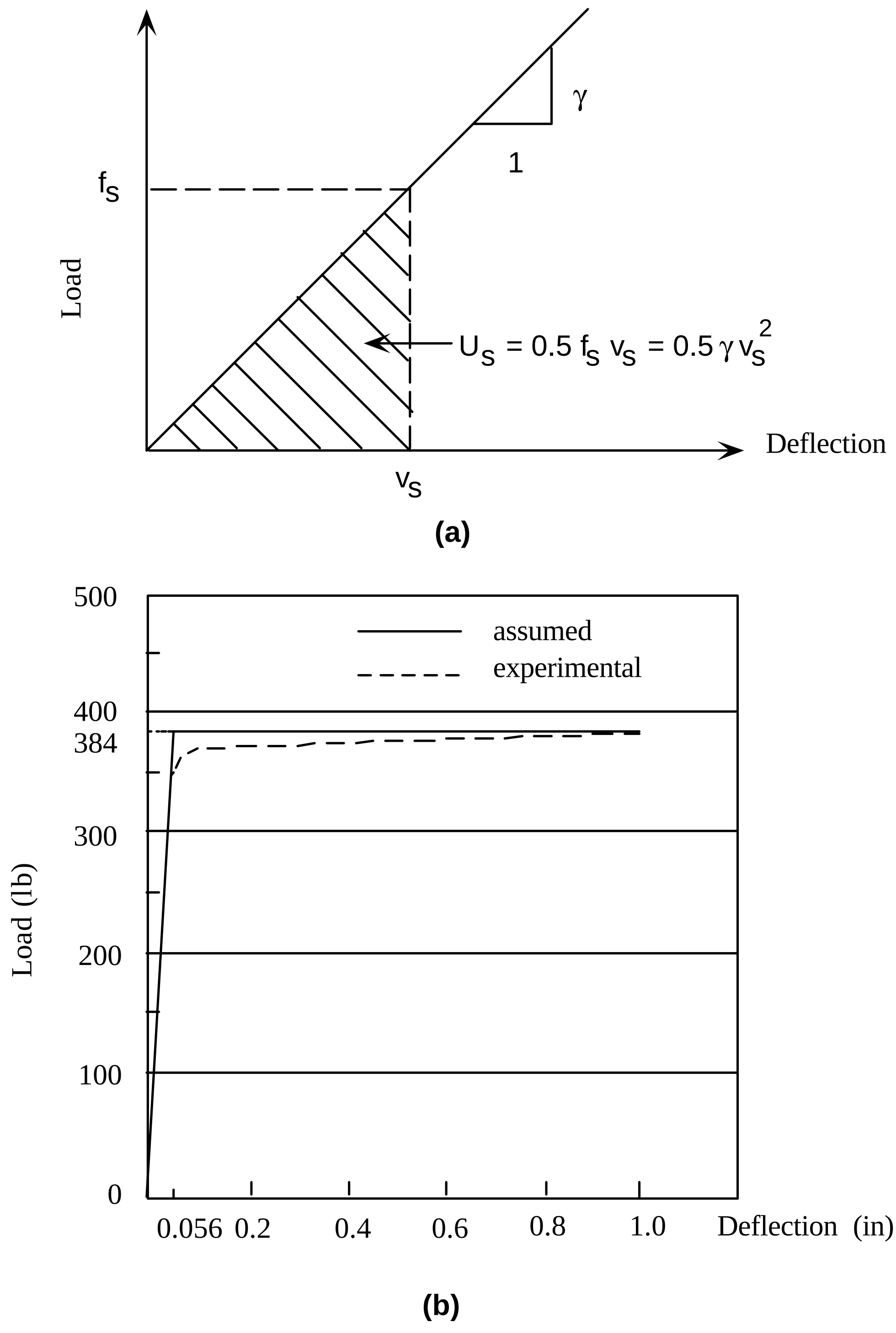

Figure 3.4 Load-Deflection Curve: (a) Linear Spring; (b) Nonlinear Spring

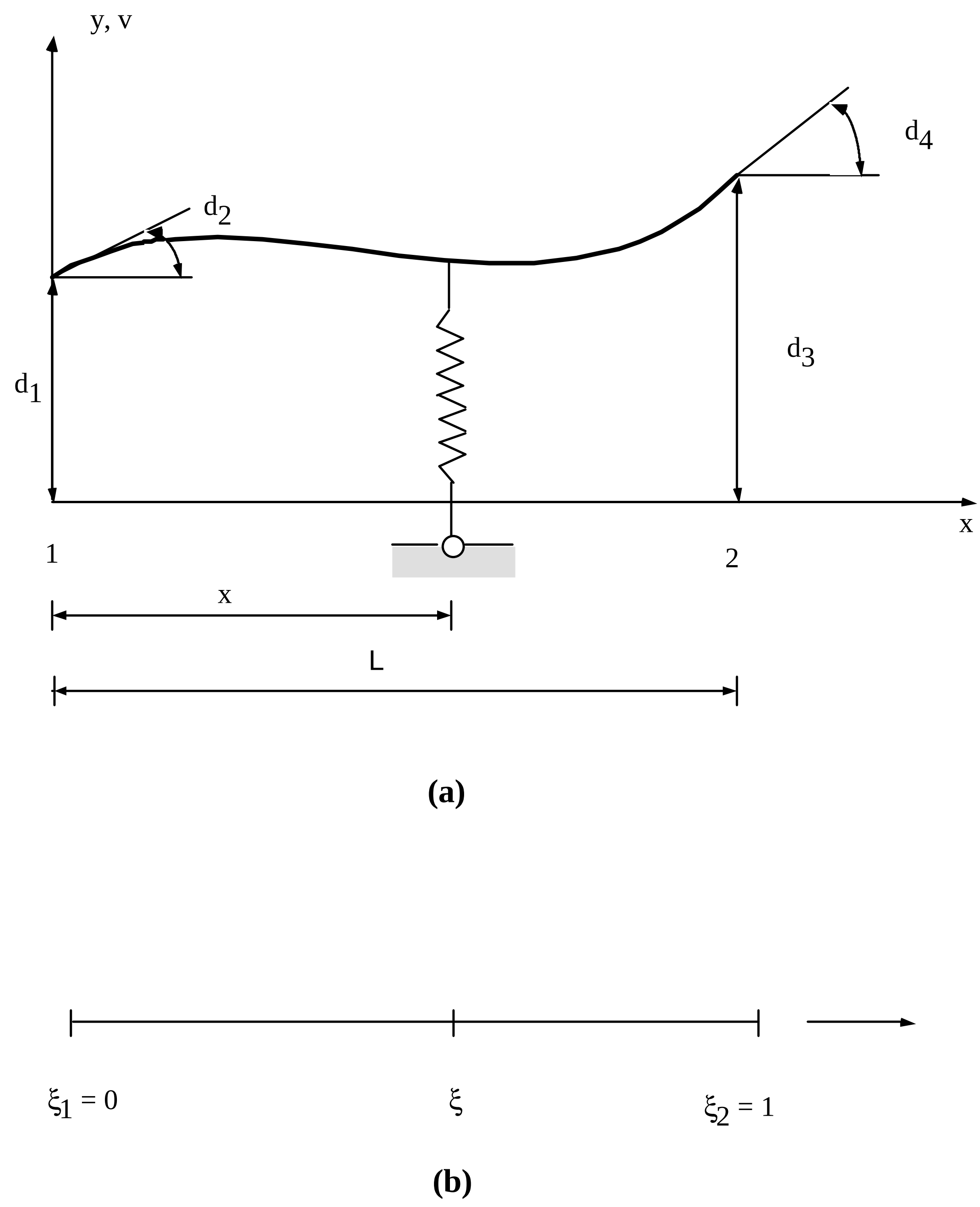

Figure 3.5 Plane Beam with Discrete Connector

From Equations (3.21) and (3.22), the spring energy can be written as

$$U_s = \quad \frac{1}{2} d^T N_s^T \gamma N_s d = \frac{1}{2} d^T k_s d$$

where k_s is the spring stiffness matrix and is given by

$$k_s \quad = \quad N_s^T \gamma N_s$$

$$= \quad \gamma \begin{bmatrix} N_1 \\ N_2 \\ N_3 \\ N_4 \end{bmatrix} \begin{bmatrix} N_1 & N_2 & N_3 & N_4 \end{bmatrix}$$

$$= \quad \gamma \begin{bmatrix} g_1 & g_2 & g_4 & g_7 \\ & g_3 & g_5 & g_8 \\ & & g_6 & g_9 \\ \text{sym.} & & & g_{10} \end{bmatrix} \tag{3.24}$$

where

$$\begin{aligned}
\gamma &= \text{spring stiffness} \\
g_1 &= N_1 N_1 \\
g_2 &= N_1 N_2 \\
g_3 &= N_2 N_2 \\
g_4 &= N_1 N_3 \\
g_5 &= N_2 N_3 \\
g_6 &= N_3 N_3 \\
g_7 &= N_1 N_4 \\
g_8 &= N_2 N_4 \\
g_9 &= N_3 N_4 \\
g_{10} &= N_4 N_4
\end{aligned} \tag{3.25}$$

and Ni’s are defined in Equation (3.23).

The total energy of the BDC element (beam and attached spring) is the sum of the internal energy of the beam (U_b) and the spring energy (U_s):

$$U = U_b + U_s = \frac{1}{2} d^T k_b d + \frac{1}{2} d^T k_s d \; = \frac{1}{2} d^T k d \tag{3.26}$$

where

k_b = plane beam stiffness matrix

k = $k_b + k_s$ = BDC stiffness matrix

When multiple springs are attached to the beam, the total energy of the BDC element is

$$\begin{aligned} U &= U_b + \sum_{i=1}^{n} U_s^i \\ &= \frac{1}{2} d^T (k_b + \sum_{i=1}^{n} k_s^i) d \end{aligned} \tag{3.27}$$

where

U_s^i = energy of the i^{th} spring

k_s^i = stiffness of the i^{th} spring

n = total number of springs

and

$k = k_b + \sum_{i=1}^{n} k_s^i$

= stiffness matrix of BDC element with multiple springs

The connector stiffness matrix for a plane beam element can be transformed into a matrix for a plane frame element using the member code (or M-code) method developed by Holzer (1985). A plane beam element and a plane frame element are shown in Figures 3.5(a) and 3.5(b), respectively. According to Figure 3.6, the M-code for transforming the plane beam element to a plane frame element is given below:

$$M = \begin{bmatrix} 2 \\ 3 \\ 5 \\ 6 \end{bmatrix} \tag{3.28}$$

This M-code can be used to map the connector stiffness matrix in Eq.(3.24) into a connector stiffness matrix for a frame element as follows:

The M-code is assigned to k_s in Eq.(3.24),

$$k_s = \gamma \begin{array}{c} \begin{array}{cccc} 2 & 3 & 5 & 6 \end{array} \\ \begin{bmatrix} g_1 & g_2 & g_4 & g_7 \\ & g_3 & g_5 & g_8 \\ & & g_6 & g_9 \\ \text{sym.} & & & g_{10} \end{bmatrix} \end{array} \begin{array}{c} \\ 2 \\ 3 \\ 5 \\ 6 \end{array}$$

and the k_s matrix for a plane frame element is

$$k_s = \gamma \begin{array}{c} \begin{array}{cccccc} 1 & 2 & 3 & 4 & 5 & 6 \end{array} \\ \begin{bmatrix} 0 & 0 & 0 & 0 & 0 & 0 \\ & g_1 & g_2 & 0 & g_4 & g_7 \\ & & g_3 & 0 & g_5 & g_8 \\ & & & 0 & 0 & 0 \\ & & & & g_6 & g_9 \\ \text{sym.} & & & & & g_{10} \end{bmatrix} \end{array} \begin{array}{c} \\ 1 \\ 2 \\ 3 \\ 4 \\ 5 \\ 6 \end{array} \tag{3.29}$$

and the g_i's are defined in Eq.(3.25).

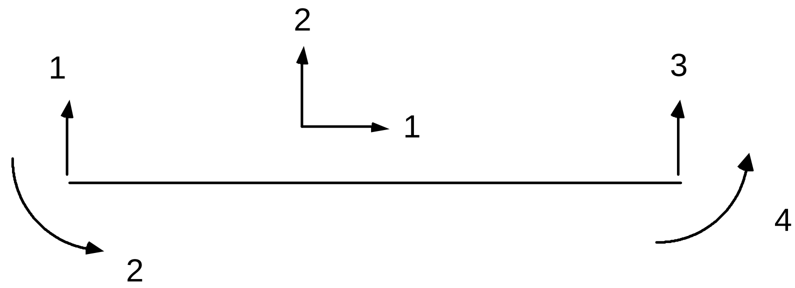

(a) Plane Beam Element

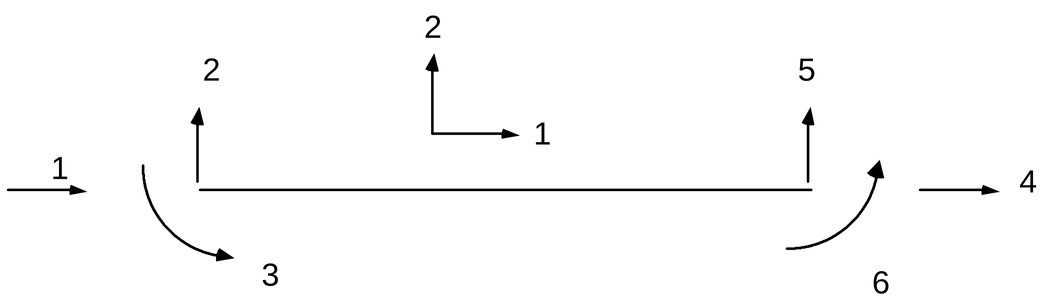

(b) Plane Frame Element

Figure 3.6 Degrees of Freedom for Plane Beam and Plane Frame Elements

The local element stiffness matrix of a plane frame element is given as (Holzer, 1985, p. 125)

$$k_b = \begin{bmatrix} \beta & 0 & 0 & -\beta & 0 & 0 \\ & 12 & 6L & 0 & -12 & 6L \\ & & 4L^2 & 0 & -6L & 2L^2 \\ & & & \beta & 0 & 0 \\ & & & & 12 & -6L \\ \text{sym.} & & & & & 4L^2 \end{bmatrix} \tag{3.30}$$

where

$$\alpha = \frac{EI}{L^3}, \qquad \beta = \frac{AL^2}{I}, \qquad \gamma = \alpha\beta = \frac{EA}{L}$$

E = modulus of elasticity

I = moment of inertia of the cross-sectional area

L = length of the element

A = cross-sectional area

3.3.2 Formulation of 3-D BDC Stiffness Matrix

The three-dimensional frame element has a total of 12 DOF, 6 at each node, as shown in Figure 3.7. Since the dome model is analyzed with space beam elements, it is necessary to formulate a 3-D stiffness matrix of the beam-decking connector element. A space beam element with a discrete connector is shown in Figure 3.8. The axial and transverse DOF's of the frame element (DOF's 1, 3, 7, and 9 in Figure 3.7) are not considered in the beam-decking connector assembly of Figure 3.8 because the connector element provides only lateral support for the beam element. The only DOF's of the space frame element shared by the BDC element are 2, 4, 6, 8, 10, and 12, and are denoted d_1 - d_6 in Figure 3.8.

The nonlinear spring is placed tangent to the top of the beam in order to model the lateral restraint which the decking provides the beams. The nail is used to provide only the lateral resistance to beam deformation. One end of the spring is attached to the beam element through a rigid link of length h and the other end of the spring is modeled as a fixed support because the decking is assumed to be very stiff in membrane action. The membrane deflections of the decking are neglected relative to the lateral displacement and rotation of the beam element and the elongation of the spring (Holzer et al., 1994).

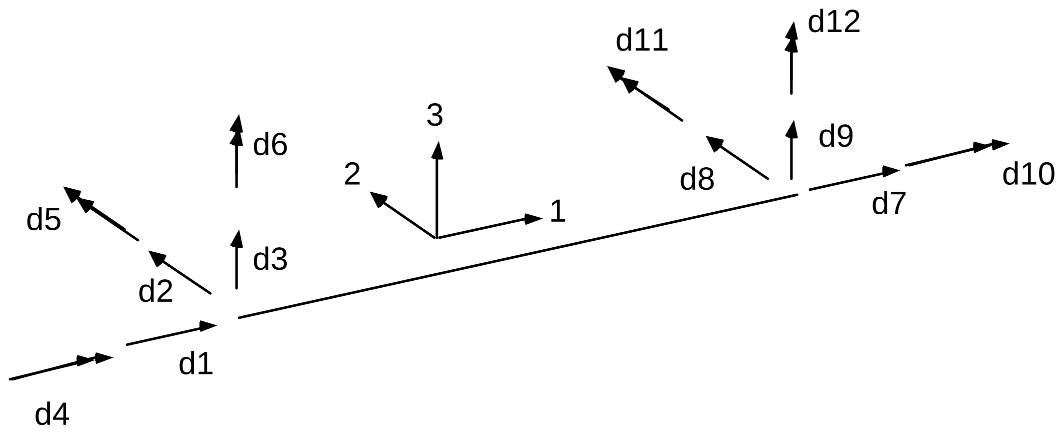

Figure 3.7 Space Frame Element

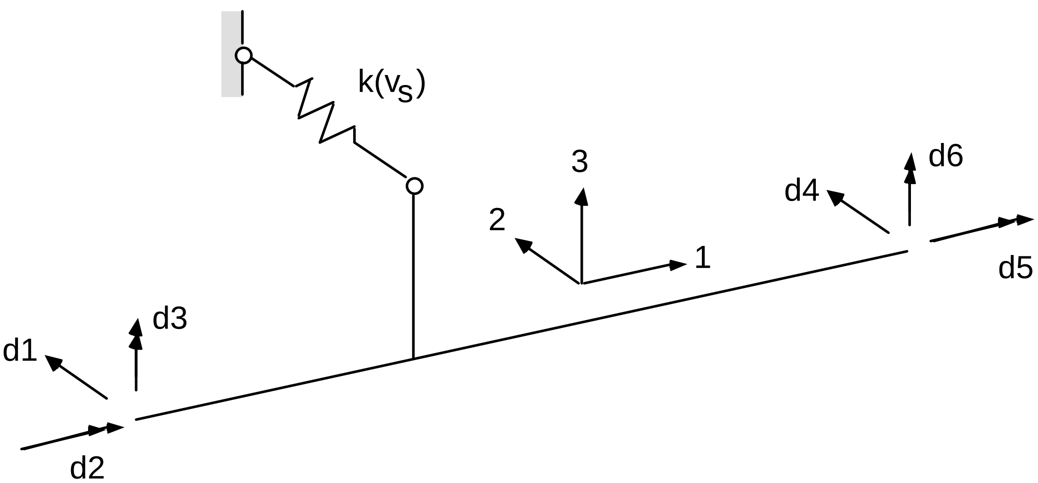

Figure 3.8 Space Beam Element with Connector

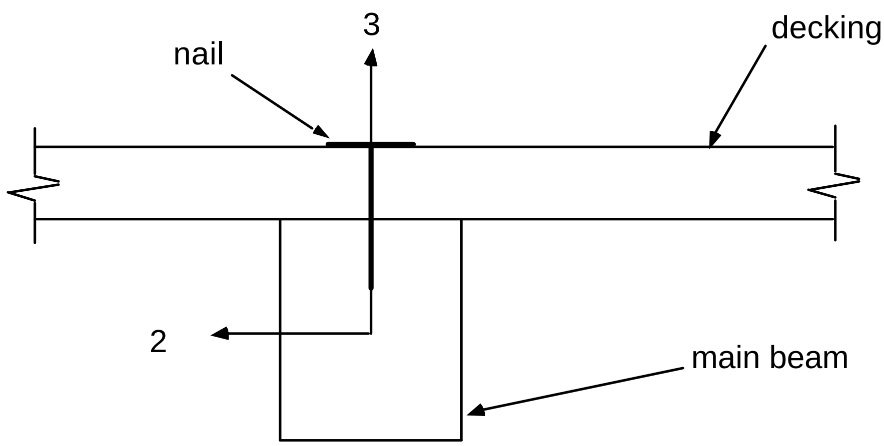

Figure 3.9 Beam-to-Decking Connection

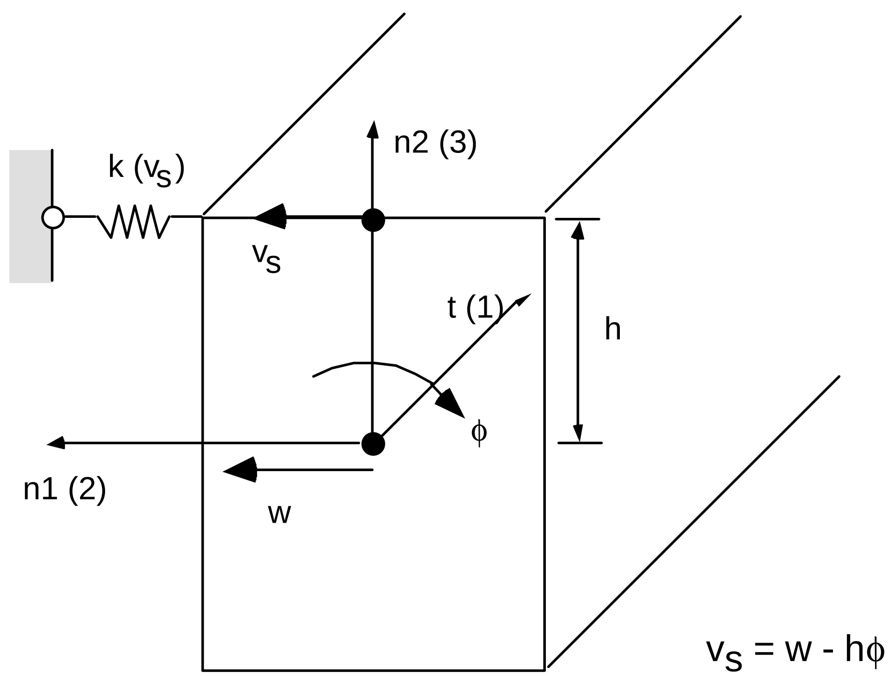

Figure 3.10 Relationship Between Nail Deflection and Nodal Deflection of Beam

Figure 3.9 shows a nailed connection between the decking and a beam, and Figure 3.10 illustrates the relationship between the spring deflection (v_s) and the nodal deflections of the beam (w and ϕ). Generally, for a spring placed at any point along the beam, the spring deflection is given by

$$v_s(\xi) = w(\xi) - h\phi(\xi) \tag{3.31}$$

where

$w(\xi)$ = deflection of the beam corresponding to transverse deflection in the 2-direction and bending about the 3-axis

h = rigid link length

$\phi(\xi)$ = rotation of beam about 1-axis

ξ = x/L

The deflection and rotation of the beam are independent displacements and are expressed by different interpolation functions, as shown below:

$$\phi(\xi) = \begin{bmatrix} N_1^1 & N_2^1 \end{bmatrix} \begin{bmatrix} d_2 \\ d_5 \end{bmatrix} \tag{3.32}$$

where

$N_1^1 = (1 - \xi)$

and (3.33)

$N_2^1 = \xi$

$$w(\xi) = \begin{bmatrix} N_1^2 & N_2^2 & N_3^2 & N_4^2 \end{bmatrix} \begin{bmatrix} d^1 \\ d^2 \\ d^3 \\ d^4 \end{bmatrix} \tag{3.34}$$

where

$N_1^2 = N_1(\xi) = 1 - 3\xi^2 + 2\xi^3$

$N_2^2 \;=\; N_2(\xi) \;=\; (\xi - 2\xi^2 + \xi^3)L$

$N_3^2 \;=\; N_3(\xi) \;=\; 3\xi^2 - 2\xi^3$

$N_4^2 \;=\; N_4(\xi) \;=\; (-\xi^2 + \xi^3)L$

From Equations (3.31), (3.32), and (3.33), the spring deflection v_s can be expressed as

$$v_S = N_1^2 d_1 - hN_1^1 d_2 + N_2^2 d_3 + N_3^2 d_4 - hN_2^1 d_5 + N_4^2 d_6 \quad = \quad Sd \tag{3.35}$$

where

$$\begin{aligned} S &= [S(1)\;\; S(2)\;\; S(3)\;\; S(4)\;\; S(5)\;\; S(6)] \\ &= \begin{bmatrix} N_1^2 & -hN_1^1 & N_2^2 & N_3^2 & -hN_2^1 & N_4^2 \end{bmatrix} \end{aligned} \tag{3.36}$$

and

$$d \;=\; \begin{bmatrix} d_1 \\ d_2 \\ d_3 \\ d_4 \\ d_5 \\ d_6 \end{bmatrix} \tag{3.37}$$

Equation (3.35) represents the interpolation functions for a 3-D BDC element. These functions can be used to calculate the stiffness matrix of the 3-D BDC element in the ABAQUS user subroutine UEL. The following connector stiffness matrix is obtained:

$$k_s \;=\; S^T \gamma\, S$$

$$
\begin{array}{cc}
 & \begin{array}{cccccc} 2 & 4 & 6 & 8 & 10 & 12 \end{array} \\
k_s = & \left[\begin{array}{cccccc}
g_1 & g_2 & g_4 & g_7 & g_{11} & g_{16} \\
 & g_3 & g_5 & g_8 & g_{12} & g_{17} \\
 & & g_6 & g_9 & g_{13} & g_{18} \\
 & & & g_{10} & g_{14} & g_{19} \\
 & & & & g_{15} & g_{20} \\
\text{sym.} & & & & & g_{21}
\end{array}\right]
\begin{array}{c} 2 \\ 4 \\ 6 \\ 8 \\ 10 \\ 12 \end{array}
\end{array}
\tag{3.38}
$$

where

$$
\begin{array}{lll}
g_1 = S(1)\,S(1), & g_2 = S(1)\,S(2), & g_3 = S(2)\,S(2), \\
g_4 = S(1)\,S(3), & g_5 = S(2)\,S(3), & g_6 = S(3)\,S(3), \\
g_7 = S(1)\,S(4), & g_8 = S(2)\,S(4), & g_9 = S(3)\,S(4), \\
g_{10} = S(4)\,S(4), & g_{11} = S(1)\,S(5), & g_{12} = S(2)\,S(5), \\
g_{13} = S(3)\,S(5), & g_{14} = S(4)\,S(5), & g_{15} = S(5)\,S(5), \\
g_{16} = S(1)\,S(6), & g_{17} = S(2)\,S(6), & g_{18} = S(3)\,S(6), \\
g_{19} = S(4)\,S(6), & g_{20} = S(5)\,S(6), & g_{21} = S(6)\,S(6)
\end{array}
\tag{3.39}
$$

and S(1) through S(6) are given in Equation (3.36).

Analogous to the 2-D case, the above stiffness matrix must be transformed into a 12 x 12 matrix to conform to the stiffness matrix of a space frame element which has 12 DOF (see Figure 3.7). The M-code for this transformation is as follows

$$
M = \begin{bmatrix} 2 \\ 4 \\ 6 \\ 8 \\ 10 \\ 12 \end{bmatrix}
\tag{3.40}
$$

The stiffness matrix of Equation (3.38) is then mapped into the following 12 x 12 matrix:

$$k_s = \begin{matrix} \begin{matrix} 1 & 2 & 3 & 4 & 5 & 6 & 7 & 8 & 9 & 10 & 11 & 12 \end{matrix} & \\ \begin{bmatrix} 0 & 0 & 0 & 0 & 0 & 0 & 0 & 0 & 0 & 0 & 0 & 0 \\ & g_1 & 0 & g_2 & 0 & g_4 & 0 & g_7 & 0 & g_{11} & 0 & g_{16} \\ & & 0 & 0 & 0 & 0 & 0 & 0 & 0 & 0 & 0 & 0 \\ & & & g_3 & 0 & g_5 & 0 & g_8 & 0 & g_{12} & 0 & g_{17} \\ & & & & 0 & 0 & 0 & 0 & 0 & 0 & 0 & 0 \\ & & & & & g_6 & 0 & g_9 & 0 & g_{13} & 0 & g_{18} \\ & & & & & & 0 & 0 & 0 & 0 & 0 & 0 \\ & & & & & & & g_{10} & 0 & g_{14} & 0 & g_{19} \\ & & & & & & & & 0 & 0 & 0 & 0 \\ & & & & & & & & & g_{15} & 0 & g_{20} \\ & & & & & & & & & & 0 & 0 \\ \text{sym.} & & & & & & & & & & & g_{21} \end{bmatrix} & \begin{matrix} 1 \\ 2 \\ 3 \\ 4 \\ 5 \\ 6 \\ 7 \\ 8 \\ 9 \\ 10 \\ 11 \\ 12 \end{matrix} \end{matrix} \qquad (3.41)$$

This is the local stiffness matrix of a BDC element which has been transformed to a 12 DOF format. The derivation of this matrix assumed a constant spring stiffness. However, for a segmented load-deflection curve as shown in Figure 3.4b, the spring stiffness changes for each segment of the curve. The segmented load-deflection curve can be defined in the user subroutine UEL. The various beams of the dome are oriented in different directions (i.e. their local coordinate axes are not coincident). Thus, before the BDC elements can be assembled, each local stiffness matrix must be transformed into a matrix which is based on the global axes of the assembly. This coordinate transformation process (Holzer, 1985) is also performed in the ABAQUS user supplied subroutine UEL.

The local stiffness matrix of a space frame element as shown in Figure 3.11 is given as (Holzer, 1985, p. 265)

$$
k_b = \begin{array}{cc}
\begin{array}{cccccccccccc} 1 & 2 & 3 & 4 & 5 & 6 & 7 & 8 & 9 & 10 & 11 & 12 \end{array} & \\
\begin{bmatrix}
\gamma & 0 & 0 & 0 & 0 & 0 & -\gamma & 0 & 0 & 0 & 0 & 0 \\
 & 12\beta & 0 & 0 & 0 & -6L\beta & 0 & -12\alpha & 0 & 0 & 0 & -6L\beta \\
 & & 12\alpha & 0 & 6L\alpha & 0 & 0 & 0 & -12\alpha & 0 & 6L\alpha & 0 \\
 & & & \delta & 0 & 0 & 0 & 0 & 0 & -\delta & 0 & 0 \\
 & & & & 4L^2\alpha & 0 & 0 & 0 & -6L\alpha & 0 & 2L^2\alpha & 0 \\
 & & & & & 4L^2\beta & 0 & 6L\beta & 0 & 0 & 0 & 2L^2\beta \\
 & & & & & & \gamma & 0 & 0 & 0 & 0 & 0 \\
 & & & & & & & 12\beta & 0 & 0 & 0 & 6L\beta \\
 & & & & & & & & 12\alpha & 0 & -6L\alpha & 0 \\
 & & & & & & & & & \delta & 0 & 0 \\
 & & & & & & & & & & 4L^2\alpha & 0 \\
 & \text{sym.} & & & & & & & & & & 4L^2\beta
\end{bmatrix} & \begin{array}{c} 1 \\ 2 \\ 3 \\ 4 \\ 5 \\ 6 \\ 7 \\ 8 \\ 9 \\ 10 \\ 11 \\ 12 \end{array}
\end{array}
$$

(3.42)

where

$$\alpha = \frac{EI_2}{L^3}, \quad \beta = \frac{EI_3}{L^3}, \quad \gamma = \frac{EA}{L}, \quad \delta = \frac{GJ}{L}$$

E = modulus of elasticity

I_2 = moment of inertia about the 2 axis (Figure 3.11c)

I_3 = moment of inertia about the 3 axis (Figure 3.11d)

L = length of the element

J = torsion constant

G = shear modulus

A = cross-sectional area

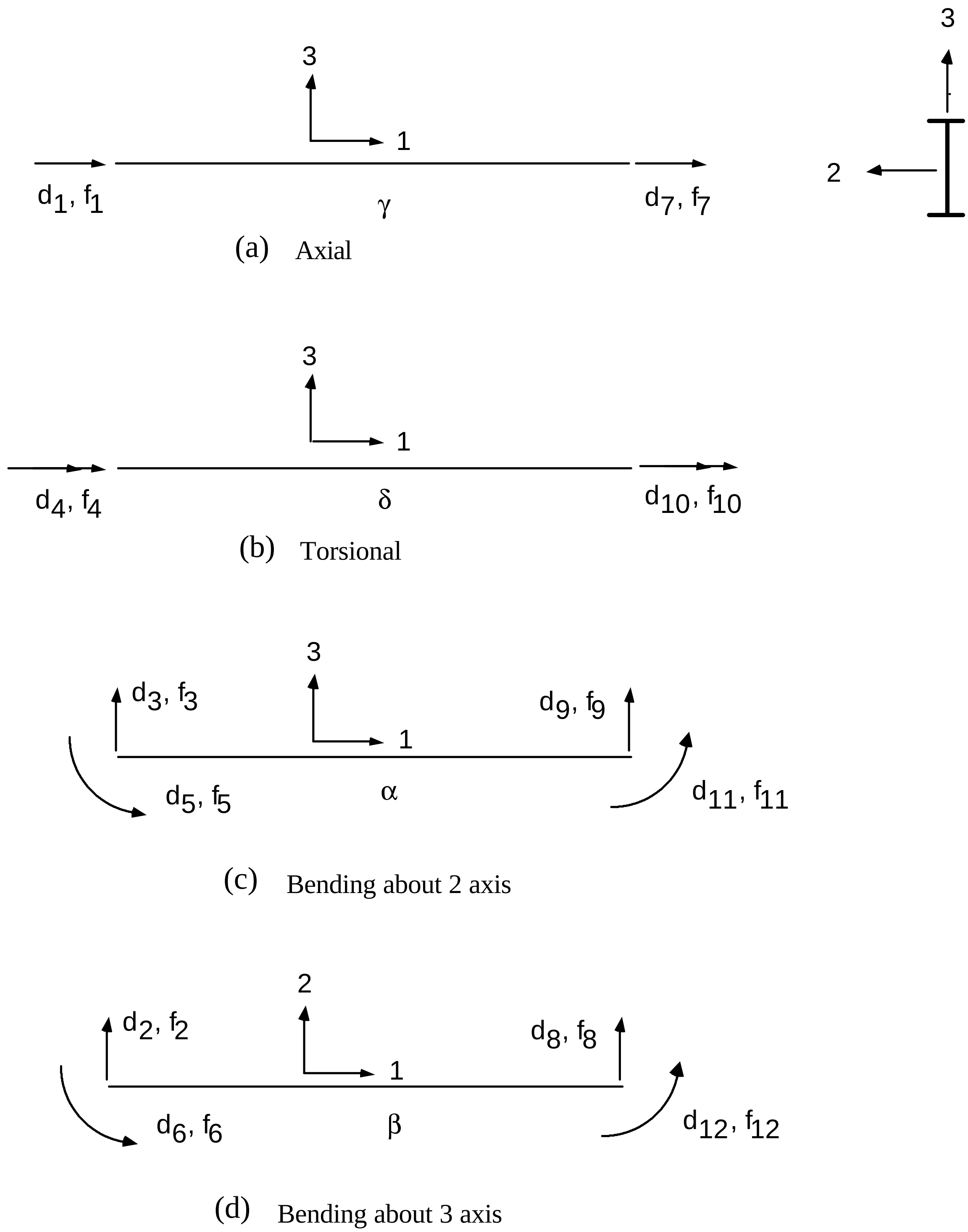

Figure 3.11 Deformation of Space Frame Element

3.4 Summary

A review of beam formulations based on Timoshenko and Bernoulli theories is presented in this chapter. The B32 beam elements are based on the Timoshenko beam theory which includes shear deformation. The B32 elements have 3 nodes and quadratic interpolation. The B33 beam elements are based on the Bernoulli-Euler beam theory. The B33 elements have 2 nodes and cubic interpolation.

Beam-decking connector (BDC) elements are introduced to simulate the effect of the decking which provides lateral support to the glulam beams.. Each BDC element includes 16 nonlinear springs which represent the nails connecting the decking to the beams. Each BDC element in the dome model shares the same nodes and degrees of freedom of the corresponding beam element through interpolation functions. Hence, the BDC elements do not add degrees of freedom to the assembly. The 2-D and 3-D connector stiffness matrices are also presented in this chapter.

Chapter 4

Analysis of Triax Dome

4.1 Introduction

This chapter is concerned with finite element analyses of a glued-laminated timber (glulam) dome. The purpose is to determine the governing failure mode and ultimate snow loads of the Crafts Pavilion dome in Raleigh, North Carolina (Fig. 4.1) and to test the hypothesis that the beam-decking connectors (B-D connectors) form the weakest link of the dome. The B-D connectors are represented by nonlinear springs which model the load-slip behavior of nails joining the beam and the decking. The dome consists of a triangulated network of curved glulam beams, a tongue-and-groove decking supported by curved purlins, and a steel tension ring. The glulam beams are joined by patented steel hubs, and the decking is nailed to the beams and purlins. The dome model is generated with the commercial finite element program I-DEAS (1995) and analyzed with ABAQUS (1995). I-DEAS was chosen because of its powerful graphical capabilities which facilitate pre- and post-processing of the dome model. ABAQUS was chosen because of its nonlinear analysis capabilities and because it allows the user to create subroutines to define elements that are not available in the standard element libraries. In this chapter, details of finite element modeling and stability analyses of the dome model are presented.

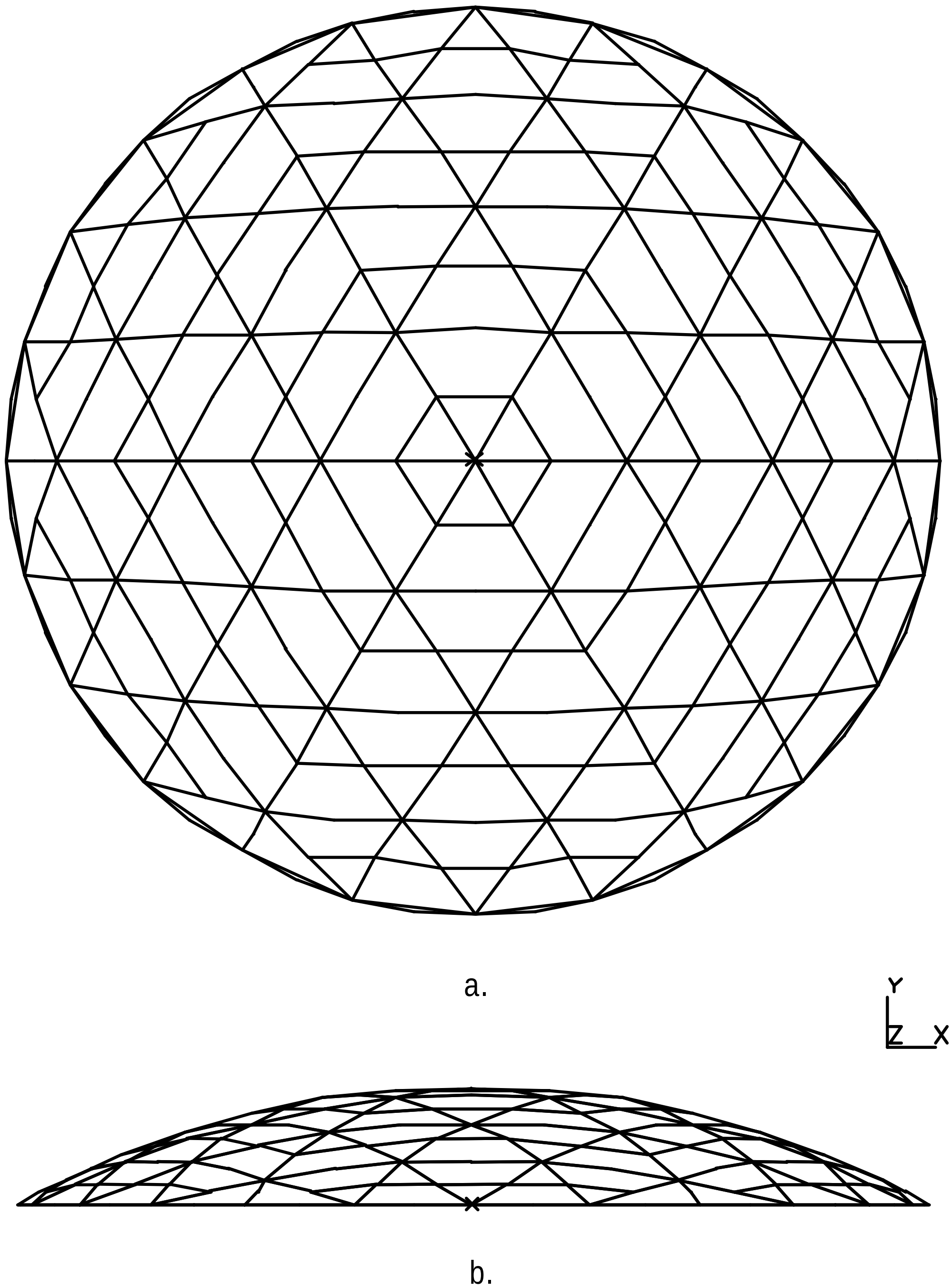

Figure 4.1 Geometry of Dome: (a) Plan View; (b) Elevation

4.2 Dome Geometry

The geometry of the dome (Fig. 4.2(a)), which is characteristic of Triax (Neal, 1973) and Varax (Eshelby and Evans, 1988) domes, is obtained by projecting a plane network of equilateral triangles onto the spherical surface of the dome. The projection is defined by rays that originate at the center of the sphere. Thus, all members lie in great circle planes and have the same radius of curvature. The dome is cyclically symmetric and is composed of six identical sectors. One of these sectors is shown in Figure 4.2(b). The dome has a span of 133 ft (40.5 m), a rise of 18 ft (5.5 m), and a radius of 133.3 ft (40.6 m) and rests on a steel tension ring. The dome is composed of 132 southern pine glulam beams. The dimensions of the members are as follows (Fig. 4.2(b)):

Main Beam I:	6.75 x 11.0 in (17.1 x 27.9 cm)
Main Beam II:	5.0 x 11.0 in (12.7 x 27.9 cm)
Base Beam:	3.0 x 12.25 in (7.6 x 31.1 cm)
Purlin:	3.0 x 8.25 in (7.6 x 21.0 cm)
Tension Ring:	1.0 x 12.0 in (2.5 x 30.5 cm)

The differences in the design of the steel hub connector are the main difference between the Varax and Triax Domes (Fig. 4.3). The Varax joint has flexural stiffness (Eshelby and Evans, 1988). The Triax joint transmits only compressive forces and is considered as a pin joint.

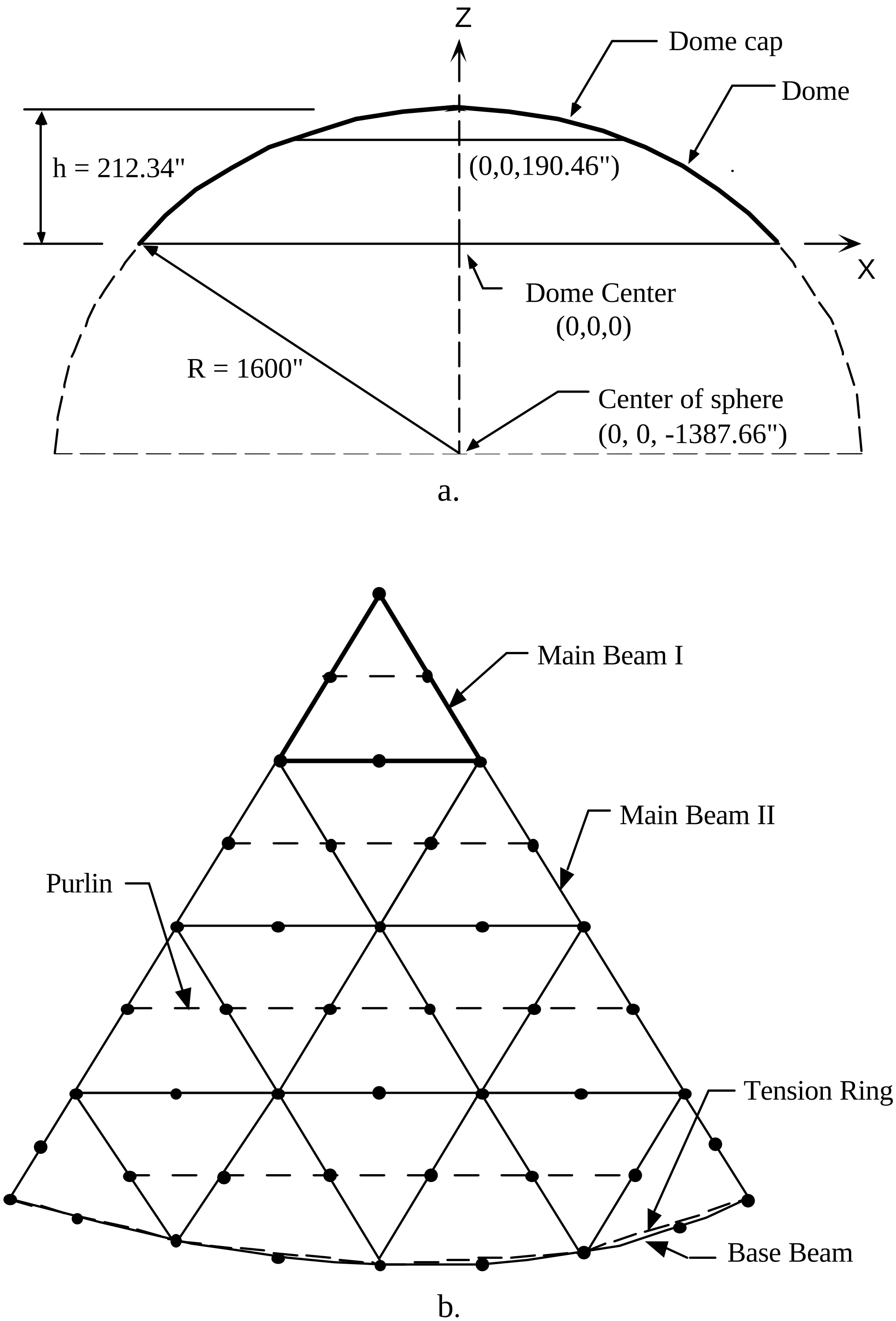

Figure 4.2 (a) Dome Geometry; (b) Dome Sector

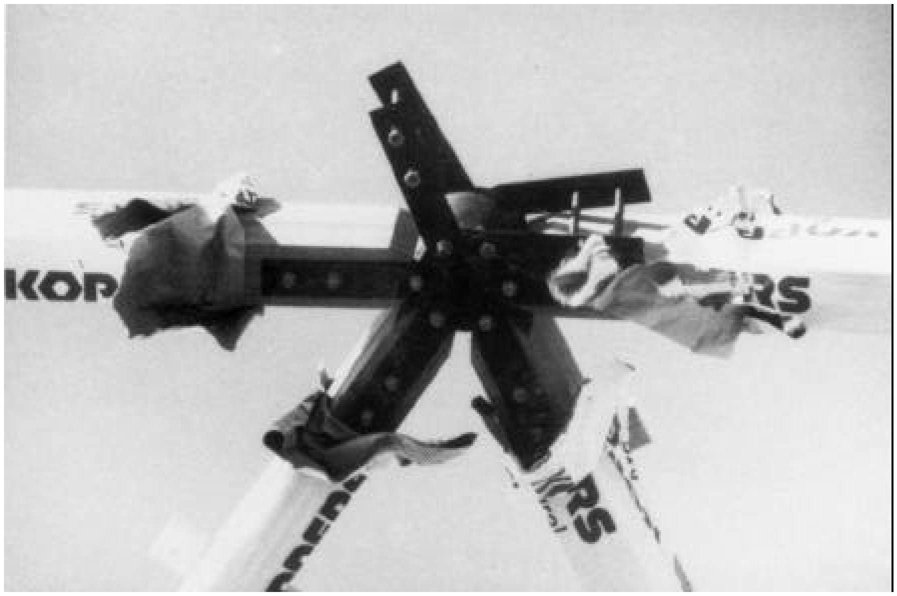

a.

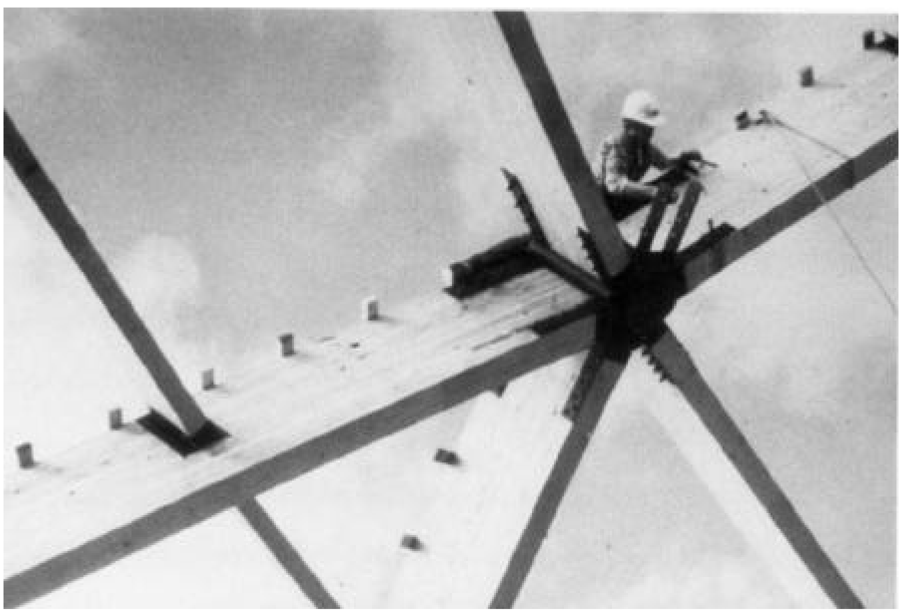

b.

Figure 4.3 Dome Joints: (a) Triax, (b) Varax

4.3 Finite Element Modeling

The dome model has undergone many improvements since it was first developed by Davalos in 1989. The dome models with various features have been constructed and evaluated to represent the behavior of the glulam dome (Holzer, et al., 1992; Holzer and Tongtoe, 1995). These features include structural members, material properties, decking, joints, design loads, load combinations, load discretization, torsion, and boundary conditions.

4.3.1 Structural Members

Davalos (1989) modeled each beam of the dome with two curved, isoparametric, 3-noded beam elements. The beam element is based on the Timoshenko beam theory which includes shear deformation. ABAQUS designates these elements as B32 elements, where B stands for beam, 3 for space, and 2 for quadratic interpolation. Wu (1991) modeled each beam of the dome with two straight, three-dimensional, Bernoulli/Euler, beam finite elements (B33). The B33 beams have cubic interpolation. Straight finite elements (B33) have two nodes, whereas curved Timoshenko elements (B32) have three nodes. Using B33 beam elements greatly reduces the number of nodes in the assembly. The radius of curvature of each beam is sufficiently large to permit each beam to be modeled with straight elements. Wu (1991) concluded that the choice of the beam finite element is not crucial in the construction of the dome model.

The curved purlins are used to support a tongue-and-groove decking of the dome. The purlins are attached to the glulam beams with steel hangers. The purlins are modeled with 108 straight truss elements (Davalos 1989).

The main function of the tension ring of the dome is to carry the induced tensile force along the base of the dome. The tension ring is modeled with 24 straight truss elements, with each element spanning between two consecutive supports (Davalos, 1989).

4.3.2 Material Properties

Although wood is an inhomogeneous, anisotropic, and highly variable material, fabrication standards for glulam beams allow one to select a single longitudinal modulus (E) and a single shear modulus (G). The glulam beams are considered to be continuous, homogeneous, and transversely isotropic. The assumption of transverse isotropy was supported by an experimental study of southern pine glulam beams (Davalos et al., 1991). Moreover, torsion tests on glulam samples have verified the assumption of transverse isotropy. Davalos (1989) analyzed the dome using a linear material law. The glulam beams are classified as E-rated southern pine (NDS, 1991) and accordingly the longitudinal elastic modulus is taken as E = 1,800,000 psi (12,400 MPa). The shear modulus isobtained from torsion tests of small glulam samples (Davalos, 1989): G = 160,000 psi (1,100 MPa).

The material properties used for the southern pine glulam beams and purlins are defined in Fig. 4.4. Three stress-strain relations are used: linear, bilinear, and nonlinear (Conners, 1989). In the linear material law, the initial elastic moduli for tension and compression are taken as E_t = 1,800,000 psi (12,400 MPa). The nonlinear normal stress-strain relation is based on a constitutive model developed by Conners (1989) with segmented strain-stress curves (Fig. 4.4). The bilinear relation is used to match the initial moduli E_t and E_c of Conners' nonlinear model. Parallel to grain stresses for linear and nonlinear material laws are tabulated in Table 4.1. Telang (1992) and Kavi (1993) incorporated the nonlinear material law in the analyses of the dome model. In the nonlinear material law, the initial elastic moduli for tension and compression are taken as E_t = 1,800,000 psi (12,400 MPa) and Ec = 2,2000,000 psi (15,200 MPa). The shear modulus of G = 160,000 psi (1,100 MPa) is used.

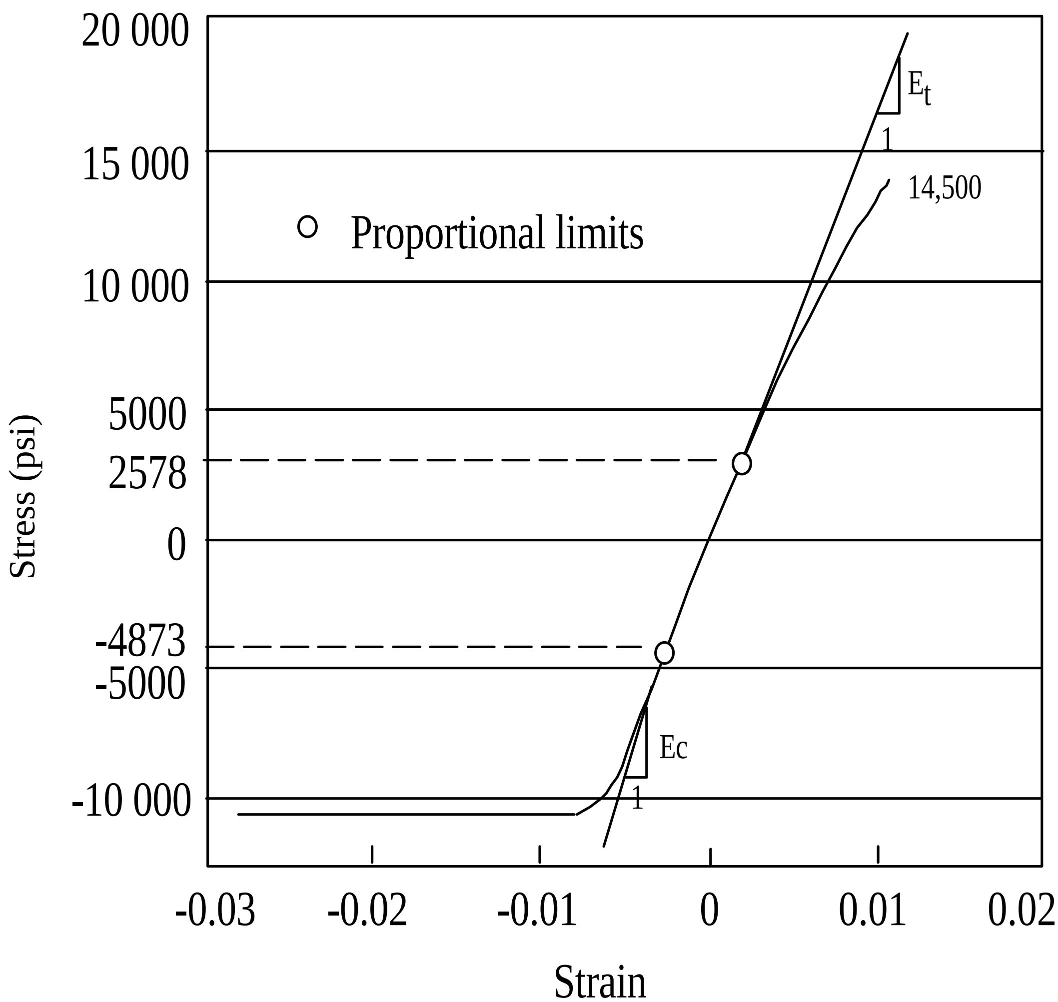

Figure 4.4 Nonlinear Material Law for Wood: G = 1.6 x 10^5 psi (1,100 MPa), E_t = 1.8 x 10^6 psi (12,400 MPa), E_c = 2.2 x 10^6 psi (15,200 MPa)

Table 4.1 Parallel to Grain Stresses for Linear and Nonlinear Material Laws

Material law	Proportional Limit Compression (psi)	Proportional Limit Tension (psi)	Ultimate Compression Stress (psi)	Ultimate Tensile Stress (psi)
Linear (Wood Handbook, 1987)	5900	8790	8500	14500
Nonlinear (Conners, 1989)	4873	2578	10496	14500

4.3.3 Modeling of Decking

The dome is covered with a 2" tongue-and-groove wood decking joined to the glulam beams and purlins with nails. Davalos (1989) did not include the effect of the decking in the dome model. Wu (1991) and Telang (1992) added a truss bracing system to model the effect of the decking. This truss bracing system consisted of a network of two-node truss elements which was connected to the glulam beams at the nodes. However, the truss bracing system does not simulate the closely spaced nail connections. Tsang (1992) introduced the beam-decking connector element model to simulate the effect of the decking to a dome cap model. When a nailed joint is subjected to a lateral load, the resulting load versus slip relationship is shown in Fig. 4.5 (Kavi 1993 and Gutshall 1994). The beam-decking connector element is an element composed of springs to represent the nails. The elongation of each spring is determined through interpolation functions from the nodal displacements of the beam elements. Therefore, the introduction of the beam-decking connector elements does not add degrees of freedom to the assembly. This modeling technique is widely used for connectors in timber structures (Dolan, 1989). The beam-decking connector elements used by Tsang (1992) were based on a linear load-deflection relationship for the springs. Kavi (1993) developed a nonlinear beam-decking connector elements. The connector elements includes 16 nonlinear springs that provide the lateral support for the glulam beam. The load-deformation curve for one nail is shown in Fig. 4.6.

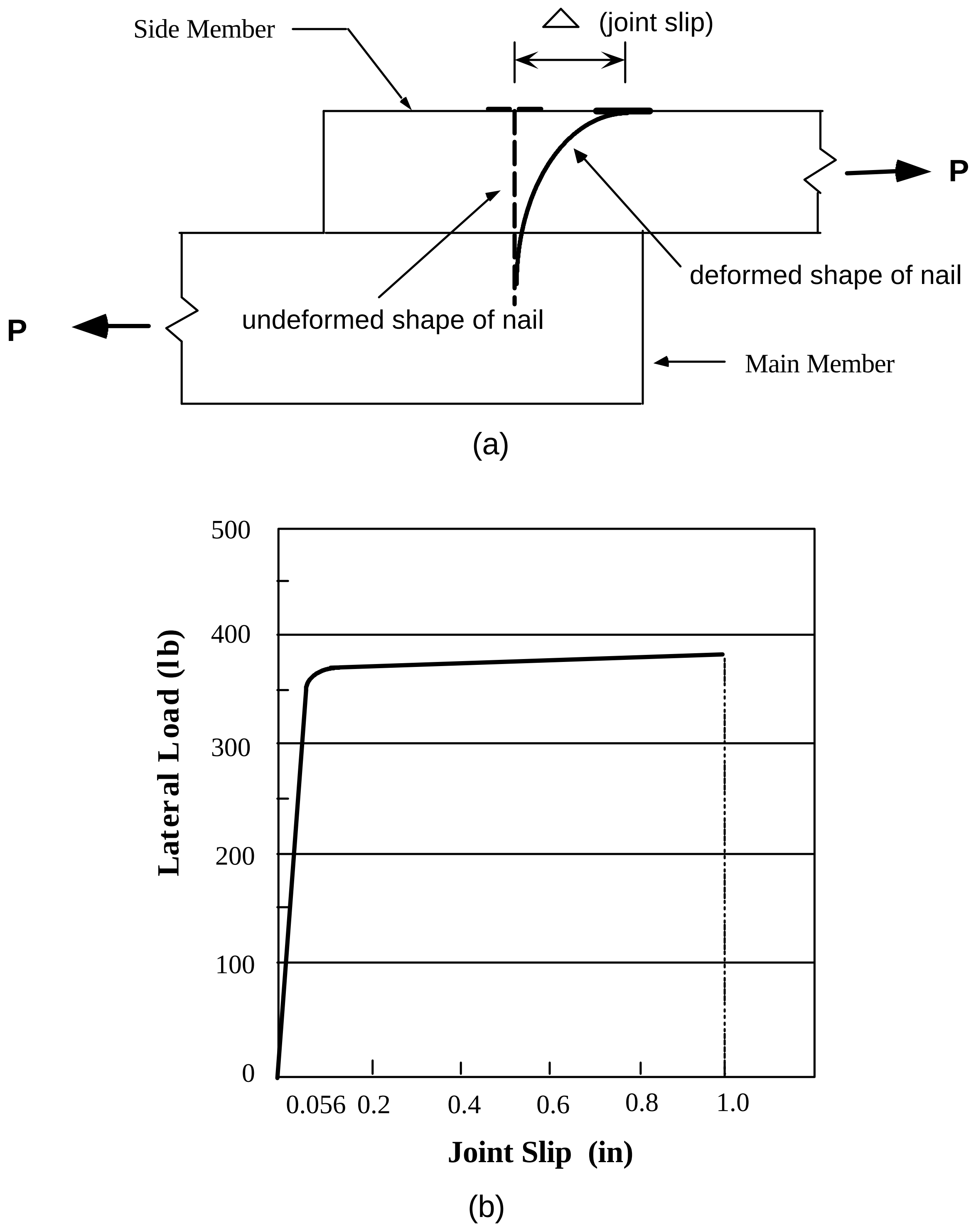

Figure 4.5 Load and Slip in Joint: (a) Joint Slip of Nailed Joint; (b) Load-Slip Curve

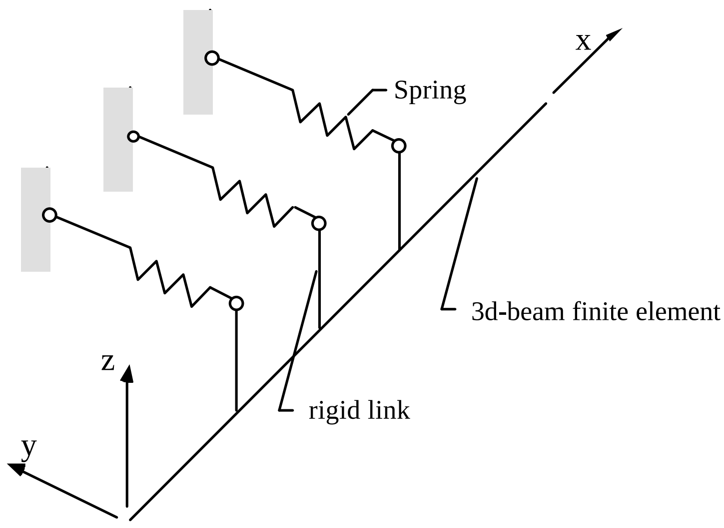

(a)

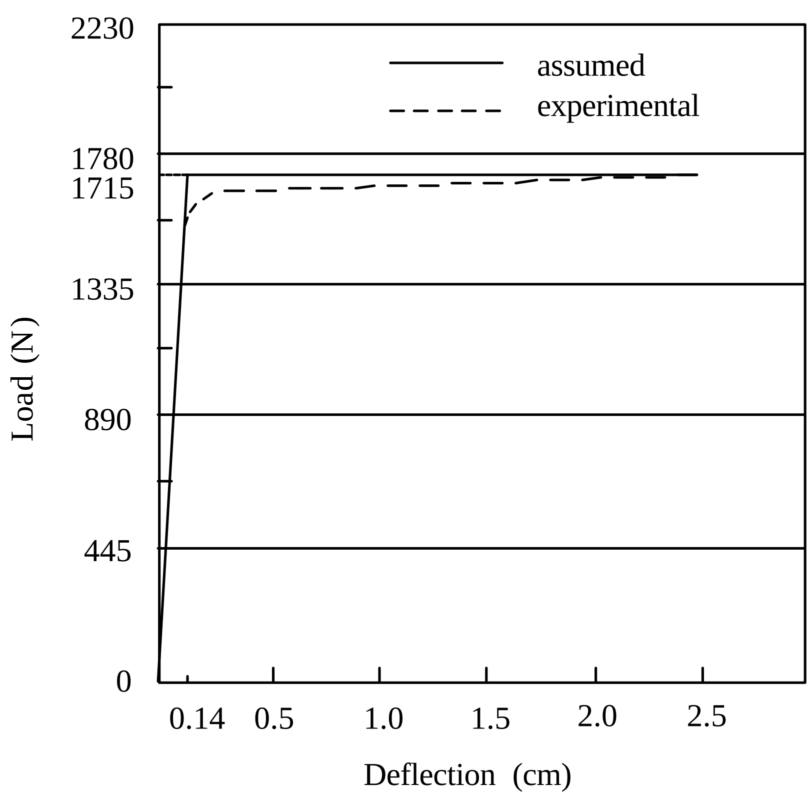

(b)

Figure 4.6 Beam-Decking Connector: (a). Connector Element; (b). Load-Slip Curve for One Nail

4.3.4 Joint Flexibility

Davalos (1989) investigated the effect of joint stiffness on the stability of the dome model. He used a six inch long, two-node, isoparametric beam (isobeam) element to model the beam-to-beam and purlin-to-beam connection. He modeled each joint with six of these connector elements joined at a common node (Davalos, 1989). He concluded that the effect of joint flexibility is significant. However, he did not include the effect of the decking on the dome model.

Wu (1991) conducted a study of the effect of joint flexibility on the dome model which used a bracing of truss elements to model the decking. He concluded that the effect of joint flexibility is not significant. However, the bracing of truss elements did not have any physical connection to the actual dome.

Kavi (1993) studied the effect of joint flexibility on a dome cap model which used beam-decking connector elements to model the decking. He concluded that the effect of joint flexibility was insignificant. However, the dome cap model does not accurately represent the behavior of the entire dome.

In this study, the effect of joint flexibility is investigated on a full dome model with beam-decking connector elements.

4.3.5 Design Loads

Design loads considered for lattice domes include dead, live, snow, wind, and seismic loads (AITC, 1985).

- **Dead Load**

The dead load pressure is obtained as follows :

Beams and purlins	2 psf
Tongue-and-groove decking	5 psf
Connectors, roofing, insulation	9 psf
Total dead load	16 psf

- **Live Load**

Live loads are those loads produced by the use and occupancy of the structure and do not include wind, snow, and earthquake loads (ASCE, 1994). The live load for the Triax dome is 20 psf which accounts for the weight imposed over the structure during construction, roofing and reroofing, and firemen and equipment (ANSI A58.1-1982, Section 4.10).

- **Snow Load**

Roof snow loads can be obtained from ground snow loads with adjustment of roof geometry and wind exposure (AITC, 1985 and ANSI A58.1-82). The snow load of 20 psf is applied over the horizontal projection of the dome model (Davalos, 1989).

- **Wind Load**

The wind load for the dome model is determined from the European Convention for Constructional Steelwork (ECCS, 1978) guidelines in conjunction with the basic wind speed given in ANSI A.58.1-82. The pressure distribution over the dome is shown in Fig. 4.7 (Wu, 1991). The ECCS specifies pressure values at three points along the midsection of the dome model in the wind direction. The values between these points can be obtained by linear interpolation.

- **Seismic Load**

Structures located in areas subject to earthquakes must be designed and constructed to resist lateral force produced by earthquake ground motions. Most building codes specify a set of lateral forces to be applied to the structures. The seismic load case of Tacoma dome, a Triax dome, (Eshelby and Evans, 1988) and the Church of the Nazarene dome, a Varax dome, (Varax Engineering Company, 1986) was not critical. The seismic load case is not considered in this study.

4.3.6 Load Combinations

The following load combinations are suggested in the analysis of glulam domes (Varax):

1. Combined dead and live loads over the entire dome
2. Combined dead load and live load over half of the dome terminating on sector lines
3. Combined dead load and live load over half of the dome terminating on sector center lines
4. Combined dead load and live load over the inner half of the dome
5. Combined dead load and live load over the outer half of the dome

6. Combined dead load and wind load
7. Combined dead load, wind load, and live load over half of the dome terminating on sector lines
8. Combined dead load, wind load, and live load over half of the dome terminating on sector center lines
9. Snow concentrations and special hanging loads.

The dome model has been analyzed for several load combinations (Davalos, 1989). Wu (1991) analyzed the effect of wind load over the dome model as shown in Fig. 4.7 and concluded that wind load is not critical. This is due to the fact that wind load results in suctions over the dome model acting in the opposite directions of dead and live loads.

The critical load combinations consist of dead and snow loads (Davalos, 1989). The pressure load composed of two independent load distributions

$$p = p_D + \lambda p_L \tag{4.1}$$

where p_D = 16 psf (766 Pa) is the design dead load pressure, p_L = 20 psf (958 Pa) is the live load pressure resulting from snow load, and λ is the proportionality factor of the live load, the load parameter.

Two load combinations (1 and 2) are considered in the analyses of the current dome model. The first load combination is composed of dead load and uniformly distributed snow load over the entire dome. The second load combination is composed of dead load and uniformly distributed snow load over half of the dome terminating on sector lines as shown in Fig. 4.8.

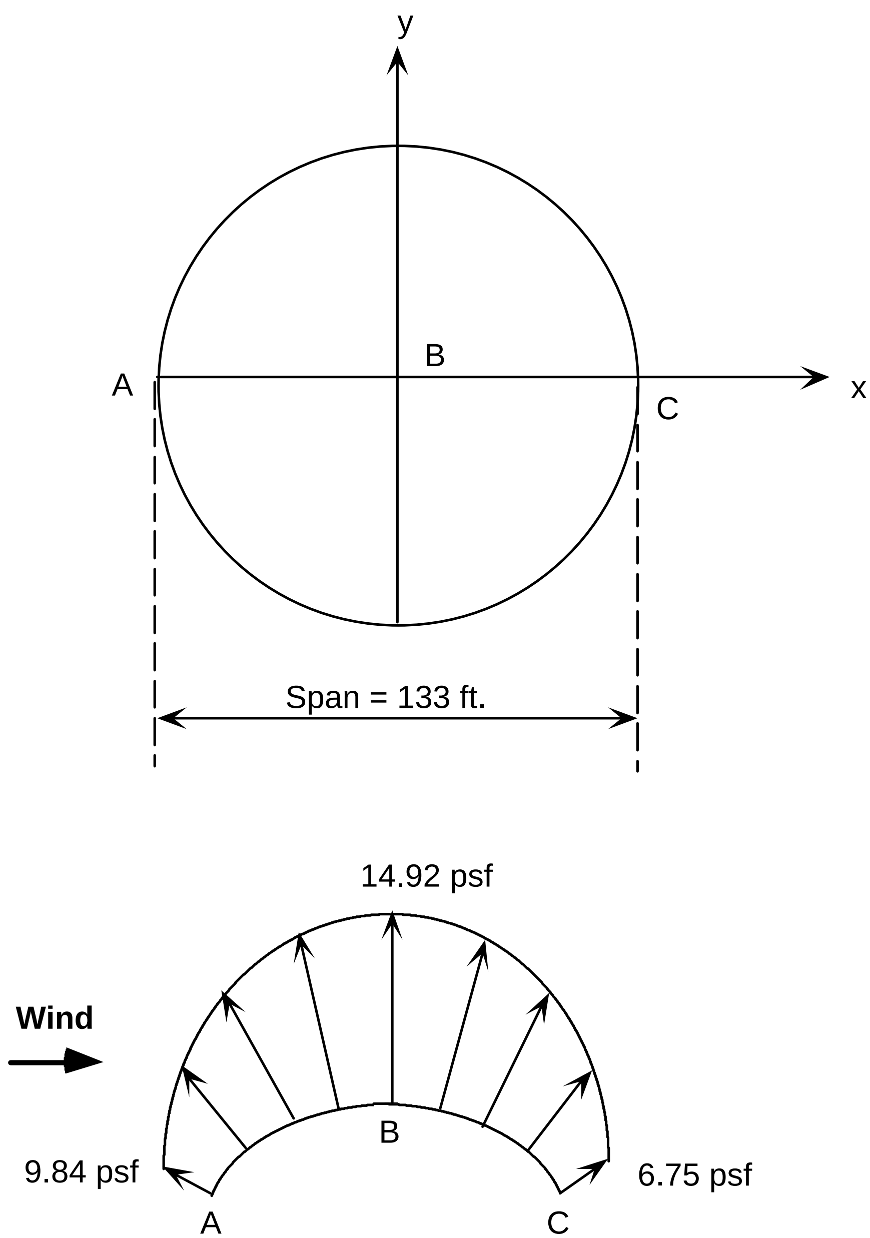

Figure 4.7 Wind Load Distribution from ECCS for the Dome Model

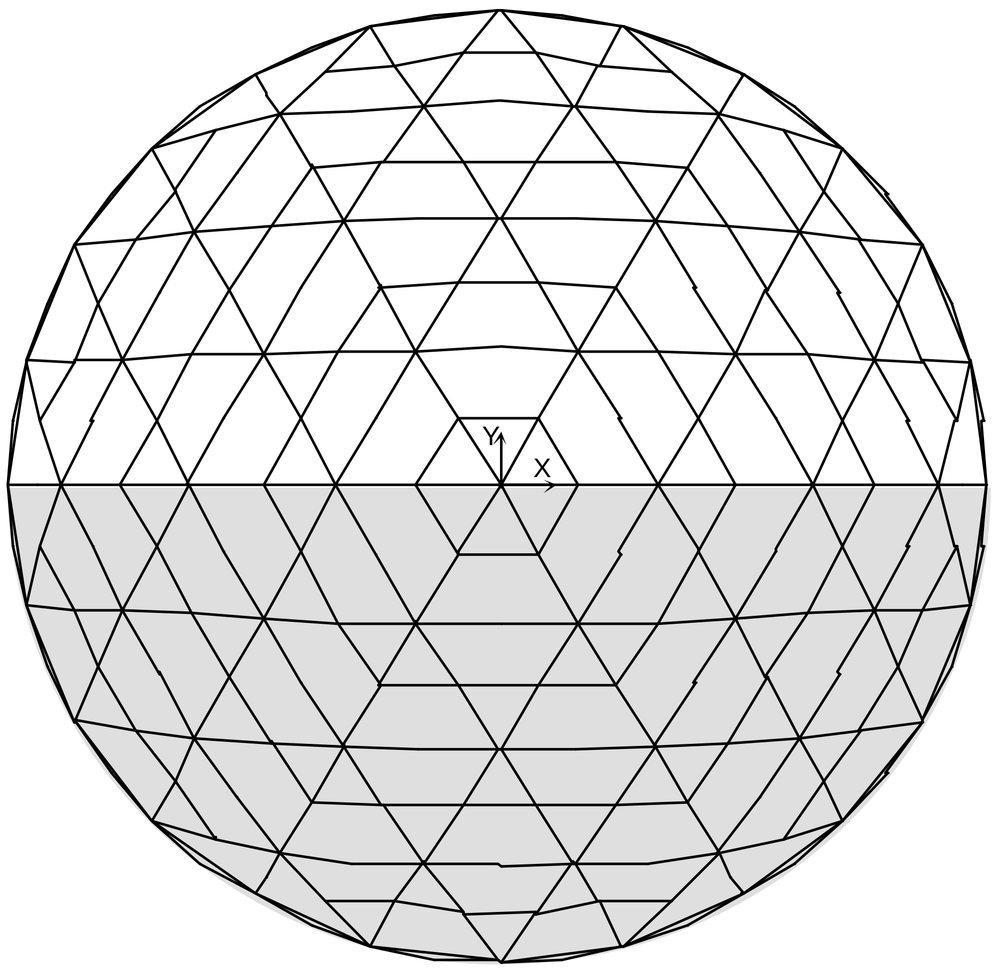

Figure 4.8 Snow Load over Half of the Dome

4.3.7 Load Discretization

There are two procedures used to transform the pressures on the decking into nodal forces applied at the beams (Holzer, et al., 1992). The first procedure is based on the concept of tributary areas (Fig. 4.9 (a)). The load pressures are first transformed from the tributary area on the decking to the beams and purlins, which are then discretized into nodal forces (Davalos, 1989). In the second procedure, the nodal forces of the dome model are generated by using shell elements (Fig. 4.9 (b)) to discretize the load pressures. Since the loading in the stability analyses is proportional, the shell elements are removed once the nodal forces are computed (Holzer et al., 1992). The advantage of the second procedure is that it can be easily implemented for a variety of load distributions and directions.

4.3.8 Torsion

Kavi (1993) incorporated Saint-Venant's torsion theory by modifying the value of the shear modulus (G) through a user subroutine. He concluded that warping has a significant effect on the torsional stiffness of beams with noncircular cross sections. In the current version of ABAQUS (V.5.5) warping can be modeled directly.

4.3.9 Boundary Conditions

Boundary constraints must be applied to remove the rigid body motion of the dome, but at the same time must allow for the steel tension ring to move freely in the radial direction (Davalos 1989). All the perimeter nodes are constrained in the Z-direction to eliminate the vertical rigid body motion. To remove the rigid body rotation of the dome about the Z-axis and the rigid body translation in the X- and Y-directions, constraints are applied at four radially opposed nodes on the steel tension ring, as shown in Figure 4.10.

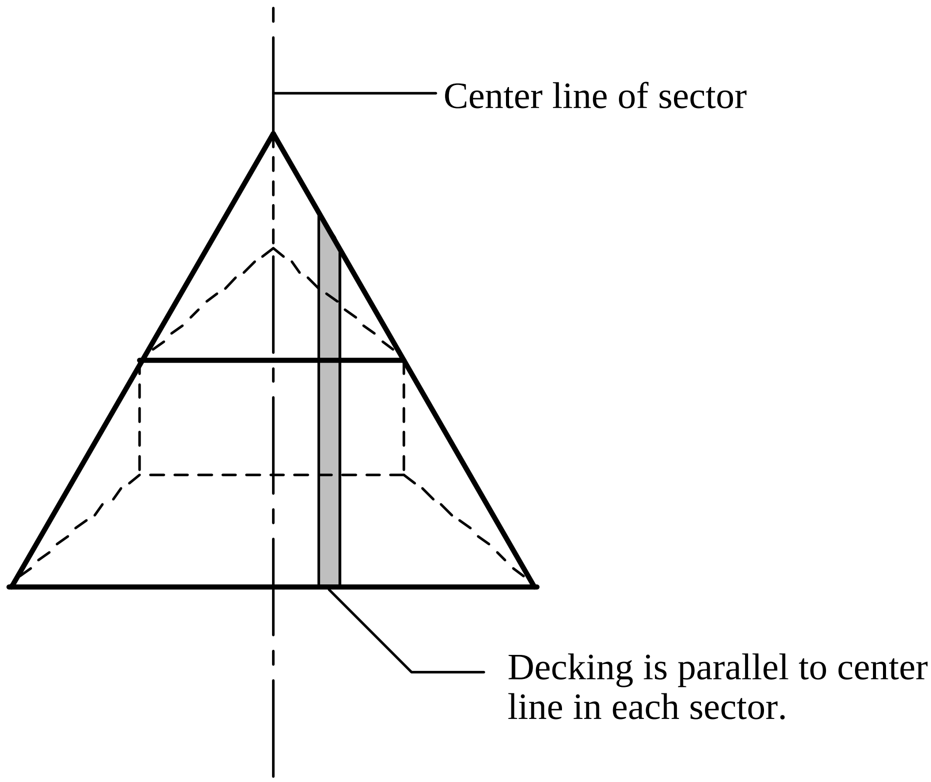

a.

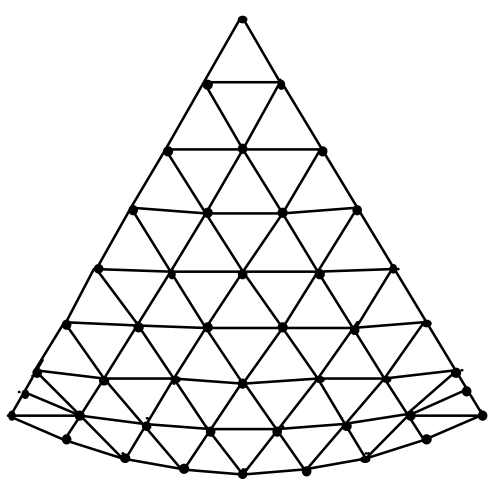

b.

Figure 4.9 (a). Load Tributary Area of One Panel ; (b). Shell Elements for One Sector

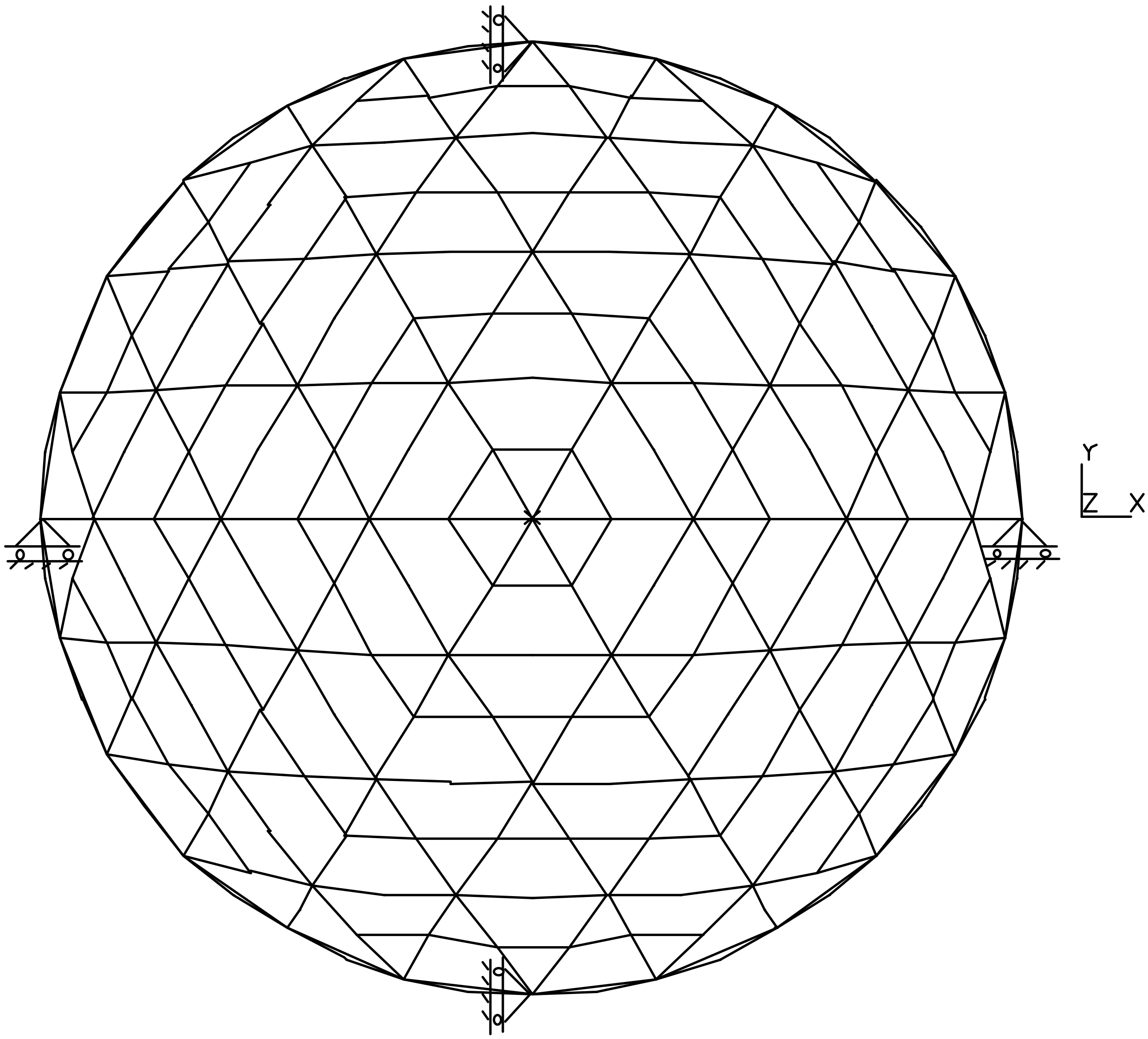

Figure 4.10 Dome Model with Restraints at Four Radially Opposed Nodes

4.4 Nonlinear Analysis

The objective of the finite element stability analysis is to compute the critical load pressure

$$p_{cr} = p_D + \lambda_{cr} p_L \tag{4.2}$$

and to predict the corresponding failure mode. Two methods have been used in the analysis of the dome. The following description of these methods of analysis are taken from Holzer and Tongtoe (1995):

(1) The nonlinear equilibrium path is traced with the Riks method. The first critical point, a bifurcation or limit point, is detected by the appearance of a zero or negative eigenvalue of the tangent stiffness matrix;

(2) the Riks method is combined with a linear eigenvalue analysis. This combined analysis is used to predict the critical load parameter,

$$^{b}\lambda_{cr} = {}^{b}\lambda + \Delta\lambda_{cr} \tag{4.3}$$

where $^{b}\lambda$ defines the base load

$$^{b}p = p_D + {}^{b}\lambda p_L \tag{4.4}$$

for which the eigenvalue analysis is performed, and $\Delta\lambda_{cr}$ is the smallest eigenvalue.

The relation between the two analysis procedures is shown in Figure 4.11. The 45^{o} line, $\lambda = {}^{b}\lambda$, passes through the critical point B, where $\lambda = {}^{b}\lambda = \lambda_{cr}$, which is computed with the Riks method. Alternatively, the critical point can be approached along the critical load prediction curve (also

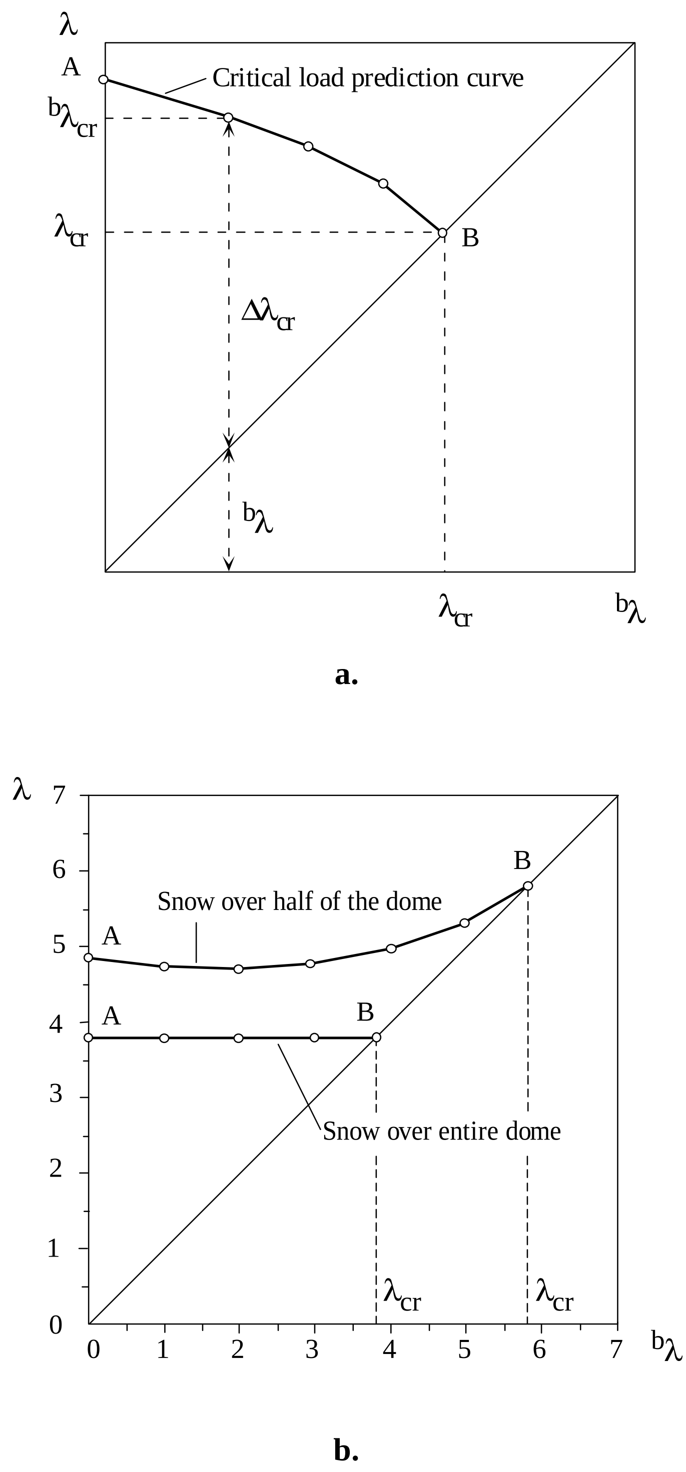

Figure 4.11 (a) Critical Load Parameters; (b) Critical Load Prediction Curves

called the eigenvalue curve (Brendel and Ramm, 1980)), resulting from a combined analysis. This curve can be determined by selecting increasing values for ${}^{b}\lambda$ and computing the corresponding eigenvalues $\Delta\lambda_{cr}$. In some cases the initial point A, ${}^{b}\lambda = 0$, provides a sufficiently accurate prediction for the critical load parameter. However, without further analysis, one cannot tell whether this value is conservative or unconservative (Cook et al., 1989).

The critical load prediction curves of the dome model with snow over the entire dome and snow over half of the dome are shown in Figure 4.11b (Holzer and Tongtoe, 1995). The analysis is based on a dome model that includes curved Timoshenko beam elements with rigid joints and geometric nonlinearity, but no decking.

4.5 Results

The results are concerned with buckling pressures, buckling modes, the effects of joint stiffness, decking models, and material laws on the stability of the dome. The finite element model of the dome consists of Bernoulli/Euler beam elements, rigid joints, geometric and material nonlinearities, and three representations of the decking: (1) no decking, (2) truss bracings, and (3) beam-decking connector elements. Three material laws are considered: linear, bilinear, and nonlinear (Conners, 1989). The results from analyses for various loading conditions, decking models, and material laws are shown in the context of Table 4.2. Maximum stresses and displacements are also closely monitored on one sector of the dome (Fig. 4.12).

Table 4.2 Critical pressure: $p_{cr} = p_D + \lambda_{cr} p_L$

Material law	Decking model	Critical load parameter, λ_{cr}	
		Full snow	Half snow
Linear	none	3.6	5.3
	truss bracing	9.3	7.2
	B-D connectors	8.5	7.6
Bilinear	none	4.4	6.5
	truss bracing	10.3	8.6
	B-D connectors	9.0	8.9
Nonlinear	none	4.4	5.3
	truss bracing	9.9	6.8
	B-D connectors	9.0	7.7

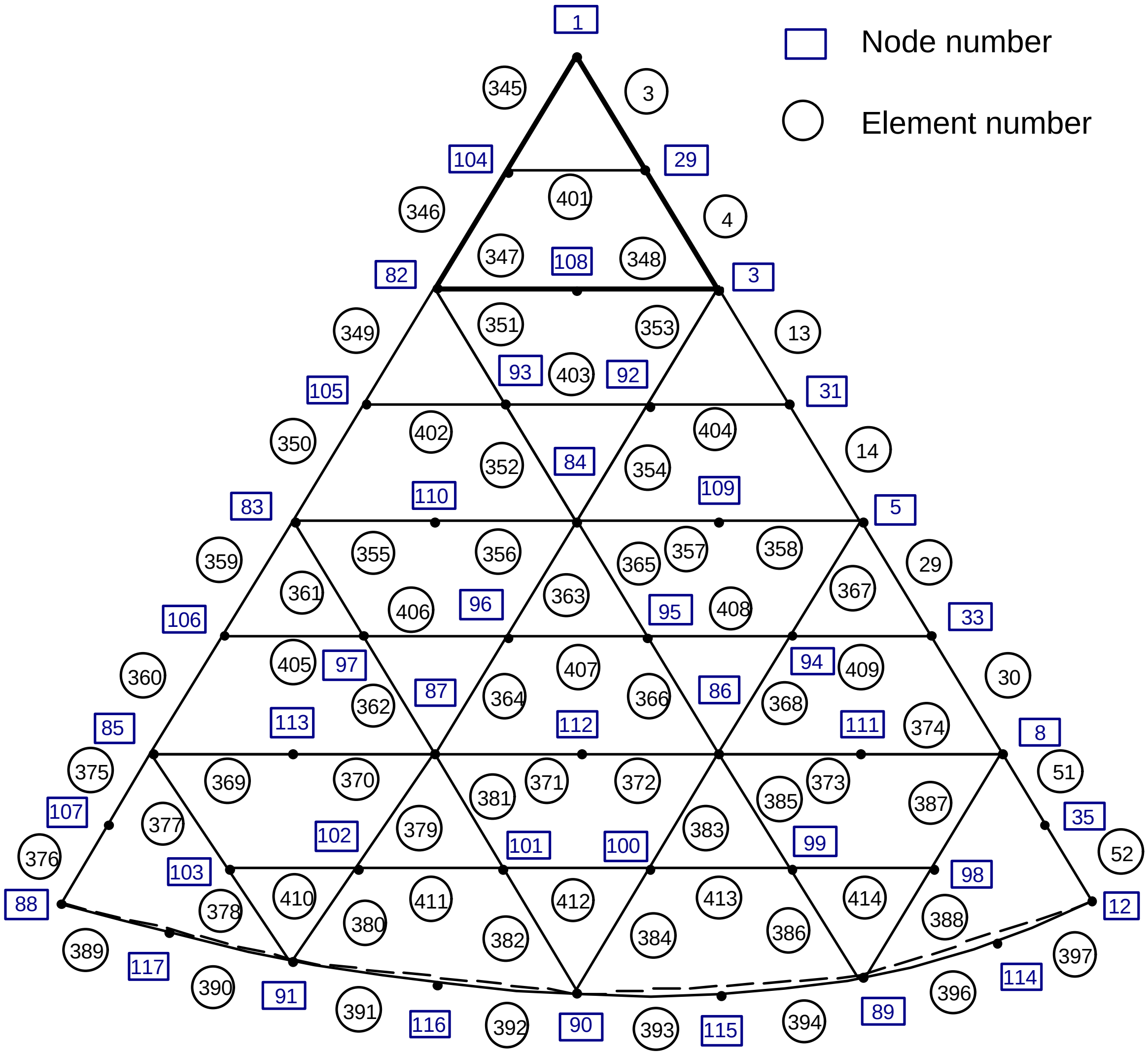

Figure 4.12 Sector of the Dome

4.5.1 Full Snow

The corresponding equilibrium paths at the apex of the dome models with nonlinear material law for various decking models and snow over the entire dome are shown in Fig. 4.13. The maximum stresses in beam elements of the dome models are tabulated in Table 4.3.

In the dome model with no decking, the dome model buckles in the form of twist buckling over the entire dome (Fig. 4.14). The critical snow load pressure increases from 3.6 for the linear material model to 4.4 for the bilinear model. For both bilinear and nonlinear material laws, the critical snow load factor is 4.4, the maximum compressive stress is 3,670 psi, and the maximum tensile stress is 2,070 psi. The maximum vertical deflection of 3.0 in. is located at the apex of the dome. Therefore, the nonlinear material law does not affect the response of the dome.

In the dome model with the truss bracing, the critical points are limit points. The resulting buckling of the dome model is shown in Fig. 4.15. The critical snow load factor is 9.9 (snow load of 198 psf), the maximum compressive stress is 9,760 psi, and the maximum tensile stress is 3,340 psi for nonlinear material law. The maximum vertical deflection of 8.8 in. is located at the apex of the dome and the nodes near the apex.

In the dome model with beam-decking connectors, the buckling mode of the dome model is shown in Fig. 4.16. The critical snow load factor is 9.0 for both bilinear and nonlinear material models. The maximum compressive stress is 7,890 psi, and the maximum tensile stress is 3,010 psi. The connectors cause the critical load parameter, λ_{cr}, to increase from 4.4 to 9.0. Material nonlinearity is not a factor for the dome model with snow load over the entire dome. Just before the critical point, a limit point, is reached, two thirds of the connectors of some beam finite elements are already disconnected as shown in Table 4.4. Maximum stresses of a dome sector just before buckling are shown in Fig. 4.17. The maximum vertical deflection of 8.8 in. is located at the apex of the dome and the nodes near the apex.

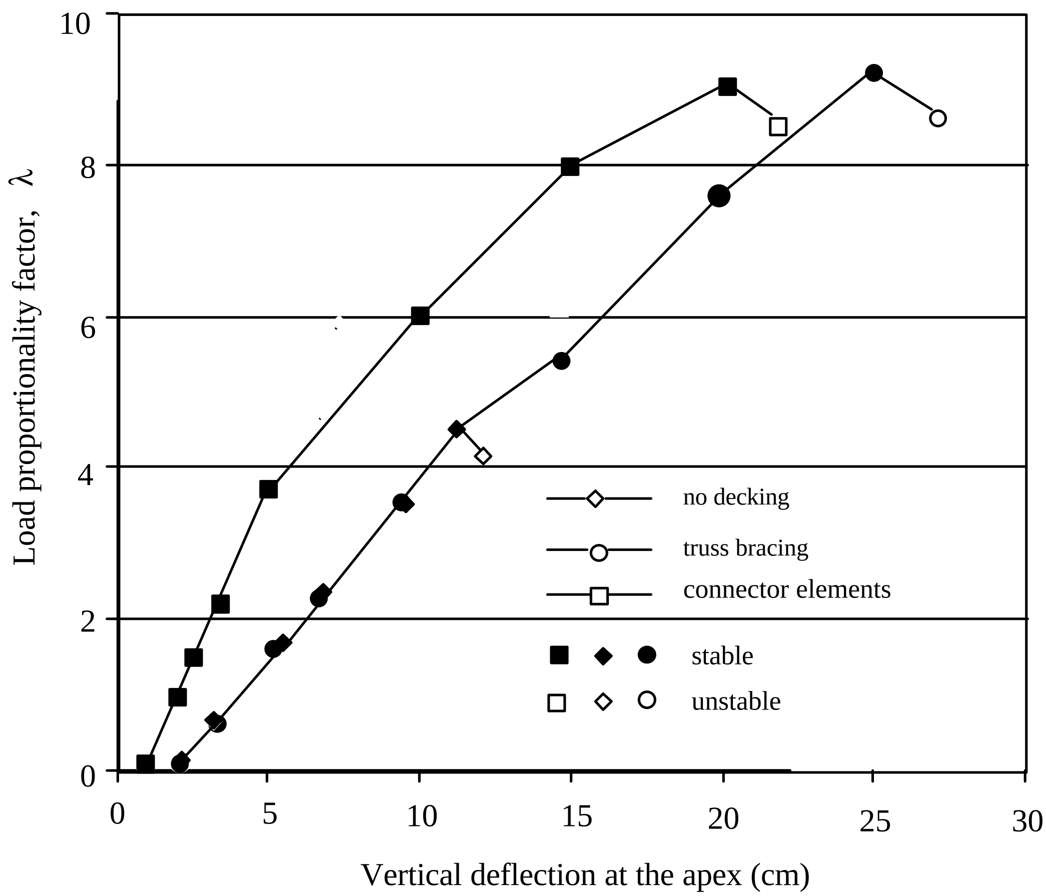

Figure 4.13 Load-Deflection Paths for Various Dome Models, Full Snow Load

Table 4.3 Stresses in the beam elements and nail deflections at critical pressures: Full Snow

Material law	Decking model	Max. tension (psi)	Max. compression (psi)	Max. nail deflection (in.)
Linear	none	2,205 (el. 369 & 374)	-3,444 (el. 51 & 375)	-
	truss bracing	2,216 (el. 369 & 374)	-6,818 (el. 51 & 375)	-
	B-D connectors	3,605 (el. 369 & 374)	-8,819 (el. 30 & 360)	2.73
Bilinear	none	2,068 (el. 369 & 374)	-3,667 (el. 51 & 375)	-
	truss bracing	3,319 (el. 369 & 374)	-11,056 (el. 51 & 375)	-
	B-D connectors	3,252 (el. 14 & 350)	-8,465 (el. 30 & 360)	2.25
Nonlinear	none	2,068 (el. 369 & 374)	-3,667 (el. 51 & 375)	-
	truss bracing	3,343 (el. 369 & 374)	-9,760 (el. 51 & 375)	-
	B-D connectors	3,010 (el. 369 & 374)	-7,890 (el. 51 & 375)	2.25

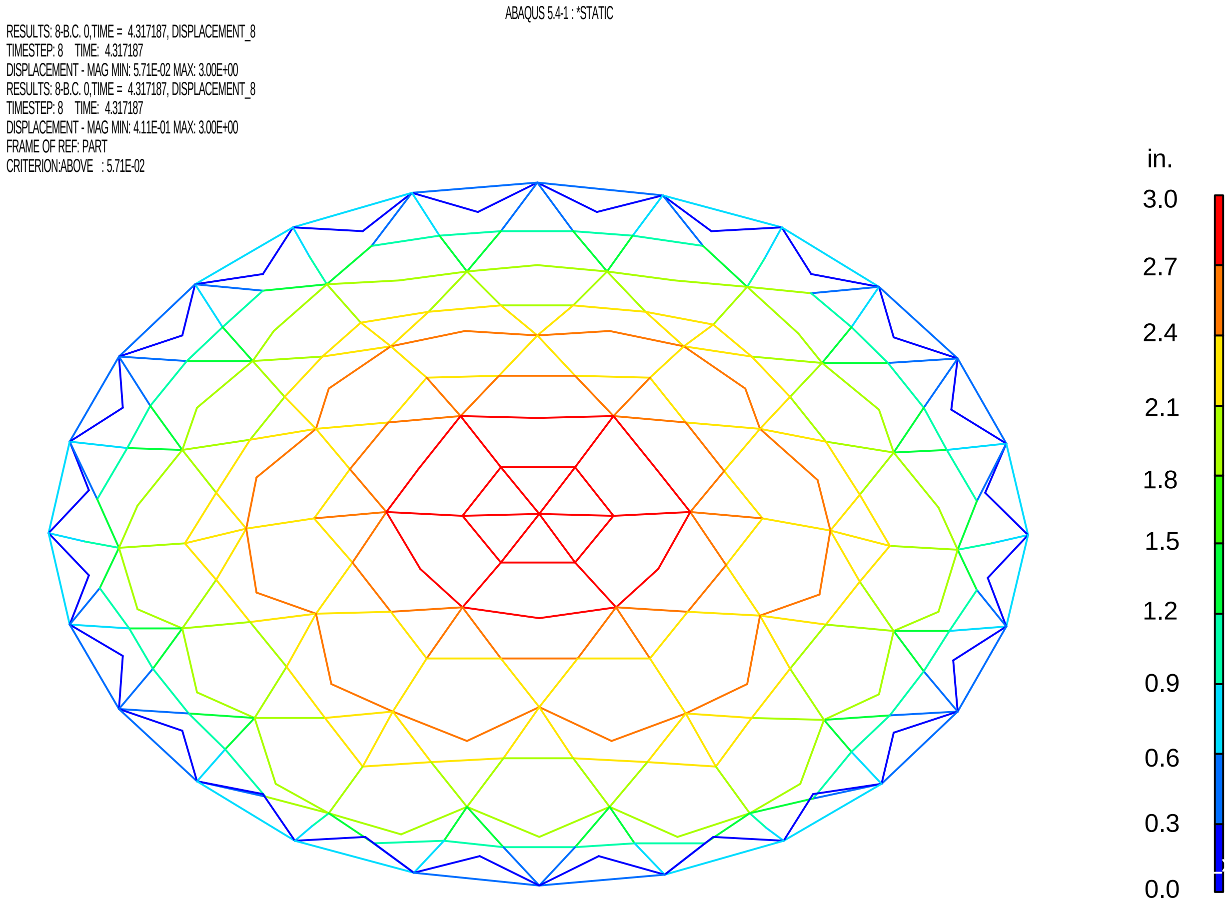

Figure 4.14 Deflection Shape of the Dome Model with no Decking and Snow Load Over Entire Dome just Before Buckling

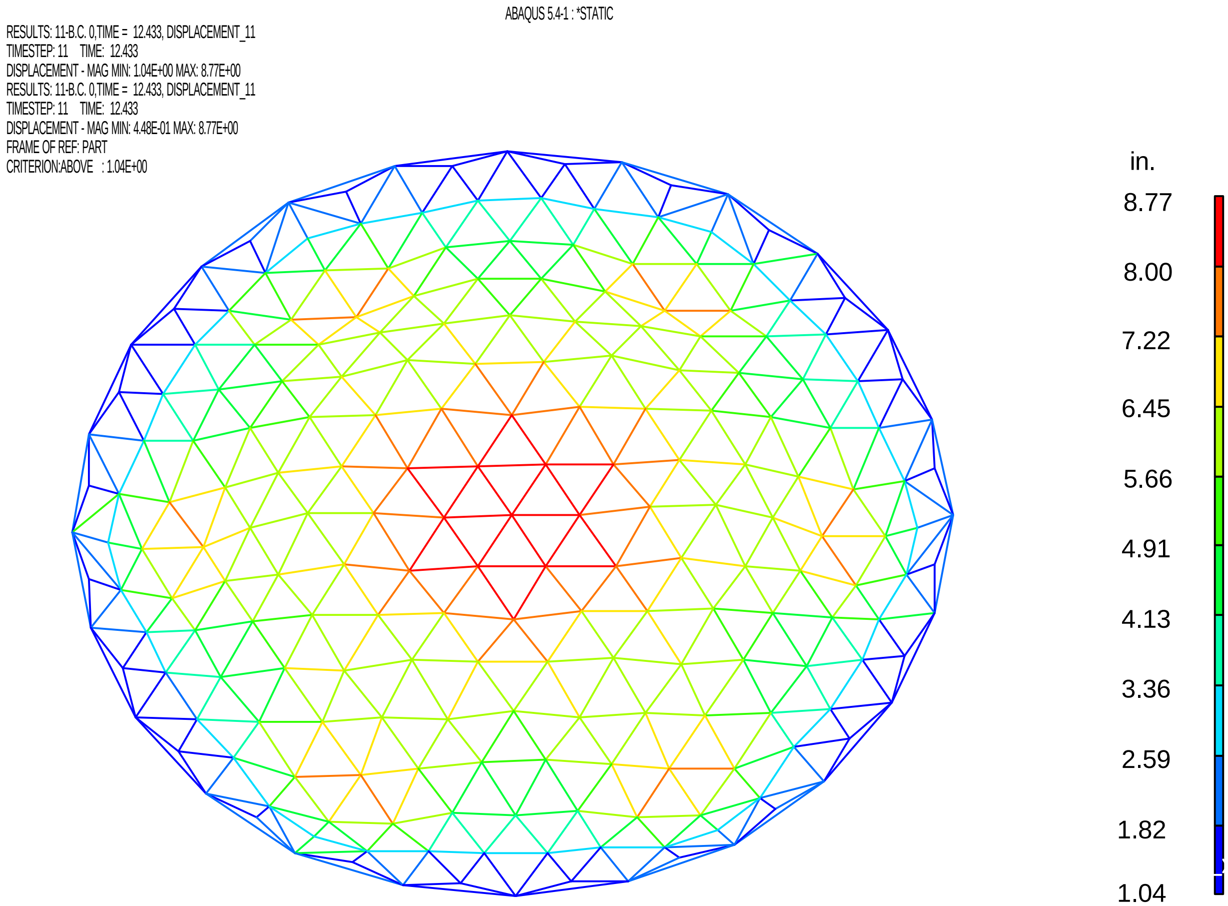

Figure 4.15 Deflection Shape of the Dome Model with Truss Bracing and Snow Load over Entire Dome just Before Buckling

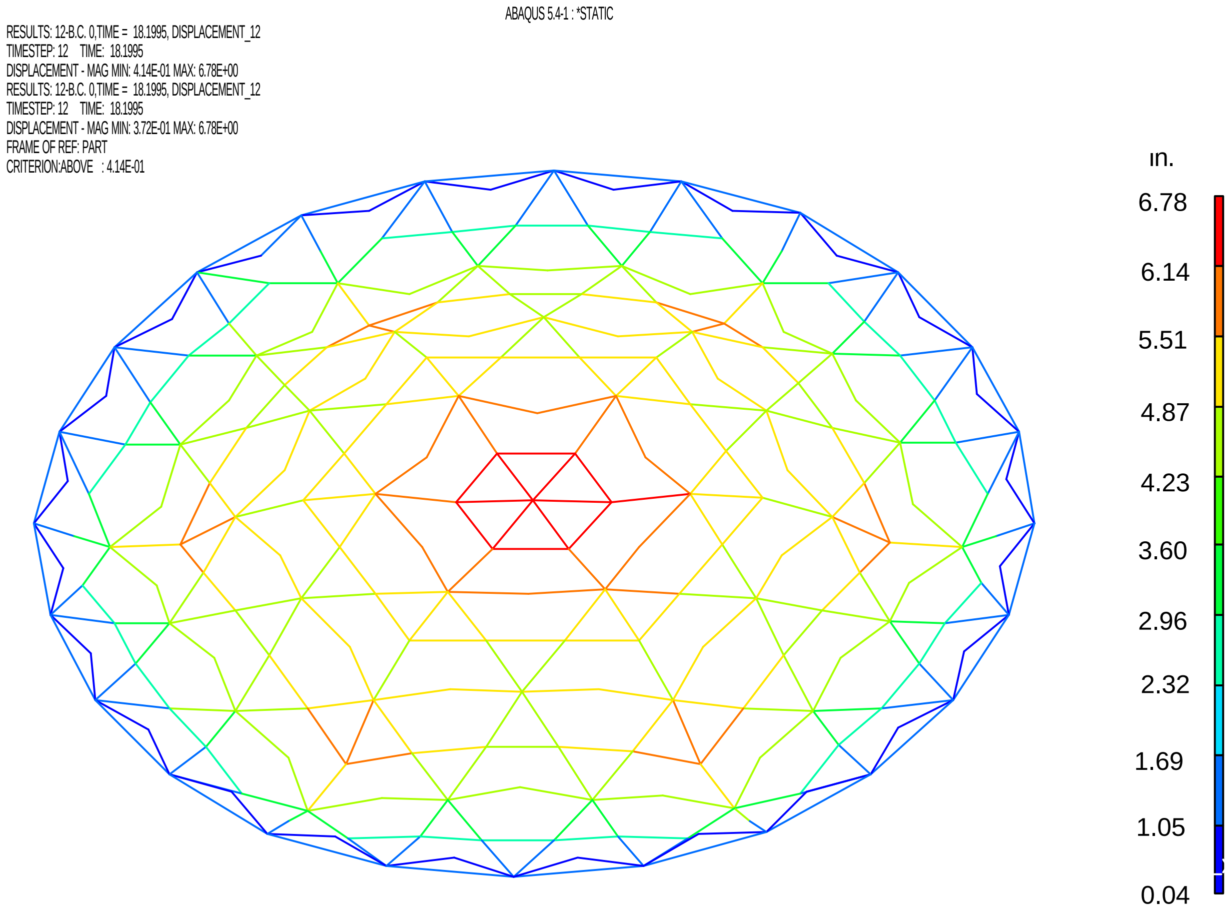

Figure 4.16 Deflection Shape of the Dome Model with Beam-Decking Connector Elements and Snow Load over Entire Dome just Before Buckling

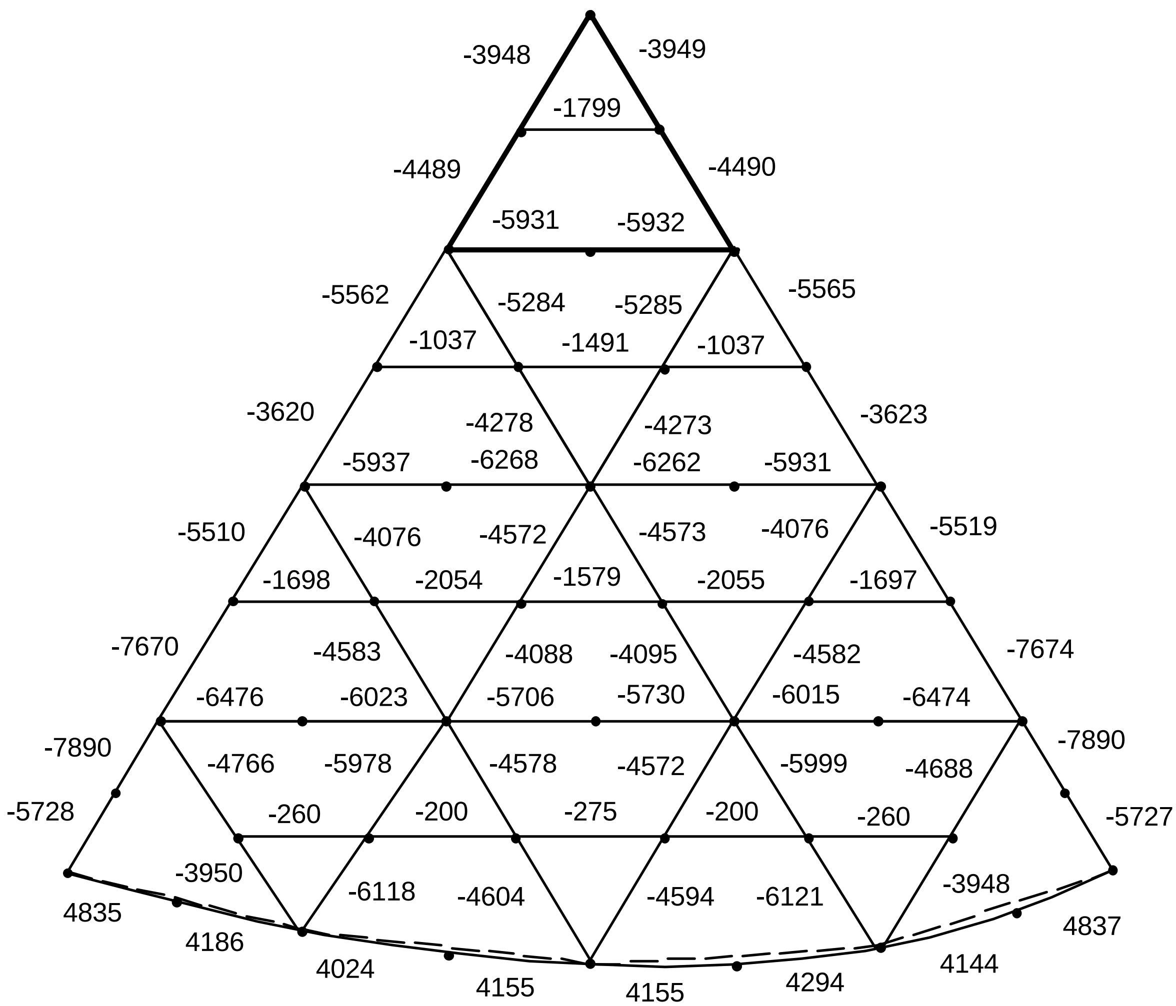

Maximum stress in tension ring: 50,900 psi

Figure 4.17 Maximum Stresses in psi just before Buckling for the Dome Model with B-D Connector Elements, Nonlinear Material, and Snow Load over the Entire Dome

Table 4.4 Nail deflections at critical pressures: Full Snow

Element number	Number of failed nails	Maximum nail deflection (in.)
28	5	1.06
35	8	1.45
36	5	1.33
347	1	1.00
550	4	1.13
859	4	1.04
716	1	1.02
714	1	1.02
718	2	1.07
724	4	1.04
720	4	1.08
722	2	1.03
867	6	1.40
868	7	1.45
220	4	1.13
355	9	1.59
356	7	1.55
357	8	1.59
358	8	1.59

Table 4.4 Nail deflections at critical pressures: Full Snow (Continued)

Element number	Number of failed nails	Maximum nail deflection (in.)
362	6	1.08
363	4	1.05
366	5	1.09
367	3	1.03
369	11	2.25
370	10	2.12
371	10	1.81
374	10	2.25
373	11	2.21
372	9	1.78
732	4	1.13
730	3	1.06
729	2	1.07
728	3	1.08
727	3	1.06
726	1	1.02
725	3	1.13
228	4	1.13
565	3	1.13

4.5.2 Half Snow

The corresponding equilibrium paths at the apex of the dome models with nonlinear material law for various decking models and snow over half of the dome are shown in Fig. 4.18. The maximum stresses in beam elements of the dome models are tabulated in Table 4.5.

In the dome model with no decking, the dome buckles prematurely in a bifurcation mode. The buckling mode indicates a localized pattern in the lower half of the dome where the snow load is applied (Fig. 4.19). For the linear material law, the maximum compressive stress (el. 355 and 358 of Fig. 4.12) exceeds the ultimate compressive stress (Table 4.1) by 43%, while the maximum tensile stress is below the proportional limit. Thus, elastic instability does not determine the critical state for this load condition. The critical snow load pressure increases from 5.3 (snow load of 106 psf) for the linear material model to 6.5 (snow load of 130 psf) for the bilinear model (Table 4.2). The critical snow load factor decreased from 6.5 for the bilinear model to 5.3 (snow load of 106 psf) for the nonlinear material law model. Therefore, nonlinear material does affect the response of the dome model. The maximum compressive stress of the beam elements is 10,250 psi, and the maximum tensile stress is 7,850 psi. Just before the critical pressure is reached, the vertical deflection at the apex of the dome is 2.3 in. and the maximum vertical deflection of 7.4 in. is located at nodes 109 and 110 (Fig. 4.12).

In the dome model with the truss bracing, the buckling mode of the dome model is shown in Fig. 4.20. The critical snow load factor is 6.8 (snow load of 136 psf), the maximum compressive stress is 5,790 psi, and the maximum tensile stress is 3,110 psi for the nonlinear material law. Just before the critical load, a bifurcation point, is reached, the vertical deflection at the apex of the dome is 3.3 in. and the maximum vertical deflection of 6.4 in. is located near the apex at nodes 29 and 104 (Fig. 4.12).

In the dome model with beam-decking connectors, the buckling mode of the dome model is shown in Fig. 4.21. The critical snow load factors are 7.6, 8.9, and 7.7 for linear, bilinear , and nonlinear models, respectively (Table 4.2). The maximum compressive stress is 6,158 psi, and the maximum tensile stress is 3,480 psi for the nonlinear model. The connectors cause the critical load parameter, λ_{cr}, to increase from 5.3 to 7.7 (Table 4.2). Just before the critical pressure, a bifurcation point, is reached, fifteen beam elements have failed connectors and half of the connectors of some beam finite elements are already disconnected as shown in Table 4.6. Maximum stresses of a dome sector just before buckling are shown in Fig. 4.22. The vertical deflection at the apex of the dome is 2.5 in. and the maximum vertical deflection of 6.02 in. is located near the apex at nodes 29 and 104 (Fig. 4.12).

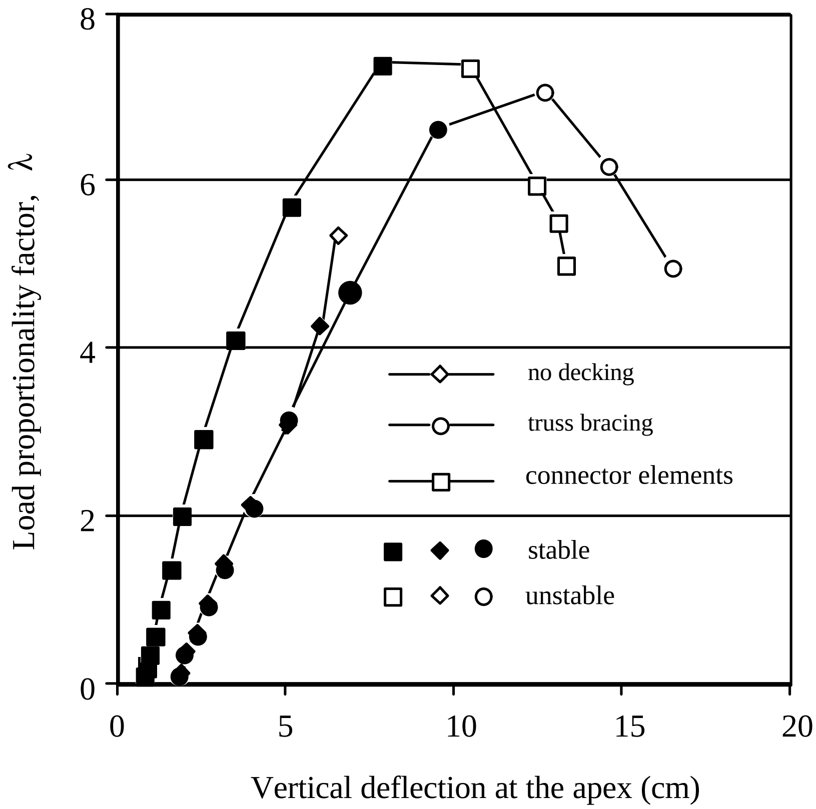

Figure 4.18 Load-Deflection Paths for Various Dome Models, Half Snow Load

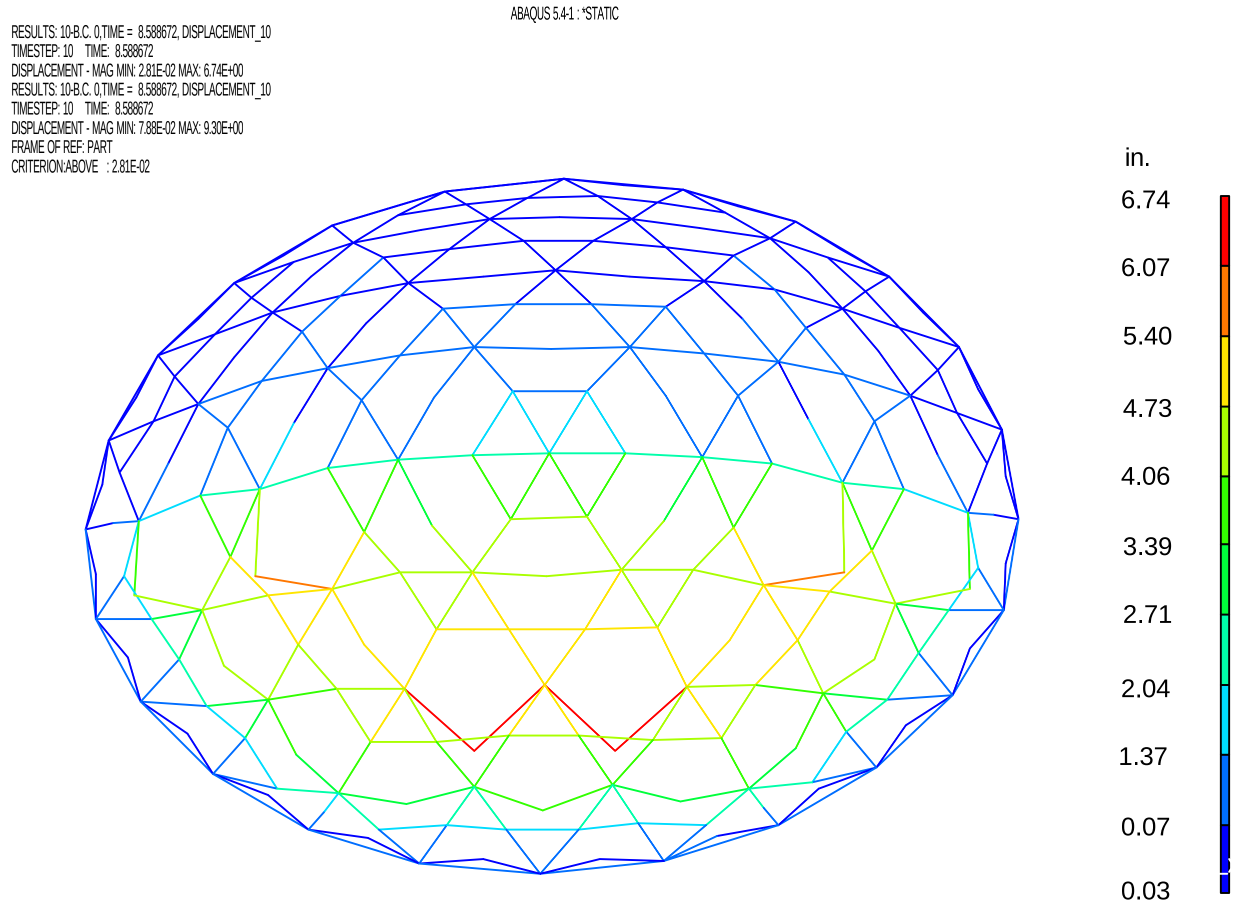

Figure 4.19 Configuration Shape of the Dome Model with No Decking and Snow Load over Half the Dome just Before Buckling

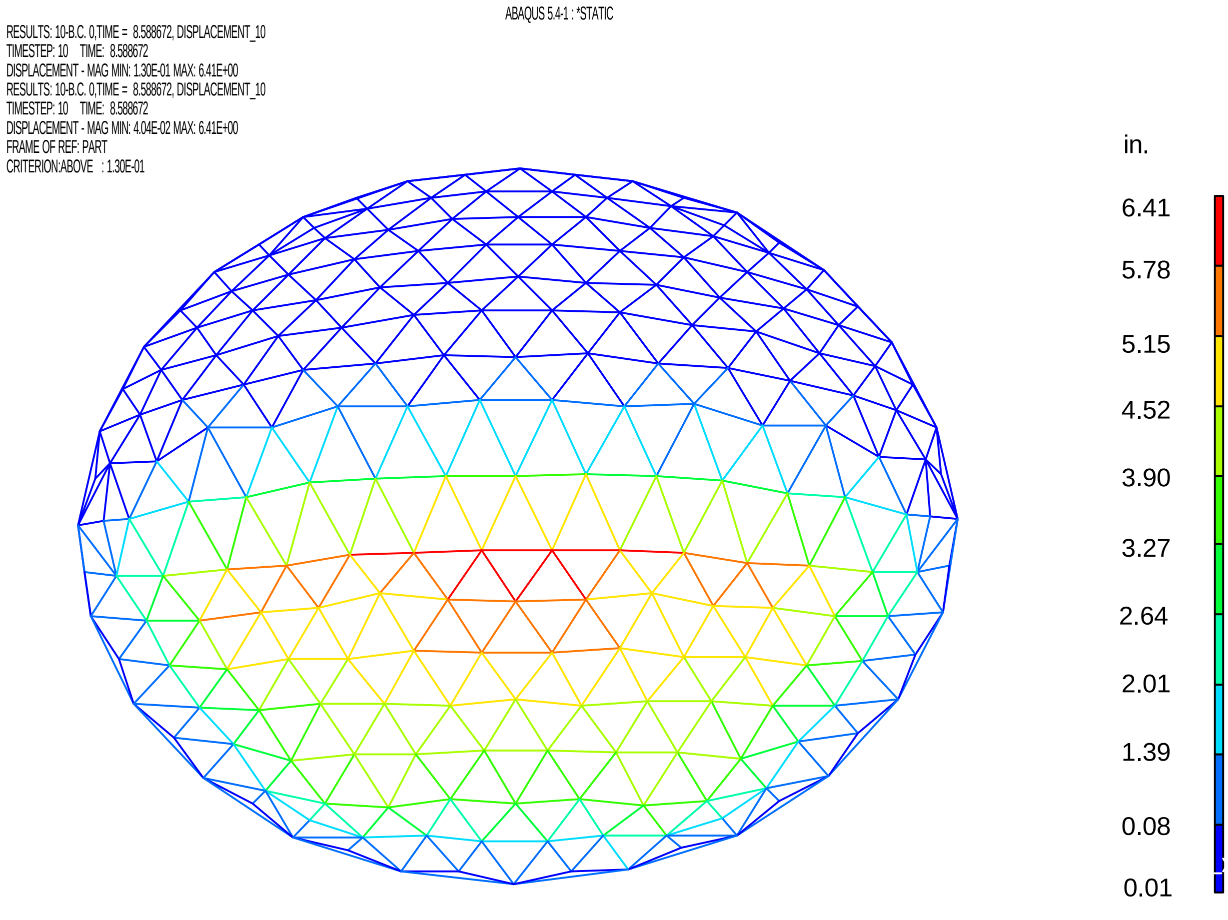

Figure 4.20 Configuration Shape of the Dome Model with Truss Bracing and Snow Load over Half the Dome just Before Buckling

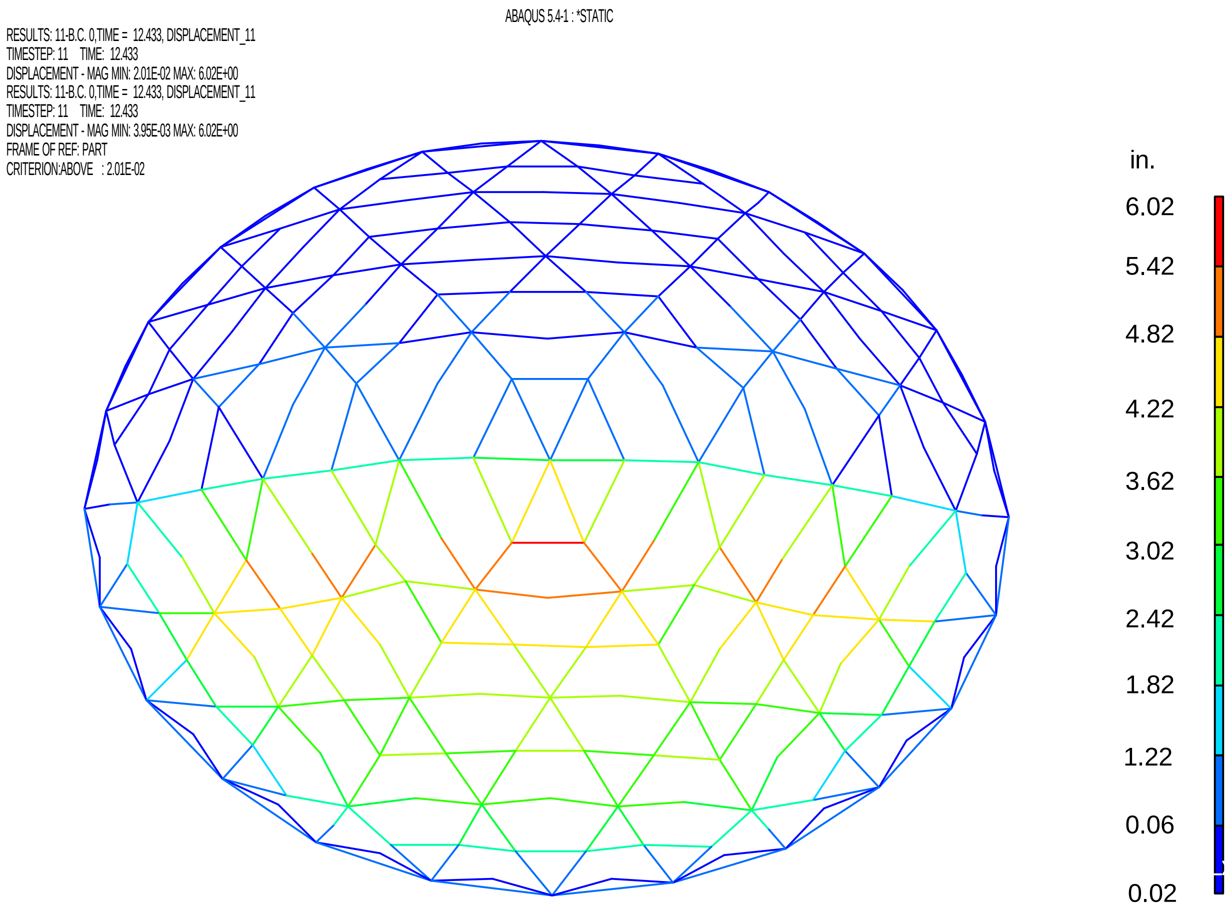

Figure 4.21 Configuration Shape of the Dome Model with Beam-Decking Connectors and Snow Load over Half the Dome just Before Buckling

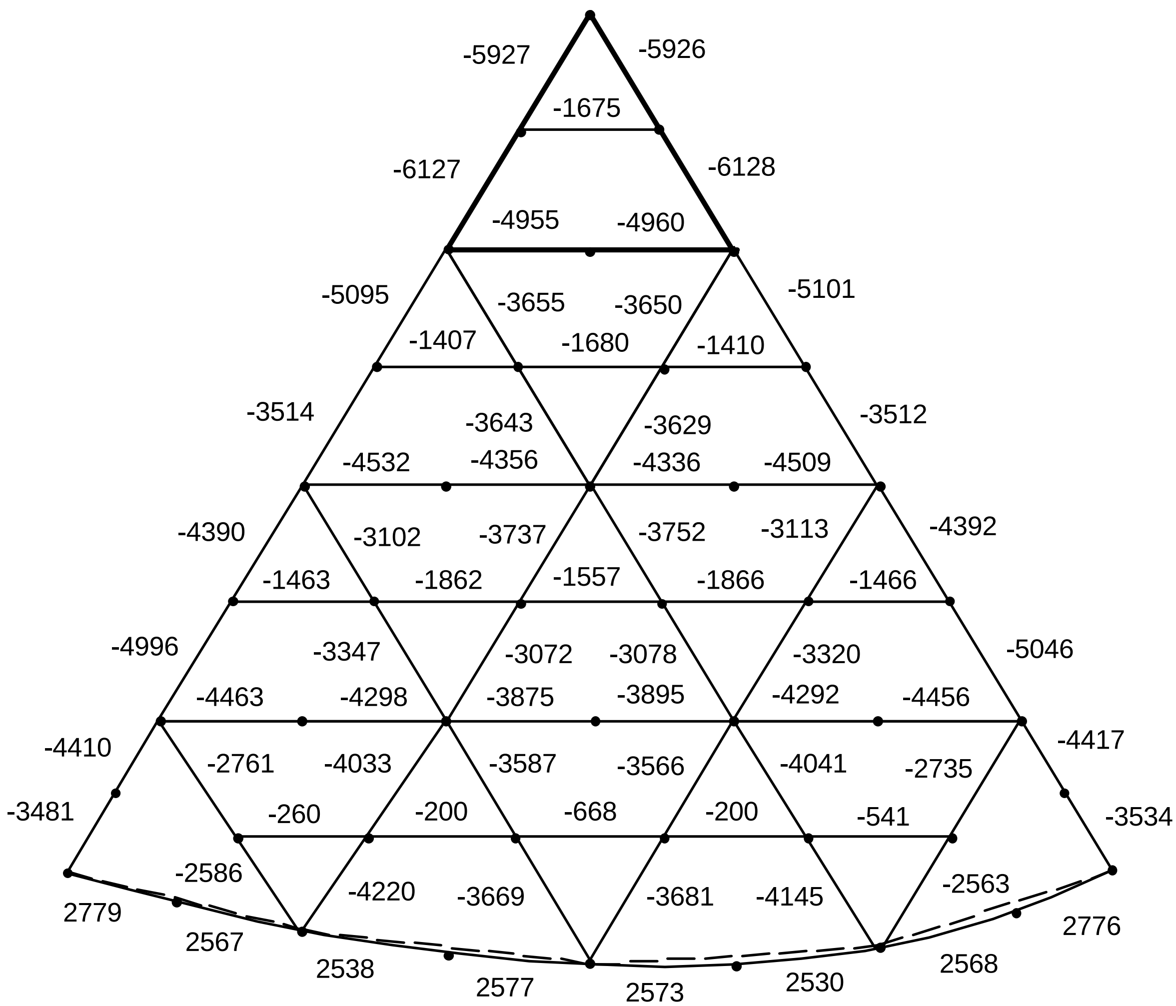

Maximum stress in tension ring: 31,000 psi

Figure 4.22 Maximum Stresses in psi just before Buckling for the Dome Model with Connector Elements, Nonlinear Material, and Snow Load over Half the Dome

Table 4.5 Stresses in beam elements and nail deflections at critical pressures: Half Snow

Material law	Decking model	Max. tension (psi)	Max. compression (psi)	Max. nail deflection (in.)
Linear	none	8,650 (el. 355 & 358)	-12,176 (el. 355 & 358)	-
	truss bracing	3,714 (el. 3 & 345)	-5,445 (el. 4 & 346)	-
	B-D connectors	4,328 (el. 3 & 345)	-7650 (el. 347 & 348)	1.52
Bilinear	none	7,215 (el. 355 & 358)	-12,023 (el. 355 & 358)	-
	truss bracing	3,115 (el. 3 & 345)	-5,445 (el. 51 & 375)	-
	B-D connectors	3,480 (el. 3 & 345)	-6,158 (el. 4 & 346)	1.69
Nonlinear	none	7,850 (el. 355 & 358)	-10,250 (el. 355 & 358)	-
	truss bracing	3,110 (el. 3 & 345)	-5,792 (el. 51 & 375)	-
	B-D connectors	3,480 (el. 3 & 345)	-6,158 (el. 4 & 346)	1.46

Table 4.6 Nail deflections at critical pressures: Half Snow

Element number	Number of failed nails	Maximum nail deflection (in.)
28	4	1.04
859	3	1.03
355	6	1.19
356	5	1.16
357	6	1.19
358	5	1.19
362	4	1.03
363	2	1.01
366	2	1.01
369	8	1.46
370	6	1.38
371	9	1.43
374	7	1.46
373	7	1.44
372	8	1.41

4.6 Effects of Variations in Joint Stiffness

One of the main objectives of this study is to find out the effects of variations in the joint stiffness on the response of the dome model. So far, all the joints in the dome models were considered to be rigid. However, the connections between the beams are considered as pin in Triax joints (Fig. 4.3(a)) and flexible for Varax joints (Fig. 4.3(b)). Variations in joint stiffness can be simulated by varying the values of moments of inertia of beam-beam connector elements. The hub connecting the space beams is represented by 6 beam-beam connector elements (B33).

Table 4.7 and 4.8 indicate that the contribution of the beam-decking connectors to the load-carrying capacity of the dome is more significant than those of the beam-beam joint stiffness. For the dome model with beam-decking connectors, the critical load factors vary little with changes in the beam-beam joint stiffness. The effect of variations in the beam-beam joint stiffness is significant for the dome models without decking.

Table 4.7 Snow Over Entire Dome: $p_{cr} = p_D + \lambda_{cr} p_L$

Beam-Beam Joint Stiffness	λ_{cr} **without effect of decking**	λ_{cr} **with effect of decking**
rigid	4.78	9.40
75%*	4.62	8.41
50%*	3.21	8.09
25%*	2.68	8.08

*% of moments of inertia of beam

Table 4.8 Snow Over Half the Dome: $p_{cr} = p_D + \lambda_{cr} p_L$

Beam-Beam Joint Stiffness	λ_{cr} **without effect of decking**	λ_{cr} **with effect of decking**
rigid	5.37	7.32
75%*	4.47	7.31
50%*	4.05	7.30
25%*	3.96	7.25

*% of moments of inertia of beam

4.7 Locations of Applied Loads

In the dome model, the loads are applied to the beam at the joints along the centroidal axis. In reality, the loads are applied on top of the beams. To test the sensitivity of dome behavior to locations of the applied loads, the live load is applied on top of the beams through a rigid link as shown in Figure 4.23. The results of the analyses are shown in Table 4.9. The results of the analyses indicated that the loads can be applied to the nodes along the centroidal axis because they do not have a significant effect on the ultimate load capacity of the dome.

Table 4.9 Sensitivity of Applied Loads

Dome model	**Critical load parameter, λ_{cr}**	
	Full snow	Half snow
Loads applied on the centroidal axis	9.0	7.7
Loads applied on top of beam	8.8	7.68

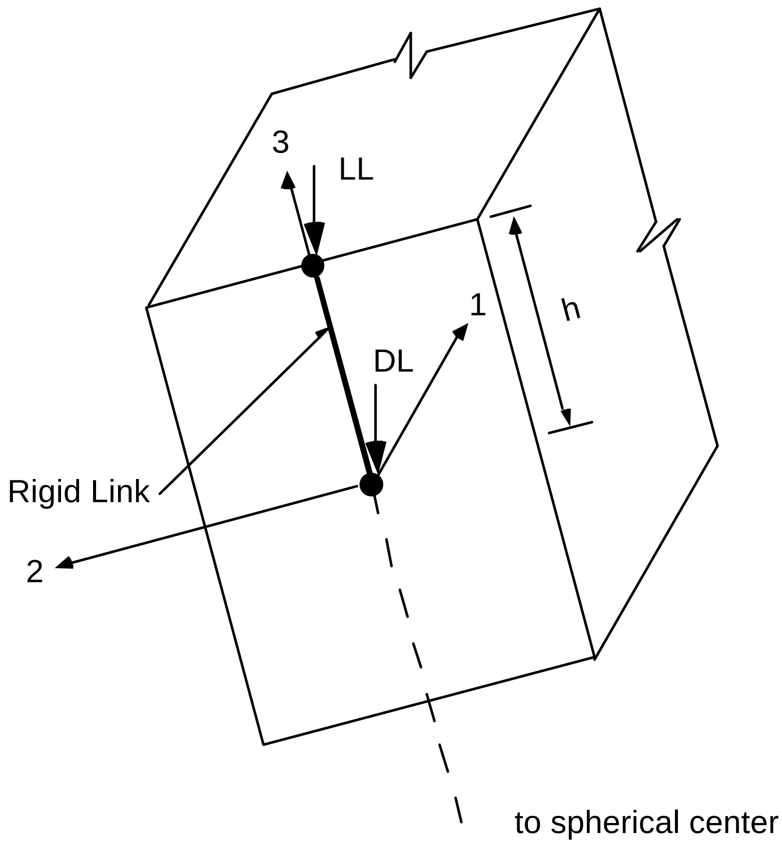

Figure 4.23 Beam Element with Live Load Applied to Top of Beam

4.8 Summary

The Crafts Pavilion dome in Raleigh, North Carolina, is analyzed with the finite element stability method to determine the governing failure mode and ultimate snow loads. Modeling considerations include 3-D beam finite elements, transverse isotropy, torsional warping, beam-decking connectors, geometric and material nonlinearities, the discretization of pressure loads, and boundary conditions. The following conclusions can be drawn from this study:

1. The beam-decking connectors contribute significantly to the ultimate load capacity of the dome model, and connector failures seem to trigger failure of the dome model.

2. Material nonlinearity is not a factor for the dome models with snow load over the entire dome. The nonlinear material behavior is closely linked with the failure mode for the dome model with snow over half of the dome.

3. The effect of beam-beam joint flexibility of a full dome model with beam-decking connector elements is included in this study. Tables 4.7 and 4.8 show that variations in the joint stiffness have little effect on the buckling load in the presence of decking.

The assumptions made in the formulation of the finite element model are updated in Table 4.10 (Whitlow, 1995).

Table 4.10 Summary of Assumptions in Dome Modeling

Component	Model	Reason
Curved Beams	Straight FE's (B33), Bernoulli-Euler theory, can be used to model curved beams.	Straight FE's (B33) have two nodes, whereas curved Timoshenko elements (B32) have three nodes. Using straight beam elements greatly reduces the number of nodes in the assembly. The radius of curvature of each beam is sufficiently large to permit each beam to be modeled with straight elements. Wu (1991) concluded that the choice of the beam finite element is not crucial in the construction of the dome model.
Beam-to-Beam Joints	Assumed to be rigid	Davalos (1989) found the effect of joint flexibility to be significant. However, the dome model he studied neglected the effect of the decking. Wu (1991) studied the effect of joint flexibility on the dome model which used a bracing of truss elements to model the decking. He concluded that the effect of joint flexibility is not significant. However, the bracing of truss elements did not have any physical connection to the actual dome. Kavi (1993) studied the effect of joint flexibility on a dome cap model which used beam-decking connector elements to model the decking. He concluded that the effect of joint flexibility was insignificant. However, the dome cap model does not accurately represent the behavior of the entire dome. The effect of joint flexibility of a full dome model with beam-decking connector elements is included in this study. Tables 4.7 and 4.8 show that variations in the joint stiffness have little effect on the buckling load in the presence of decking.

Table 4.10 Summary of Assumptions in Dome Modeling (Continued)

Component	Model	Reason
Steel Tension Ring	Steel truss element	The tension ring is modeled by twenty-four truss elements, with each element spanning between two consecutive supports (Davalos, 1989).
Decking	Modeled with nonlinear beam-decking connector elements	The connector elements simulate the behavior of the nails joining the top of the beam and the decking. The beam-decking connectors contribute significantly to the ultimate load capacity of the dome model, and connector failures seem to trigger failure of the dome model.
Torsion	Saint-Venant's model for torsion of rectangular beams	Kavi (1993) incorporated Saint-Venant's torsion theory by modifying the value of the shear modulus (G) through a user subroutine. In the current version of ABAQUS (V. 5.5) warping can be modeled directly. The effects of warping is significant for beams with rectangular cross sections.
Geometric Response of the Dome	Nonlinear Geometry	Davalos (1989) determined that geometric nonlinearities must be considered in the analysis of the dome.
Loading Conditions	Full Snow Half Snow	Wu (1991) analyzed the effect of wind loading on the dome and concluded that wind loads are not critical. The half snow load case has proven to be the controlling snow load case.
Load Discretization	Shell elements	The nodal forces are generated by using shell elements to discretize the surface pressure. Since the loading is proportional, the shell elements can be removed once the nodal forces are computed.

Table 4.10 Summary of Assumptions in Dome Modeling (Continued)

Component	Model	Reason
Material Properties	Linear, bilinear, and nonlinear material laws. Assumption of Transverse Isotropy	The nonlinear normal stress-strain relation is based on the work by Conners (1989). The assumption of transverse isotropy was supported by an experimental study of southern pine glulam beams (Davalos et al., 1991). The assumption permits one to select a single modulus (E) and a single shear modulus (G). Moreover, torsion tests on glulam samples have verified the assumption of transverse isotropy. Material nonlinearity is not a factor for the dome models with snow load over the entire dome. The nonlinear material behavior is closely linked with the failure mode for the dome model with snow over half of the dome.
Boundary Conditions	All perimeter nodes are fixed in the Z- direction. Two opposite nodes along the X-axis are fixed in the Y-direction. Two opposite nodes along the Y-axis are fixed in the X-direction.	The constraints must eliminate the rigid body motions of the dome but must allow for the tension ring to move freely in the radial direction (Davalos, 1989).

Chapter 5

Analysis of Varax Dome

5.1 Introduction

This chapter is concerned with finite element stability analyses of the Church of the Nazarene dome in Corvallis, Oregon (Fig. 5.1). The dome is analyzed to determine the governing failure mode and ultimate snow loads. The dome consists of a triangulated network of curved glulam beams, a tongue-and-groove wood decking supported by curved purlins, and a steel tension ring. A typical dome sector is shown in Fig. 5.2. The glulam beams are joined by patented steel hubs (Varax) as shown in Fig. 5.3 (Tissaoui, 1991), and the decking is nailed to the beams and purlins. The dome model is pre- and post-processed by I-DEAS (1995) and analyzed by ABAQUS (1995). The principle objective of this chapter is to test the hypothesis that the beam-decking connectors (B-D connectors) form the weakest link of the dome. The beam-decking connectors are represented by nonlinear springs which model the load slip behavior of nails between the beam and the decking. Another objective of this chapter is to study the effects of variations in the joint stiffness. The joints are modeled by beam-beam connectors (B-B connectors) whose moments of inertia are used to control the joint stiffness. Geometric and material nonlinearities are considered in this study. The geometry, finite element modeling, and finite element stability analyses of the dome are presented in this chapter.

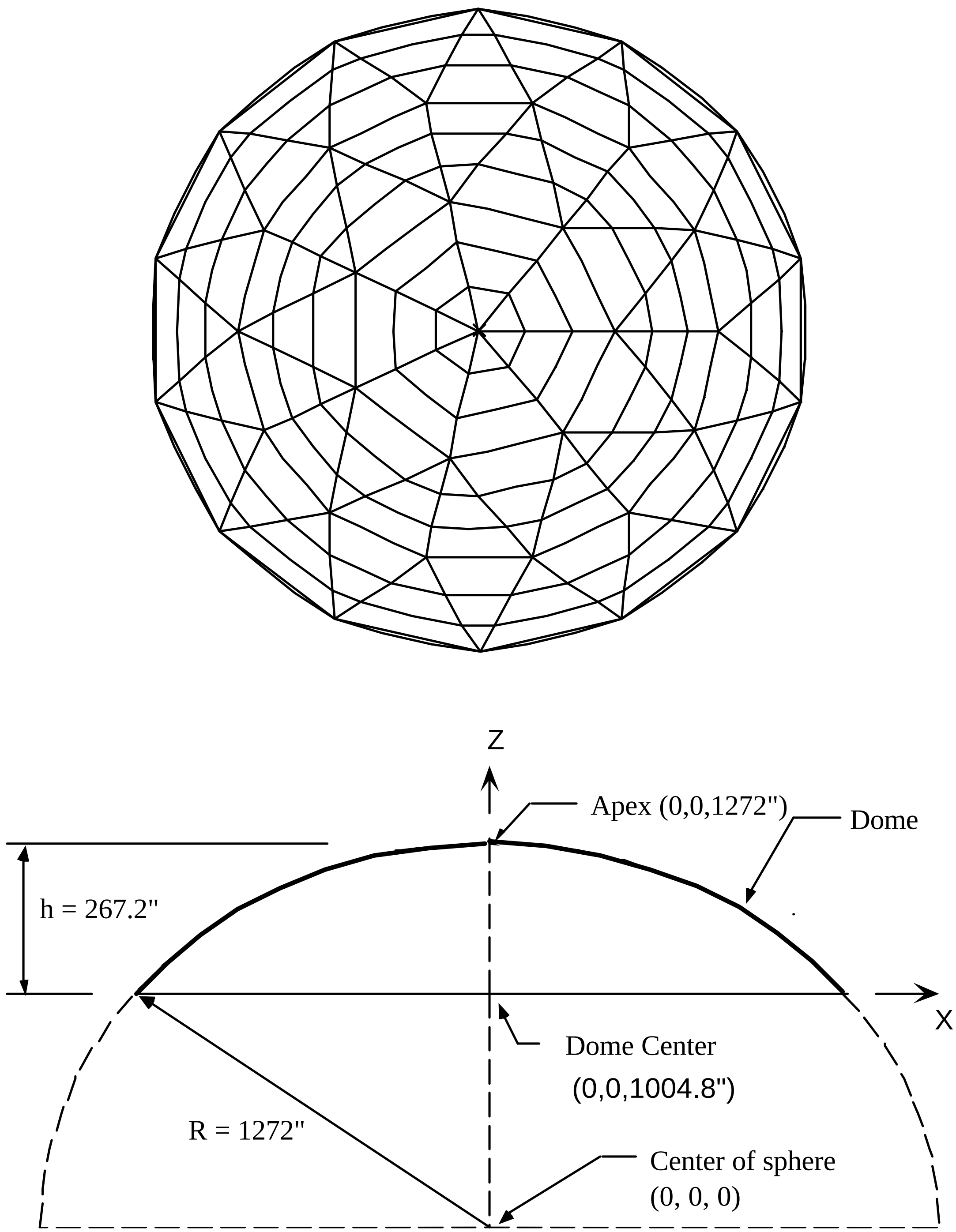

Figure 5.1 Geometry of Dome

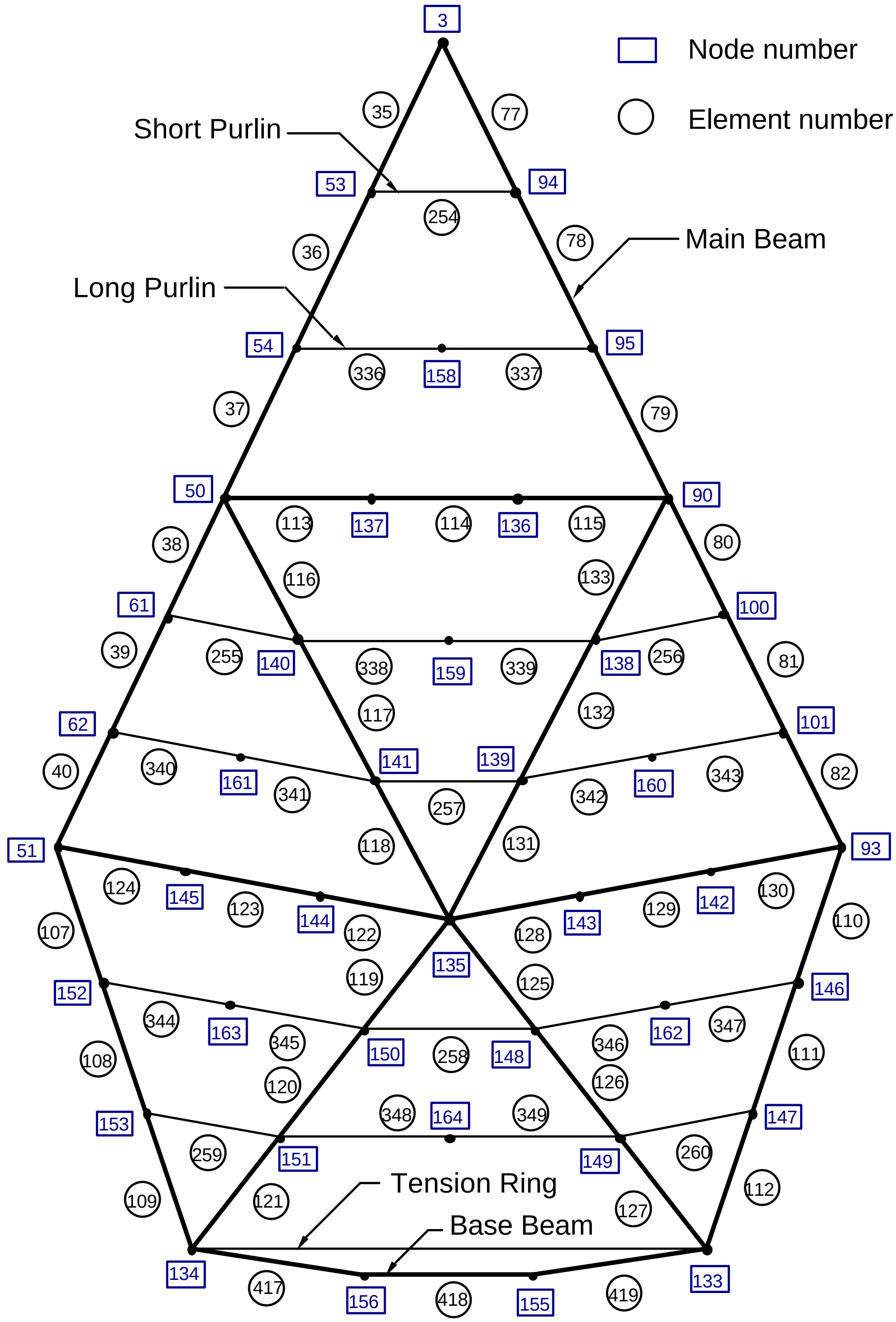

Figure 5.2 Dome Sector

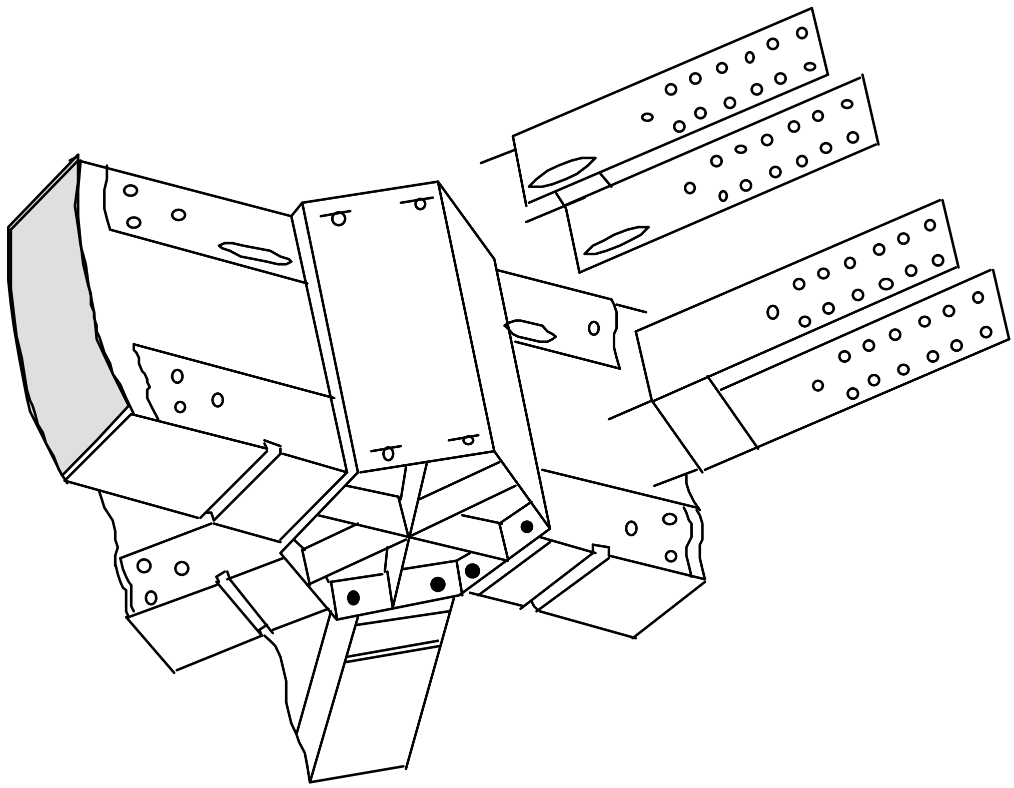

(a). Varax steel hub connector

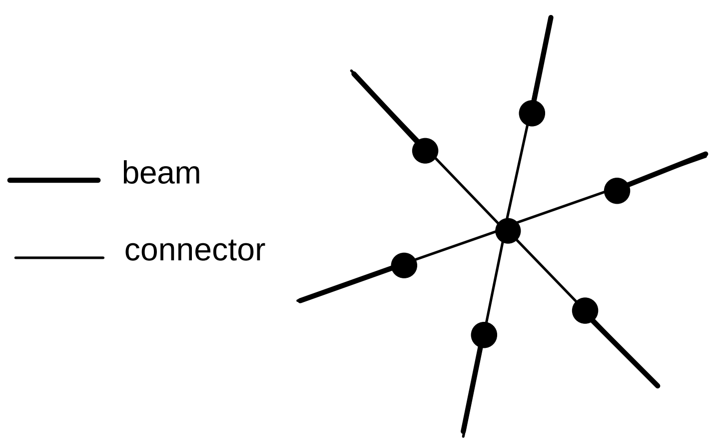

(b). Typical Joint

Figure 5.3 Modeling of the Space Joints.

5.2 Dome Geometry

The geometry of the Church of the Nazarene dome, which is characteristic of Varax domes (Eshelby and Evans, 1988), is similar to the geometry of the Triax dome in Chapter 4 except that it is composed of seven identical sectors and is supported by fourteen columns. The dome has a span of 130.6 ft (39.8 m), a rise of 22.4 ft (6.8 m), and a radius curvature of 106.5 ft (32.5 m) and rests on a steel tension ring. The dome is covered with 2-inch tongue-and-groove wood decking and composed of 77 beams and 112 purlins. The dimensions of the members are as follows:

Main Beam :	5.125 x 12.0 in (13.0 x 30.5 cm)
Short Purlin:	3.125 x 7.5 in (7.9 x 19.0 cm)
Long Purlin:	5.125 x 7.5 in (13.0 x 19.0 cm)
Base Beam:	5.125 x 22.0 in (13.0 x 55.9 cm)

5.3 Finite Element Modeling

The dome models with various features are constructed and evaluated to represent the behavior of the glulam dome. The models are created with I-DEAS and exported to ABAQUS for nonlinear analyses. The results from ABAQUS are then imported back to I-DEAS for post-processing (graphical interpretation of the results). I-DEAS was selected because of its powerful graphical capabilities in creating the dome models and displaying the results. ABAQUS was chosen as the finite element program to analyze the behavior of the dome because of its excellent nonlinear analysis capabilities. In this chapter, structural members, material properties, joints flexibility, boundary conditions, design loads and load discretization are presented.

5.3.1 Structural Members

Both beams and purlins of the dome are modeled with three-dimensional, beam finite elements (B33). The B33 beam elements are based on the Bernoulli/Euler beam theory, which ignores transverse shear deformations. The B33 beam element has two nodes, whereas the B32 Timoshenko beam element, which includes transverse shear deformations, has three nodes. Due to the large curvature of the beams, Wu (1991) considered effect of curvature of the beam elements (curved B32 vs. straight B33) on the dome model. Although the B33 beam element could be curved. He concluded that the effect of curvature was not crucial in the construction of the dome model. A mesh of three element per beam is used in this study because our main interest is the qualitative behavior of the dome. Using the B33 elements greatly reduces the total number of nodes of the dome model. The steel tension ring is modeled with straight truss elements.

5.3.2 Material Properties

The beams and purlins of the Varax dome are constructed with glued-laminated (glulam) southern pine. Tissaoui (1991) analyzed the dome using a linear material law. In this study, linear, bilinear, and nonlinear material laws are considered. The longitudinal elastic moduli for tension and compression are taken as E_t = 1,800,000 psi (12,400 MPa) and E_c = 2,200,000 psi (15,200 MPa), respectively (Fig. 4.4). The shear modulus is not included because the beam model ignores the shear deformations.

5.3.3 Joint Flexibility

To study the effect of variations in joint stiffness, a six inch long, two-node, B33 element is used to model the beam-to-beam connections. Moments of inertia of the B-B connectors are used to control the joint stiffness. The cross-sectional dimensions of the connector elements are varied to modify the moments of inertia and therefore the stiffness of the connector elements. The hub connecting the space beams is represented by 6 connector elements at a standard node and 7 connector elements at the apex.

The height and width of the joint elements are modified by a reduction factor "c_0" such that their moment of inertia is reduced by a factor of "c", as shown in Figure 5.4.

a = original width of beam

b = original height of beam

c_0 = width and height reduction factor

c = stiffness reduction factor

I = original moment of inertia

I' = reduced moment of inertia of the hinge elements

$$I = \frac{ab^3}{12}, \; I' = \frac{c_0^4 ab^3}{12}; \; I' = cI, \quad c = c_0^4$$

$$\text{Stiffness reduction (\%)} = \frac{I - I'}{I} \times 100\%$$

The connector elements have the original dimensions of the main beam. In this study, the dome model is analyzed with beam stiffness reduction factors of 0, 25, 50, and 75%. The relations of the stiffness reduction factors are presented in Table 5.1.

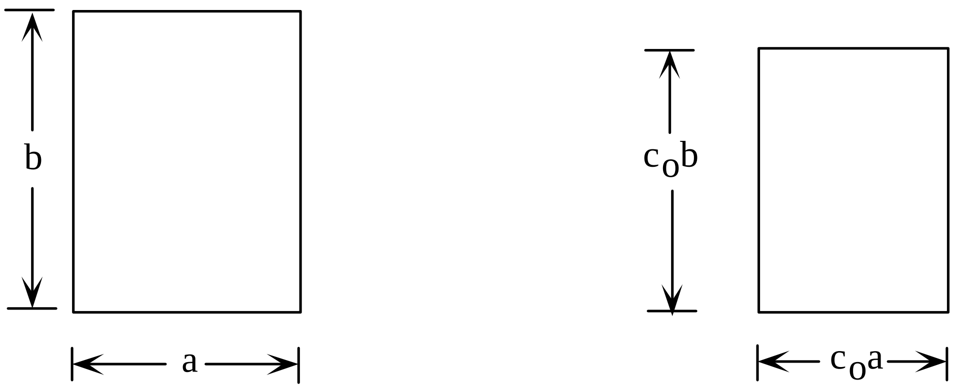

$I = \frac{1}{12} ab^3$ $\quad$ $I' = cI$ where $c = c_o^4$

(a) $\quad$ (b)

Figure 5.4 (a) Original beam dimensions; (b) Connector element with reduced dimensions

Table 5.1 Connector element dimensions for reduced stiffness

Stiffness reduction factor (%)	Width and height reduction factor, c_o	Reduced height (in)	Reduced width (in)
0	1.0	12.00	5.13
25	0.931	11.17	4.77
50	0.841	10.09	4.31
75	0.707	8.49	3.62

5.3.4 Boundary Conditions

The boundary conditions are applied to remove rigid body displacements of the dome but at the same time allow for the steel tension ring to move freely in the radial direction. Since the dome model is defined in rectangular coordinates, the perimeter nodes are specified in cylindrical coordinates using the TRANSFORM card (Appendix A) in ABAQUS. The perimeter nodes are then restrained in the tangential and vertical directions while allowed to translate in the radial direction and rotate in any direction as shown in Fig. 5.5.

5.3.5 Design Loads

The design loads consist of dead and snow loads. The design snow load is 25 pounds per square foot of the horizontal projection (per UBC). The dead load pressure is obtained as follows (Varax Engineering Company, 1986) :

Grid framing	2.76 psf
Decking	5.00 psf
Connections	0.54 psf
Roofing	1.50 psf
Insulation	4.50 psf
Miscellaneous	0.70 psf
Total dead load	15.00 psf

Two load cases are considered in the analyses of the dome model: snow over the entire dome and snow over half of the dome (Fig. 5.6).

Wind and seismic load cases were analyzed for this dome and revealed no forces in excess of those in the snow load cases (Varax Engineering Company, 1986). Therefore, they are not considered in this study.

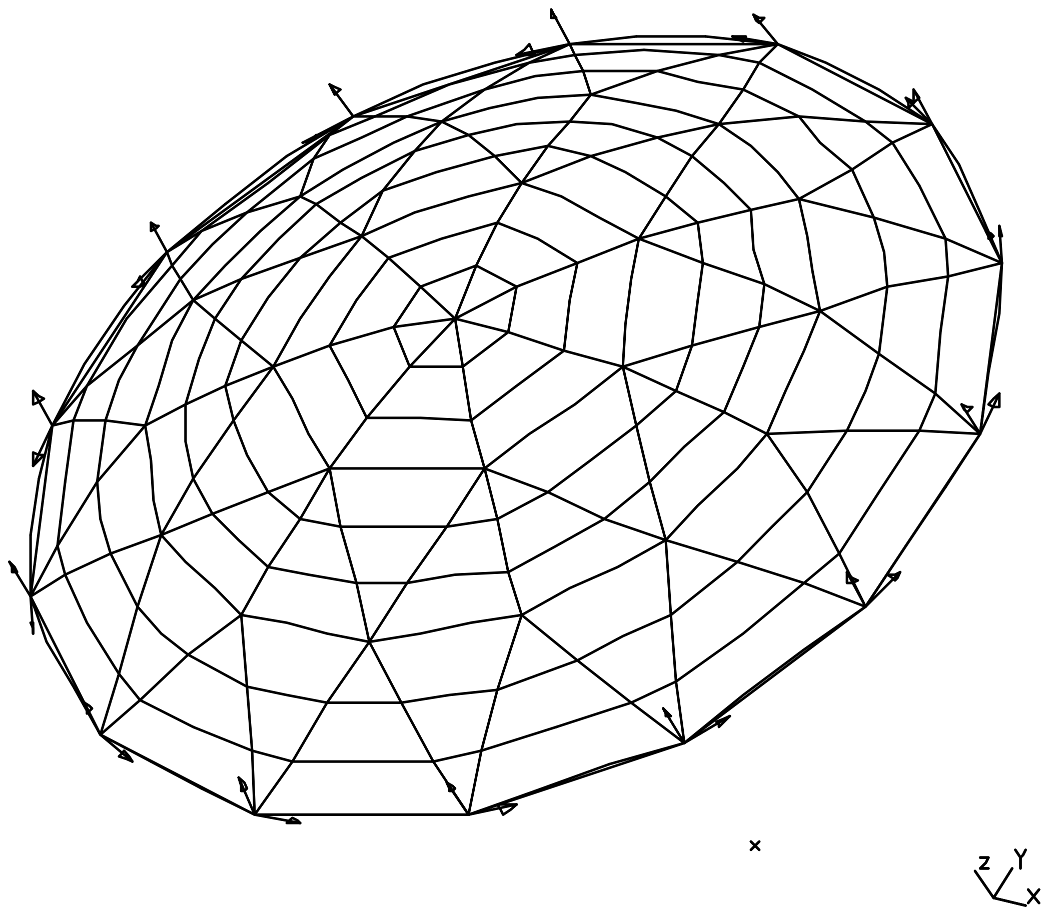

Figure 5.5 Boundary Conditions

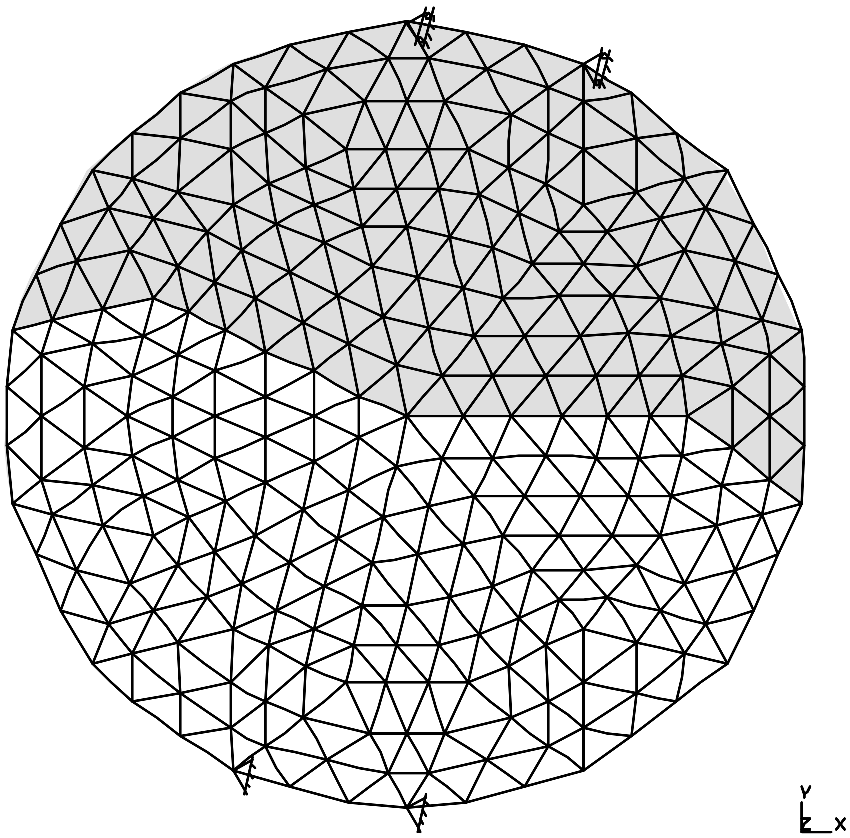

Figure 5.6 Snow Load over Half of the Dome.

5.3.6 Load Discretization

The nodal forces of the dome model are generated by using shell elements to discretize the load pressures and performing a linear analysis with ABAQUS. Since the loading in the stability analyses is proportional, the shell elements are removed once the nodal forces are computed. The procedure for discretization of loads is as follows (Holzer, et al., 1992):

1. All nodes of the dome model are fixed.
2. Pressure in the opposite sense of the actual pressure is applied to the shell elements in a linear analysis to compute the reactions of all nodes.
3. The shell elements are removed and the reactions are applied at the nodes of the beams.

The load on the shell elements is specified by using the body weight (lb/in^3) of the shell elements, the BZ option in ABAQUS. In Appendix A, the dead load of the dome is specified by using the body weight of the shell directly because it truly represents the body weight of the dome. However, the snow load must be specified over the plan area rather than the surface area of the dome as shown in Appendix B. For the dome model, the thickness of the shell elements is given as 0.001 in. to make its body weight negligible. Therefore, the dead and snow loads of 15 psf (0.1042 psi) and 25 psf (0.1736 psi) are specified as 104.2 lb/in^3 and 173.6 lb/in^3, respectively.

5.3.7 Decking

The effect of the decking is considered in two ways: (1) the decking is neglected and (2) it is represented by beam-decking connector elements. The connector elements are nonlinear springs that model the behavior of the nails joining the top of the beams with the decking (Fig. 4.5a). The elongation of each spring is determined through interpolation functions from the nodal displacements of the beam element. Hence, the springs do not add degrees of freedom to the assembly. The load-deformation curve for one nail is shown in Fig. 4.5b. When the elongation of a spring during the analysis reaches 1 in. (2.5 cm), the spring is disconnected.

5.4 Linear Analysis

The dome model is first subjected to a linear finite element analysis in ABAQUS. Nonlinear analyses are then applied to the dome model to trace the equilibrium paths and to determine the first critical point. The linear analysis is conducted to verify the integrity of the dome model. The response of the dome model should be symmetric under symmetric loading. Two load cases are considered:

- Dead load (15 psf) + Snow load over the entire dome
- Dead load (15 psf) + Snow load over half of the dome.

5.4.1 Linear Analysis Results: Full Snow

The response of the dome model under the symmetric load (snow load over the entire dome) is symmetric as shown in Fig. 5.7. The maximum vertical displacement of 1.6 in. is located at the nodes on the long purlins near the bottom of each sector. The vertical displacement of the apex is 1.2 in. The radial displacement of the boundary nodes, where the nodes are restrained in the tangential and vertical directions, is 0.4 in. The maximum horizontal displacement located at the nodes on the base beams is 1.6 in.

The maximum stresses of each element members are shown in Fig. 5.8. The maximum compressive stress is 2300 psi located on the long purlins near the bottom of each sector. The maximum tensile stress is 2850 psi located on the base beams. The maximum tensile stress in the tension ring is 14,570 psi which is less than the allowable stress of 26,000 psi (Varax Engineering Company, 1986).

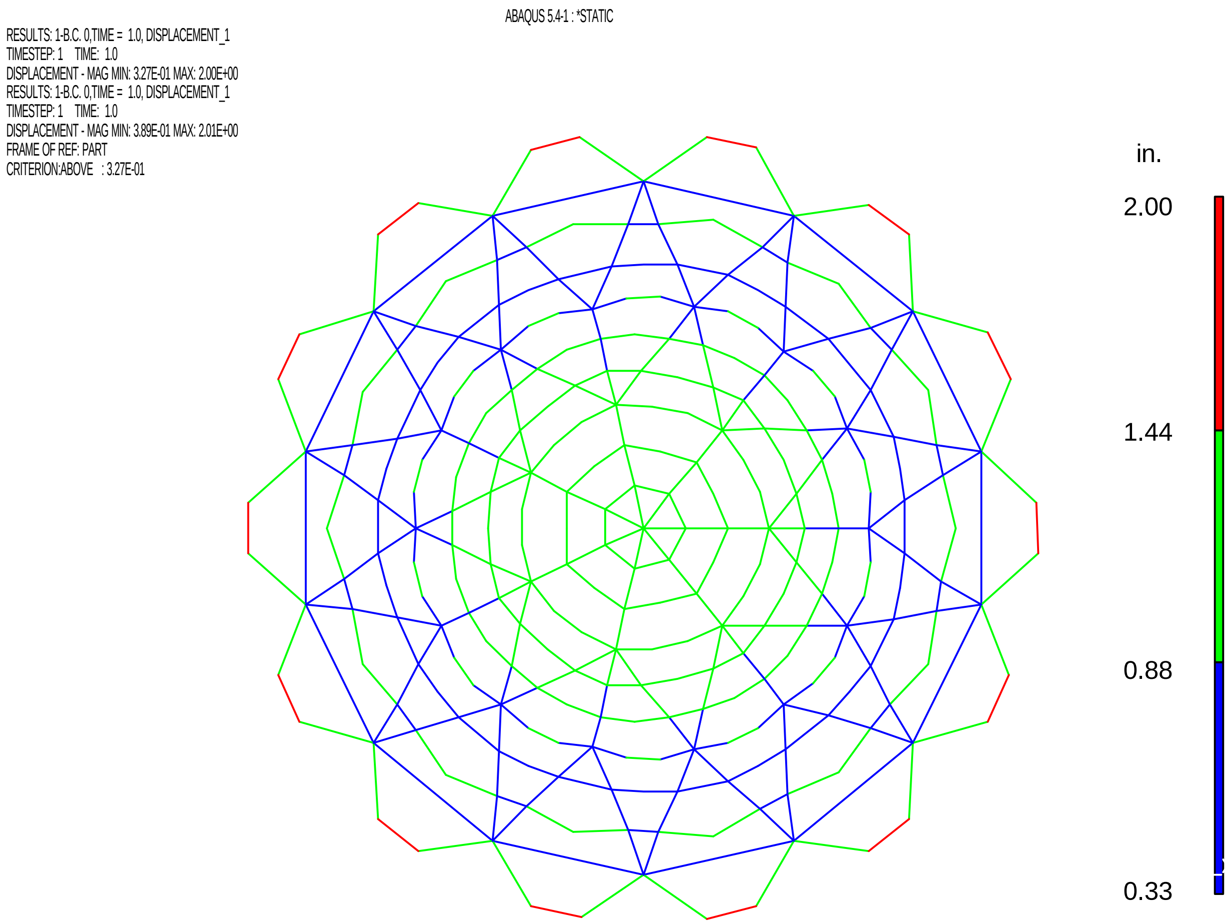

Figure 5.7 Displacement Contours for the Dome Model with Snow Load over the Entire Dome in the Linear Analysis

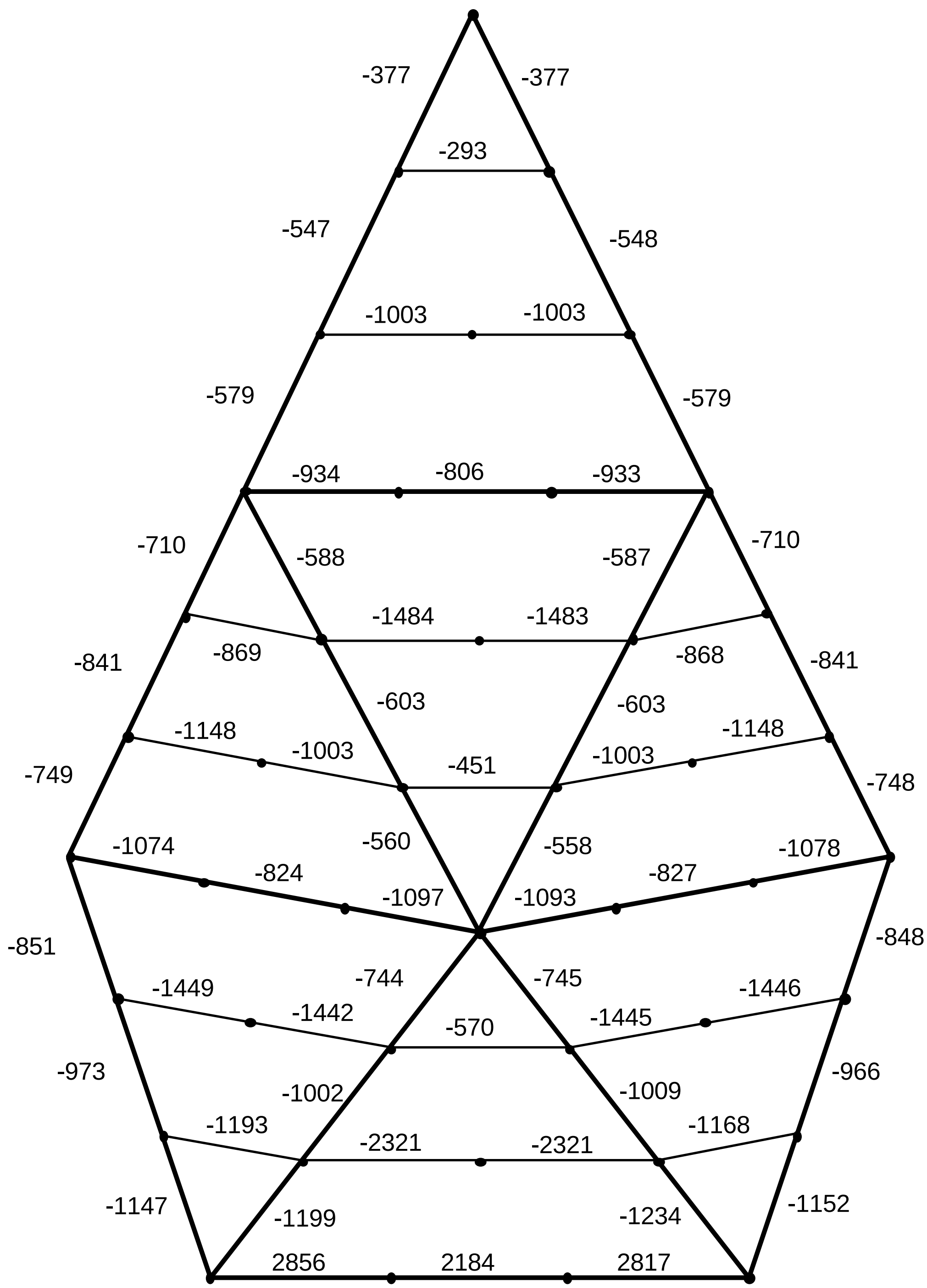

Stress in tension ring: 14,583 psi

Figure 5.8 Maximum Stresses in psi for the Dome Model with Snow Load over the Entire Dome in the Linear Analysis

5.4.2 Linear Analysis Results: Half Snow

The maximum displacements are located in the upper half of Fig. 5.9 where the snow load is applied. The maximum vertical displacement of 1.8 in. occurred on the nodes of the long purlins near the bottom of each sector. The vertical displacement of the apex is 0.8 in. The maximum horizontal displacement of 1.8 in. occurred on the base beams. The maximum radial displacement at the boundary nodes is 0.4 in.

The maximum stresses of element members for the dome model with snow over half of the dome are shown in Fig. 5.10. The maximum compressive stress of 2520 psi occurred on the long purlins near the bottom of the mid-sector where the snow load is applied. The maximum tensile stress of 2860 psi occurred on the base beams of the same sector. The maximum stress in the steel tension ring is 13,700 psi

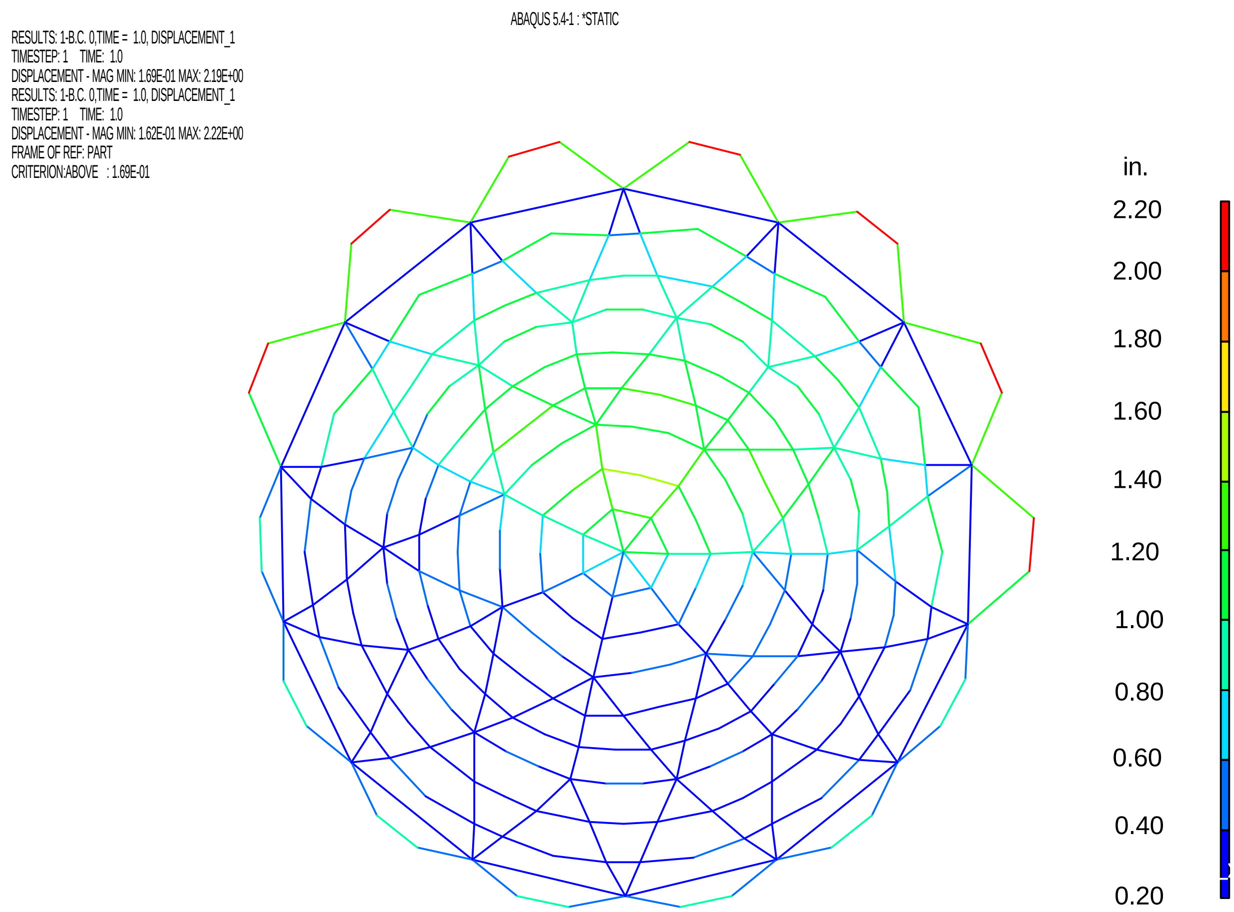

Figure 5.9 Displacement Contours for the Dome Model with Snow Load over Half the Dome in the Linear Analysis

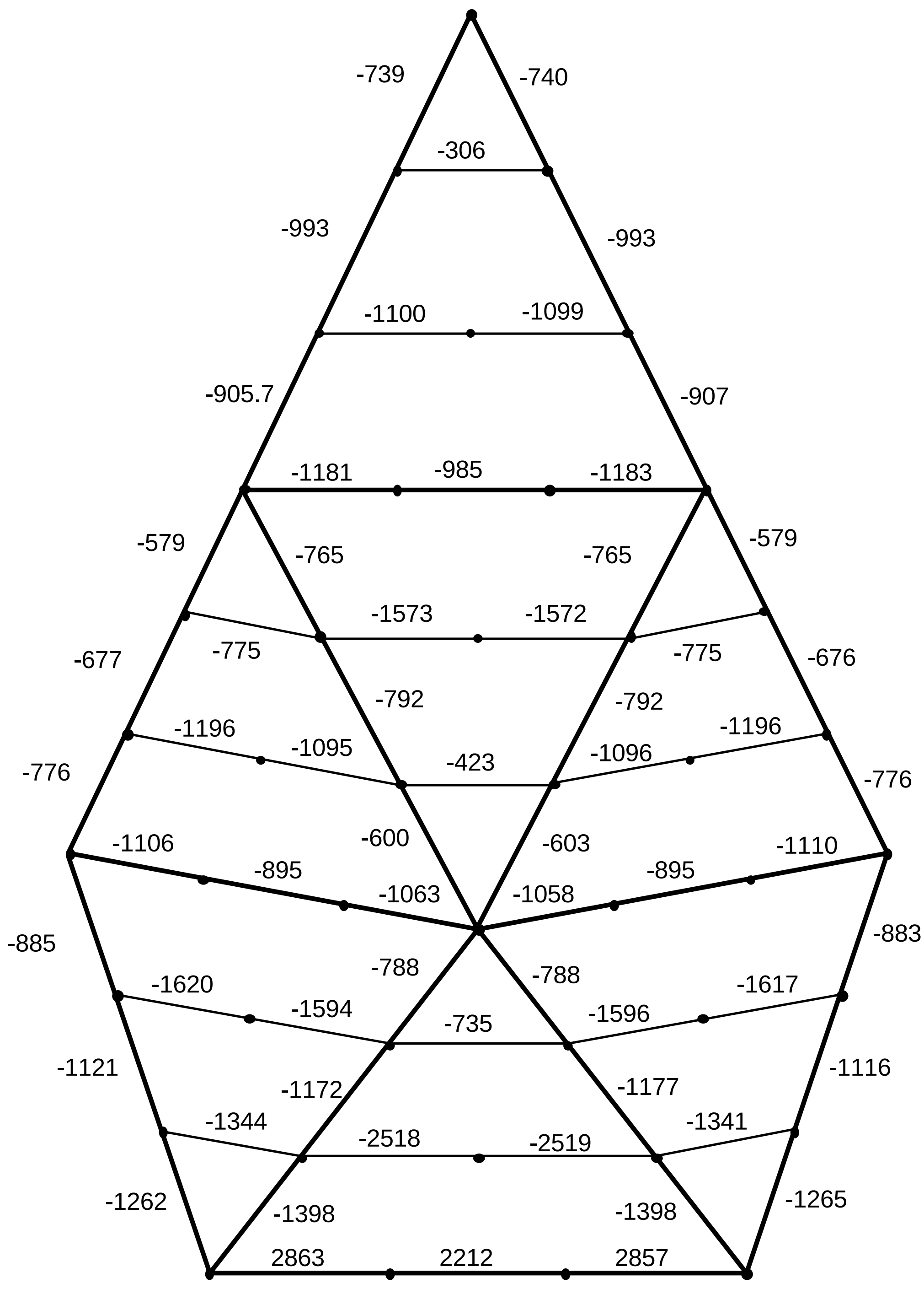

Stress in tension ring: 13,693 psi

Figure 5.10 Maximum Stresses in psi for the Dome Model with Snow Load over Half of the Dome in the Linear Analysis

5.5 Nonlinear Analysis

Nonlinear analysis of the dome model was conducted to determine the critical snow load pressures, buckling modes, and effects of joint stiffness and connector elements on the instability of the dome. Maximum stresses and displacements were also closely monitored on one sector of the dome. Nonlinear analysis is used to trace the equilibrium path up to and beyond the critical point where the structure becomes unstable. The pressure load is composed of two independent load distributions

$$p = p_D + \lambda p_L \tag{5.1}$$

where p_D = 16 psf (766 Pa) is the design dead load pressure, p_L = 25 psf (1,197 Pa) is the live load pressure resulting from snow load over the entire dome or over half of the dome; and λ is the proportionality factor of the live load, the load parameter. The critical load pressure, p_{cr}, of the dome model can be computed as

$$p_{cr} = p_D + \lambda_{cr} p_L \tag{5.2}$$

Two incremental iterative methods are used in ABAQUS to trace the equilibrium path to the first critical point, a bifurcation point or limit point. First, the dead load (15 psf) is applied using the Newton/Raphson method. The critical snow load pressure, λ_{cr}, is obtained by scaling the snow load with the load parameter, λ, in the modified Riks method. An ABAQUS input file for the nonlinear analysis is provided in Appendix D. The first critical point, λ_{cr}, is detected by a negative eigenvalue of the tangent stiffness matrix in the message file of ABAQUS.

5.5.1 Nonlinear Analysis Results: Full Snow

The critical load parameters for various loading conditions, decking models, and material laws are shown in Table 5.2. For snow load over entire dome, the corresponding equilibrium paths at the apex of the dome models for two decking models (no decking and beam-decking connector elements) are shown in Fig. 5.11.

In the dome model without decking, the buckling mode is bifurcation in the form of twist buckling of the entire dome as shown in Fig. 5.12. The buckling mode is caused by lateral buckling of the beams, which are not restrained by the decking in this model. The critical snow load pressure increases from 3.3 for the linear material model to 5.0 for the bilinear material model. The critical snow load factor is 5.0 (snow load of 125 psf) for both dome models with bilinear and nonlinear material laws (Table 5.2). The maximum stresses are below the ultimate stress values (Fig. 4.4). The maximum compressive stress is 8,400 psi, and the maximum tensile stress is 6,100 psi as shown in Fig. 5.13.

In the dome model with beam-decking connector elements, the critical snow load factor increases from 10.6 for the linear material model to 11.1 for the bilinear material model. The critical snow load factor is 11.1 (snow load of 125 psf) for both dome models with bilinear and nonlinear material laws (Table 5.2). The maximum compressive stress is in the plastic region of the stress strain curve (plateau region) while the maximum tensile stress is beyond the ultimate stress (Fig. 4.4). The maximum compressive stress is 10,500 psi, and the maximum tensile stress is 18,530 psi as shown in Fig. 5.14. As the critical point, a bifurcation point, is reached, 135 beam elements have failed connectors and all of the beam-decking connectors of 14 beam elements are disconnected (Appendix F).

Table 5.2 Critical pressure: $p_{cr} = p_D + \lambda_{cr} p_L$

Material law	Decking model	Critical load parameter, λ_{cr}	
		Full snow	Half snow
Linear	none	3.3	5.3
	B-D connectors	10.6	7.9
Bilinear	none	5.0	6.0
	B-D connectors	11.1	8.3
Nonlinear	none	5.0	4.8
	B-D connectors	11.1	8.8

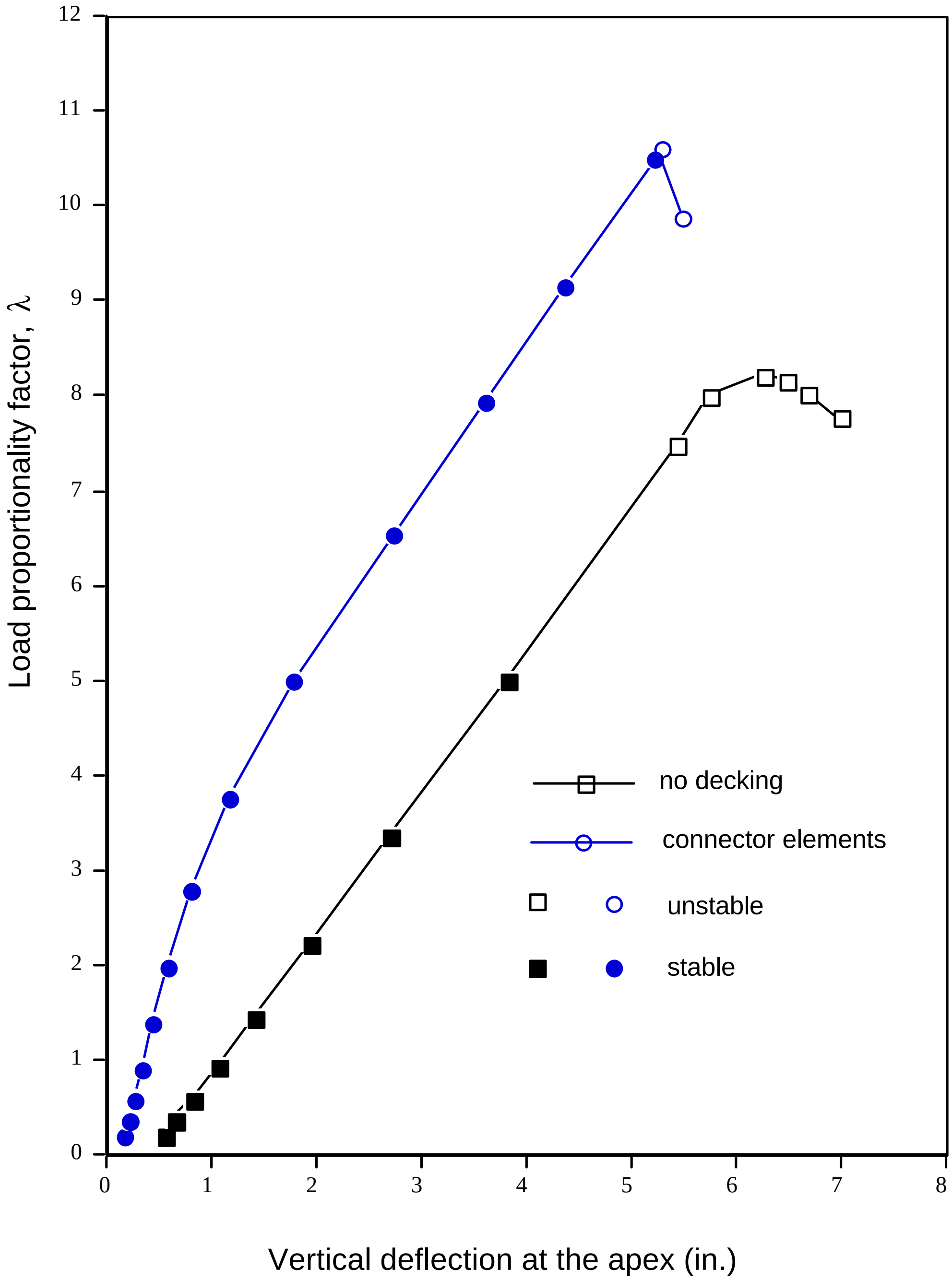

Figure 5.11 Equilibrium Paths at the Apex for the Dome Model with Snow Load over the Entire Dome

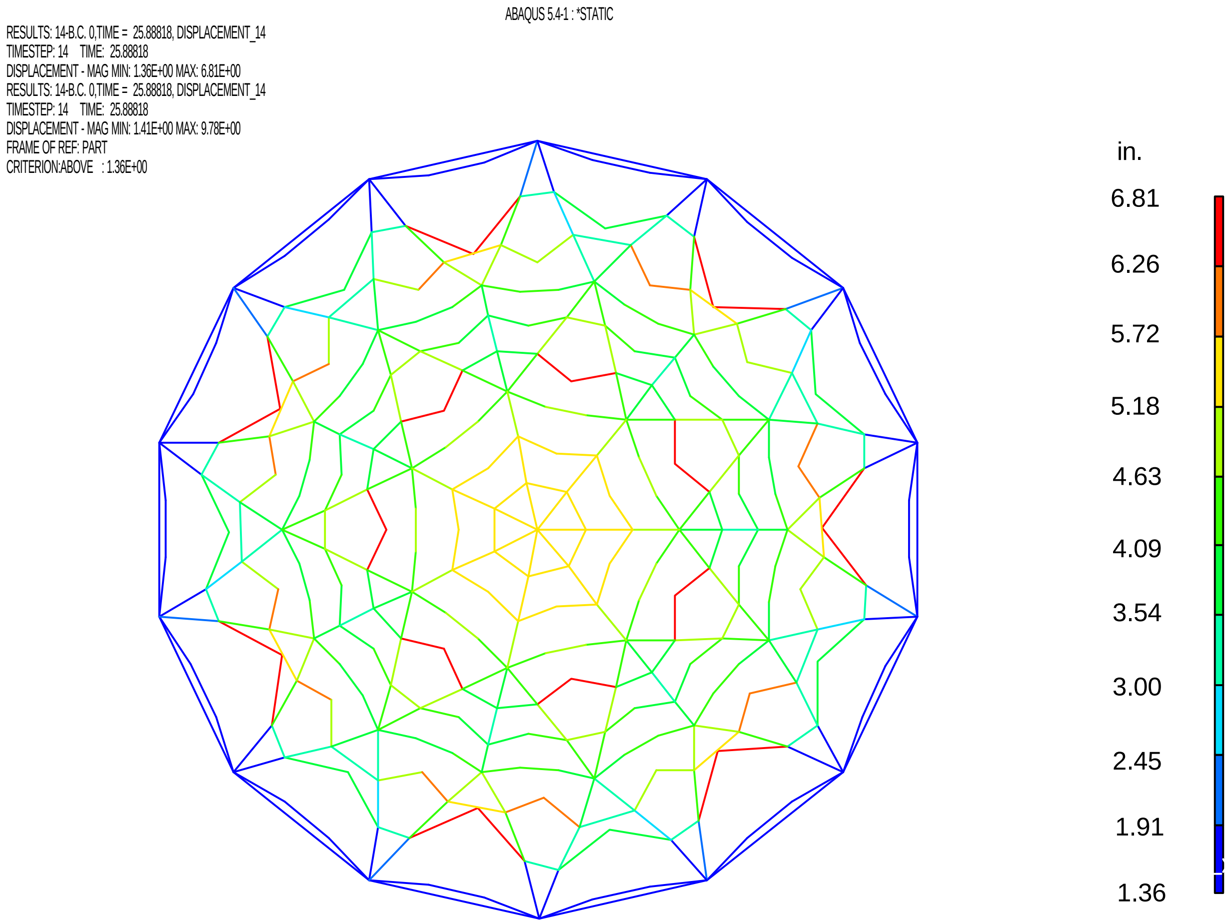

Figure 5.12 Deflection Shape of the Dome Model with Connector Elements and Snow Load over the Entire Dome just before Buckling

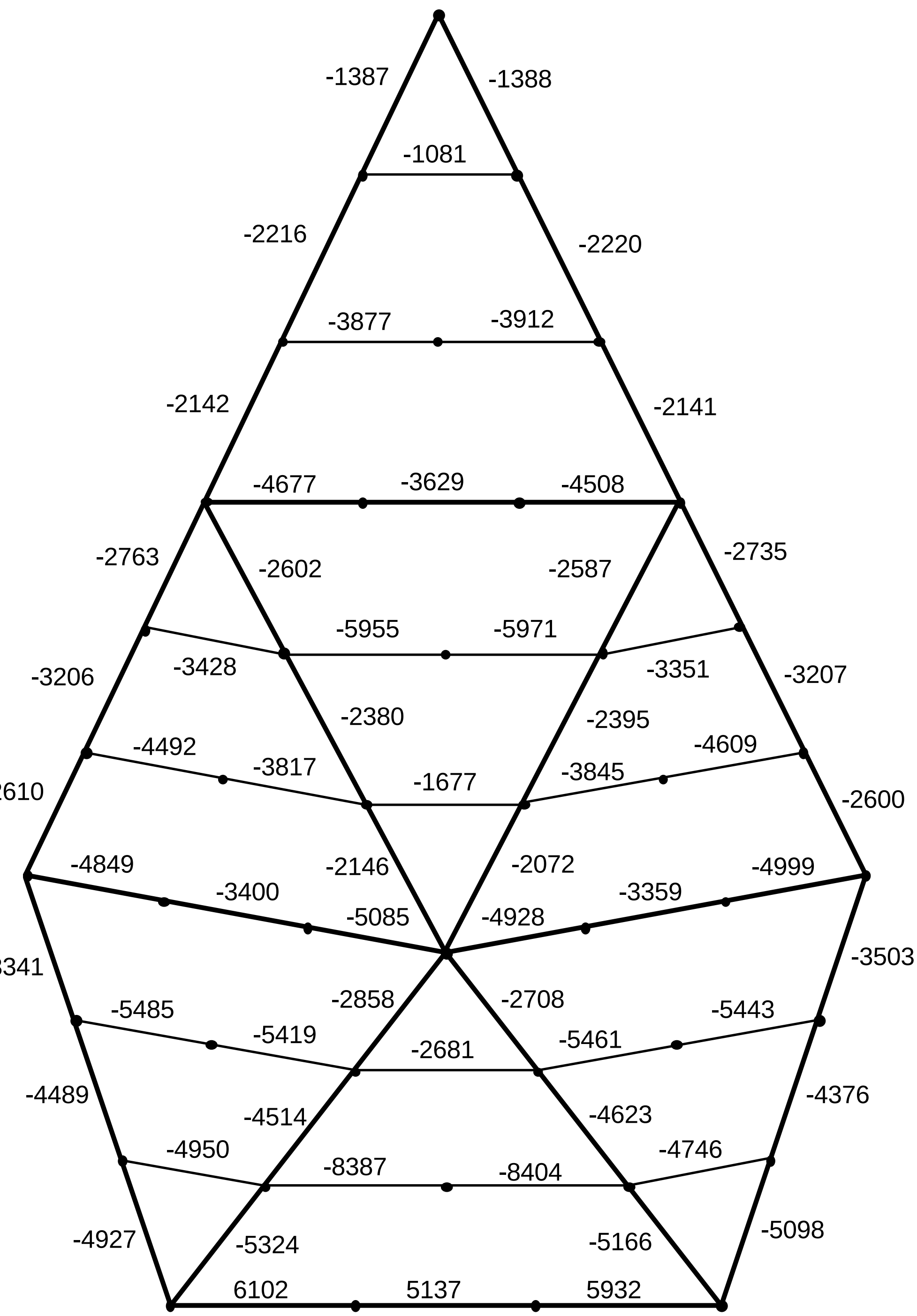

Figure 5.13 Maximum Stresses in psi just before Buckling for the Dome Model without Decking and Snow Load over the Entire Dome

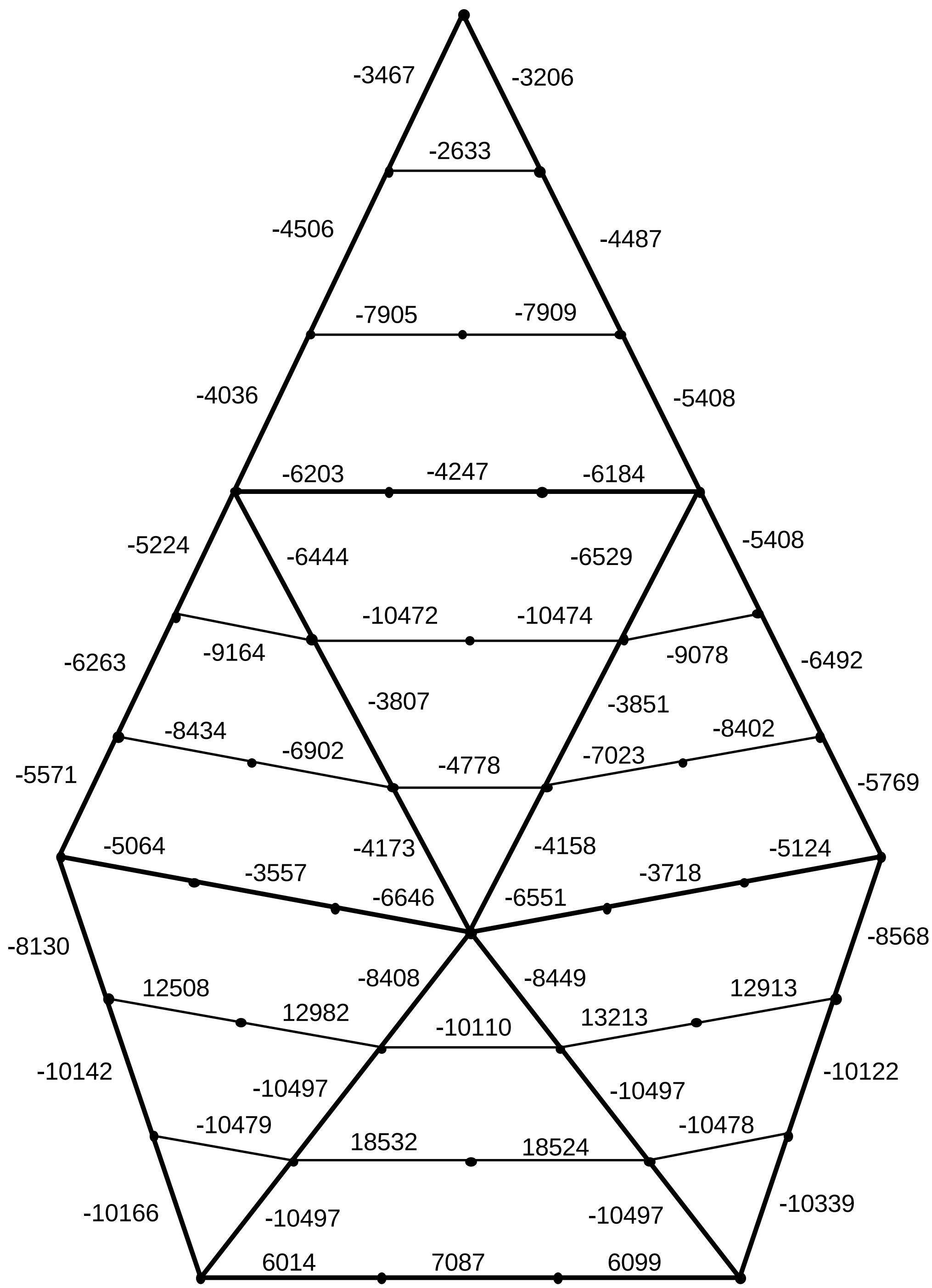

Figure 5.14 Maximum Stresses in psi just before Buckling for the Dome Model with Beam-Decking Connector Elements and Snow Load over the Entire Dome

5.5.2 Nonlinear Analysis Results: Half Snow

For snow over half the dome, the corresponding equilibrium paths at the apex of the dome models with nonlinear material law for two decking models (no decking and beam-decking connector elements) are shown in Fig. 5.15.

In the dome model without decking, the buckling mode indicates a localized pattern in the upper half of Fig. 5.16 where the snow load is applied. The critical snow load factor is 4.8 (Table 5.2). For the dome with nonlinear material law, the maximum compressive stress is between the proportional limit and the ultimate stress while the maximum tensile stress is beyond the ultimate stress (Fig. 4.4). The maximum compressive stress is 8,798 psi, and the maximum tensile stress is 15,929 psi as shown in Fig. 5.17.

In the dome model with beam-decking connector elements, the critical snow load factor is 8.8 (Table 5.2). The beam-connector elements are less effective in increasing the critical load factor than for snow over the entire dome as shown in Table 5.2. For the dome with nonlinear material law, the maximum compressive stress is at the ultimate stress while the maximum tensile stress is beyond the ultimate stress (Fig. 4.4). The maximum compressive stress is 10,497 psi, and the maximum tensile stress is 17,921 psi as shown in Fig. 5.18. As the critical point, a bifurcation point, is reached, 100 beam elements have failed connectors and all of the beam-decking connectors of 27 beam elements are disconnected (Appendix G).

Due to the unsymmetrical loading of the dome model with snow over half of the dome, the tension ring no longer moves evenly in the radial directions. A pair of pinned and roller supports are applied in opposite directions where the snow load is applied as shown in Fig. 5.6. The analyses of the dome model with and without these extra supports yield the same results.

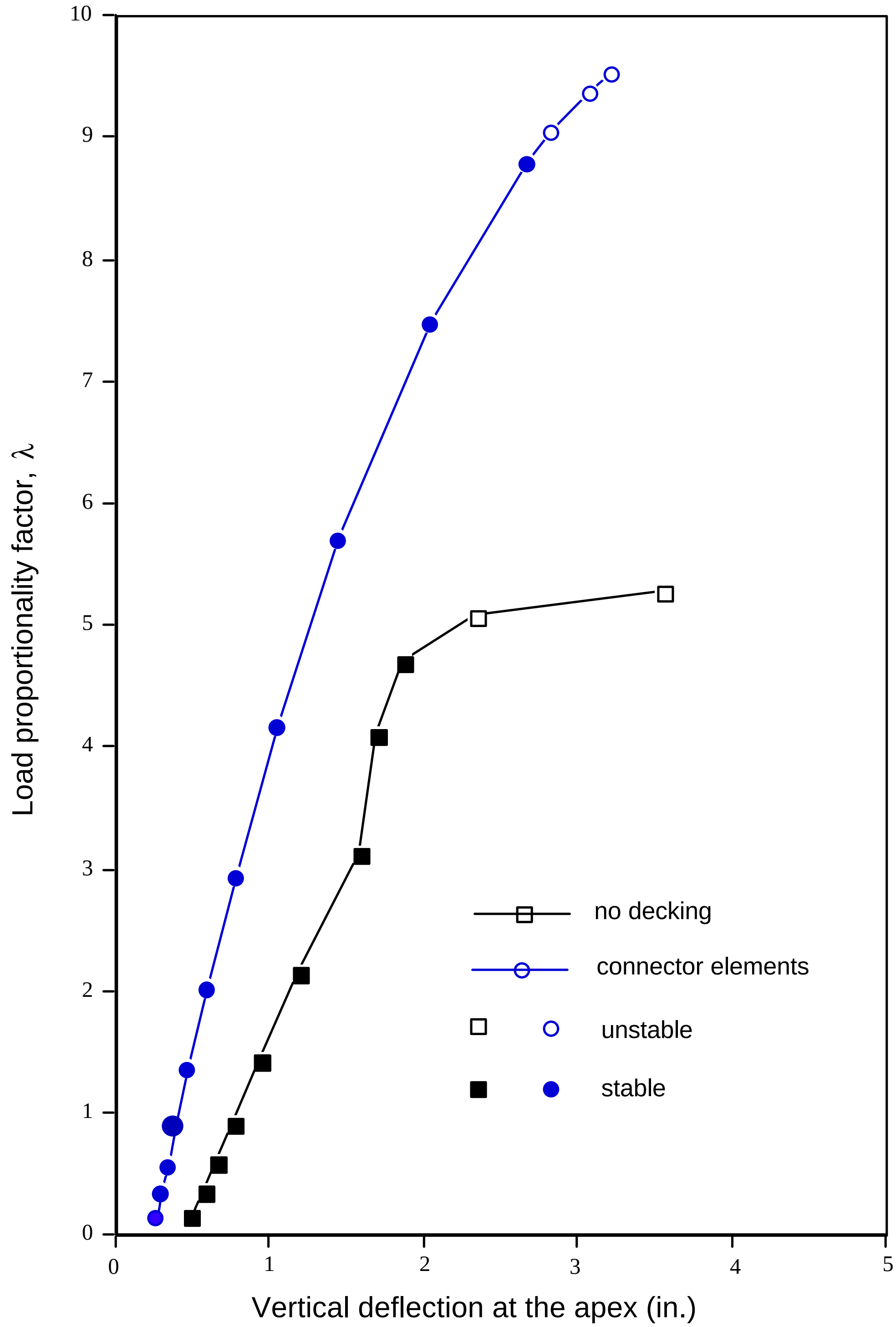

Figure 5.15 Equilibrium Paths at the Apex for the Dome Model with Snow Load over Half the Dome.

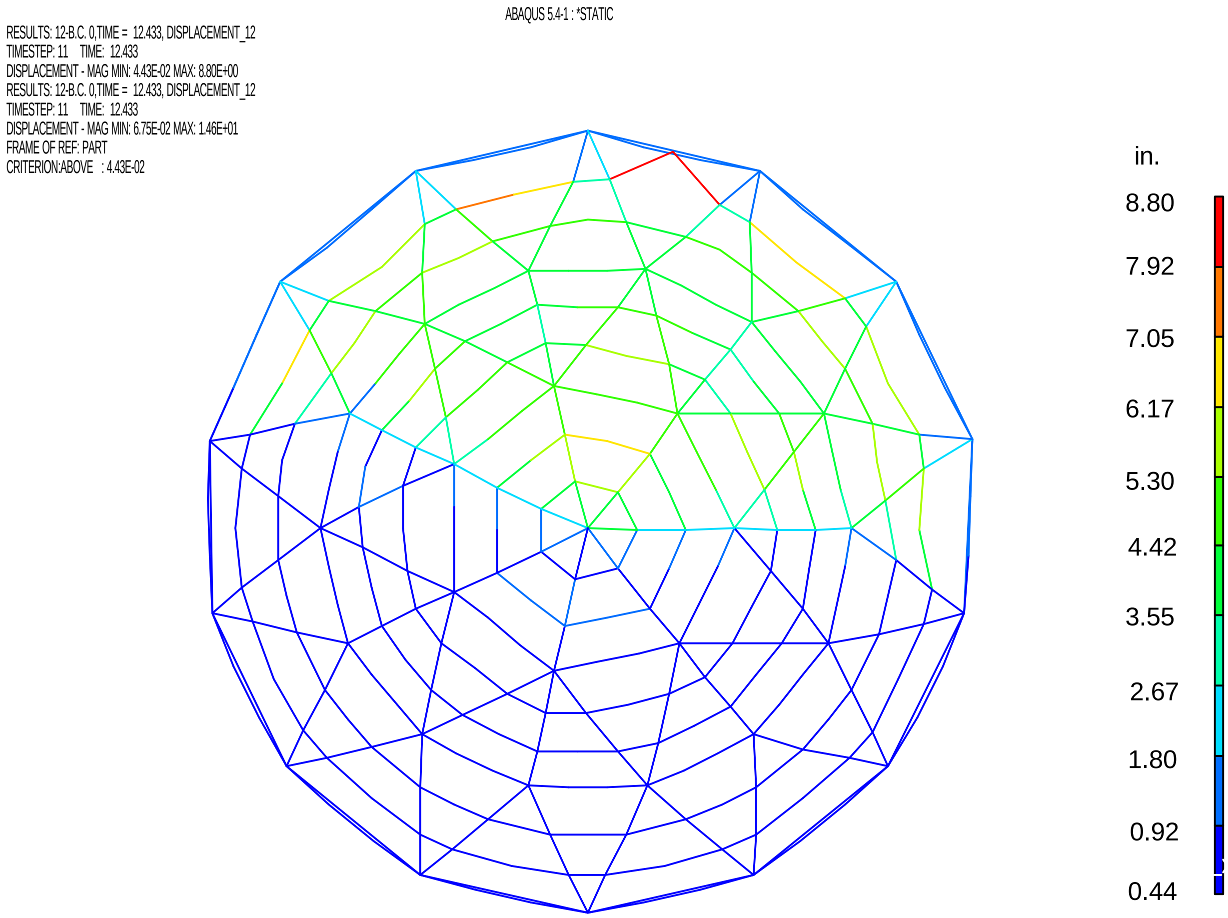

Figure 5.16 Deflection Shape of the Dome Model with Snow Load over Half the Dome just before Buckling

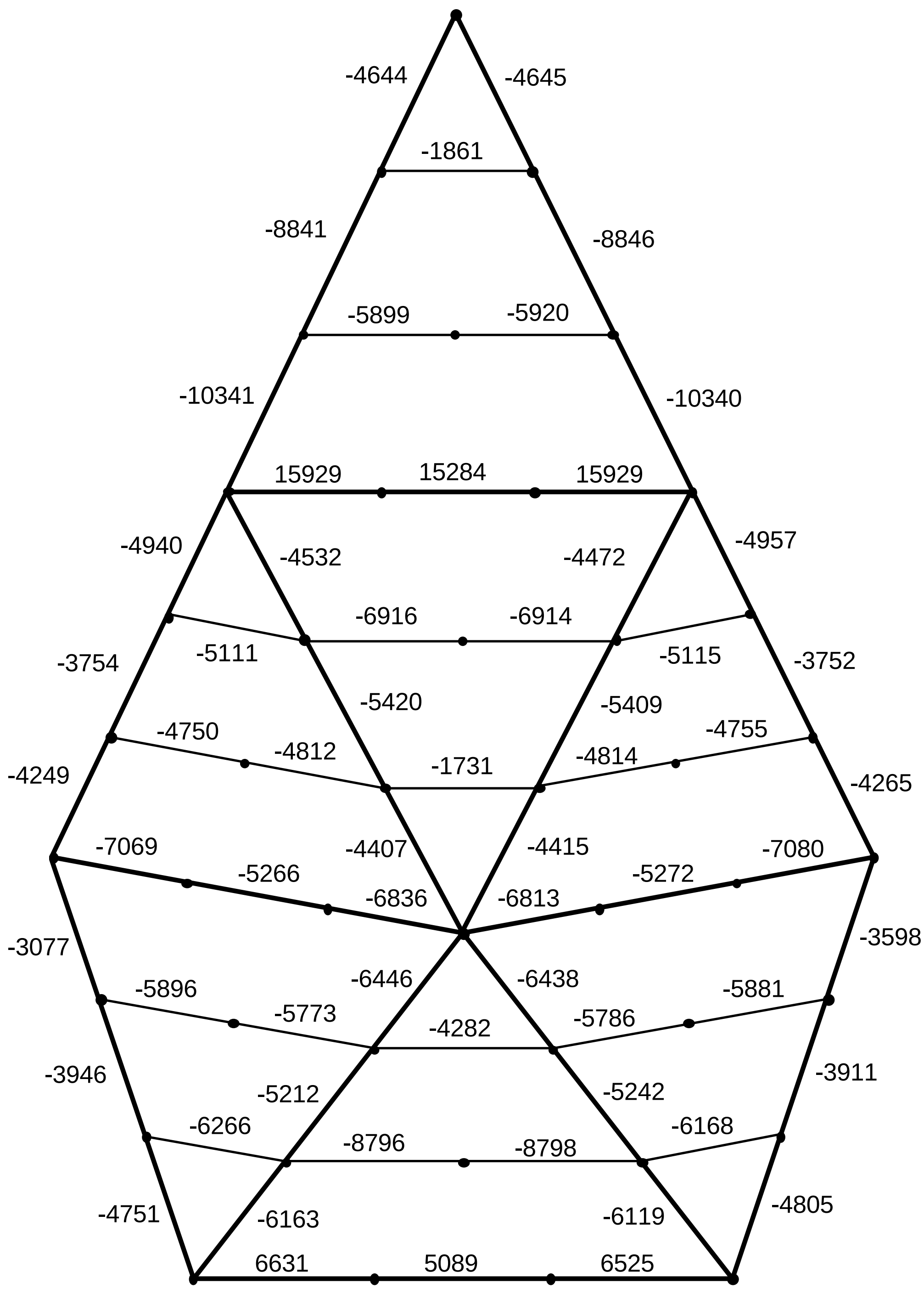

Figure 5.17 Maximum Stresses in psi just before Buckling for the Dome Model without Decking and Snow Load over Half the Dome

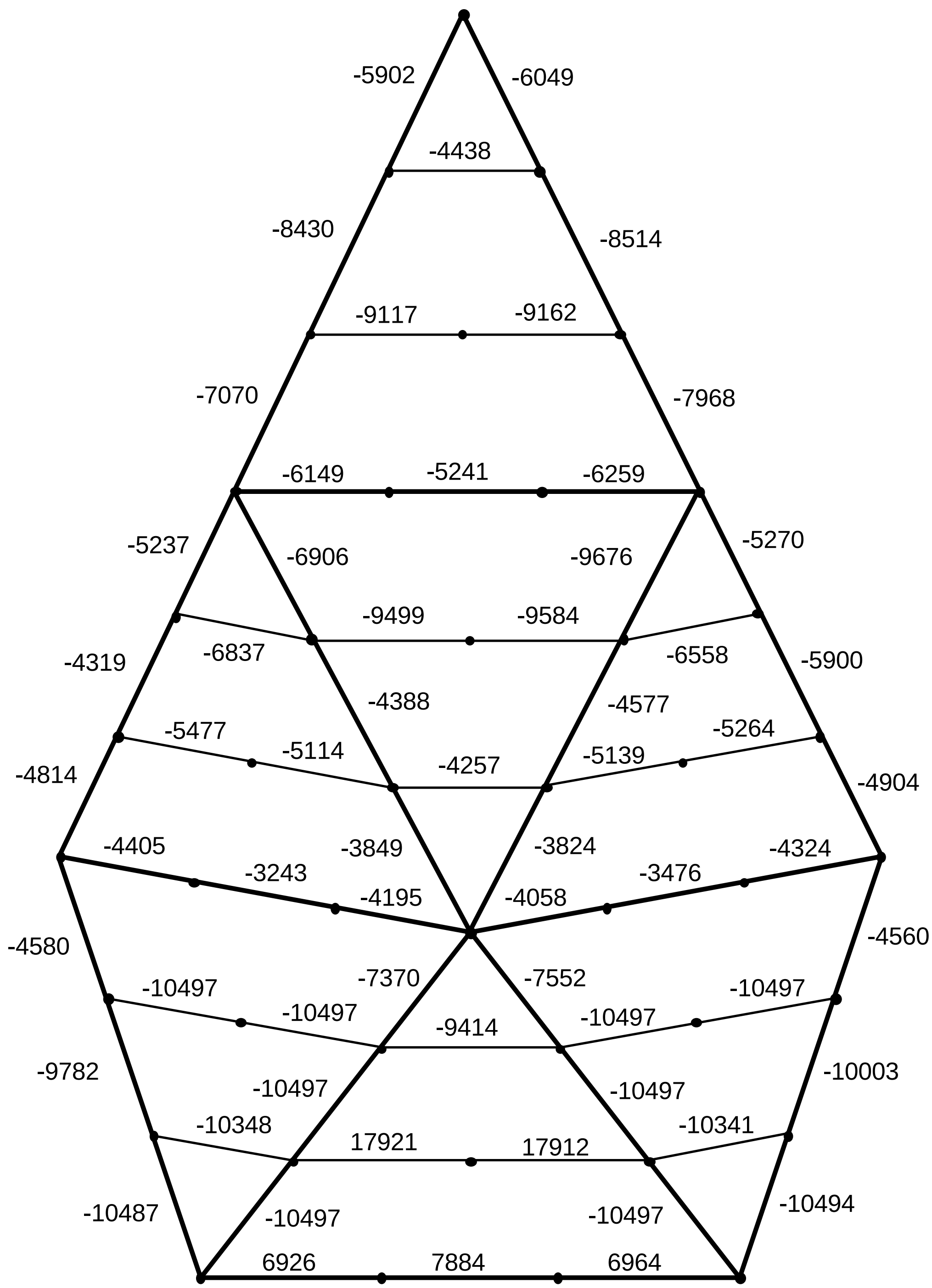

Figure 5.18 Maximum Stresses in psi just before Buckling for the Dome Model with Beam-Decking Connector Elements and Snow Load over Half the Dome

5.6 Effects of Variations in Joint Stiffness

One of the main objectives of this chapter is to find out the effects of variations in the joint stiffness on the response of the dome model. So far, all the joints in the dome models were considered to be rigid. The rigid joints do not reflect the real behavior of the joints because Varax joints have rotational stiffness (Fig. 4.3(b)). Variations in joint stiffness is simulated by varying the values of moments of inertia of beam-beam connector elements.

In the full snow load model, the contribution of the beam-connector elements to the load-carrying capacity of the dome model is more significant than that of the joint stiffness as shown in Table 5.3. The beam-connector elements are effective in increasing the critical load factor because they suppress the premature twist buckling of the dome model. The load-carrying capacity of the dome is not sensitive to variations in joint stiffness as shown in Table 5.3.

In the half snow load model, the effect of variations in the joint stiffness is significant for the dome models without decking as shown in Table 5.4. The critical load factor, λ_{cr}, is reduced from 4.7 for the rigid joints to 2.7 for the joints with 25% of moments of inertia of beam. Variations in the joint stiffness have little effect on the buckling load in the presence of beam-decking connectors.

Table 5.3 Snow over entire dome: $p_{cr} = p_D + \lambda_{cr} p_L$

Beam-Beam Joint Stiffness	**λ_{cr} without effect of decking**	**λ_{cr} with effect of decking**
rigid	5.0	11.0
75%*	4.4	10.7
50%*	4.4	10.5
25%*	4.0	9.4

*% of moments of inertia of beam

Table 5.4 Snow over half the dome: $p_{cr} = p_D + \lambda_{cr} p_L$

Beam-Beam Joint Stiffness	**λ_{cr} without effect of decking**	**λ_{cr} with effect of decking**
rigid	4.7	8.4
75%*	4.1	8.4
50%*	3.1	8.4
25%*	2.7	8.3

*% of moments of inertia of beam

5.7 Summary

The Church of the Nazarene dome in Corvallis, Oregon, is analyzed with the finite element stability method to determine the governing failure mode and ultimate snow loads. Modeling considerations include 3-D beam finite elements, transverse isotropy, beam-decking connectors, geometric and material nonlinearities, variations of joint stiffness, load discretization, and boundary conditions.

The effect of the beam-decking connectors contributes significantly to the ultimate load capacity of the dome model. The failures of the beam-decking connectors (nails) seem to trigger failure of the dome model.

The effect of variations in the beam-beam joint stiffness is significant for the dome models without decking. The critical load pressure decreases as the flexibility of the joints increases. The critical load factors vary little with changes in the beam-beam joint stiffness in the presence of beam-decking connectors.

Chapter 6

Simplified Analysis of the Dome Models

6.1 Introduction

It is very expensive and time-consuming to model and analyze a large structure with the nonlinear finite element method. One primary objective of this study is to develop a finite element model of the dome that is sufficiently simple to use in engineering practice and still produces useful results. From the nonlinear analysis of the dome models, it was determined that the beam-decking connectors form the weakest link of the dome. It was concluded that connector failures triggered the failure of the entire dome. For this reason, it is proposed that the dome be analyzed with one critical beam, located near the bottom of the dome sector as shown in Figure 6.1.

6.2 Nonlinear Analysis of Single Curved Beam

From the nonlinear analyses, the critical beams are located near the bottom of each sector of the dome. Since the nonlinear analysis of the entire dome is tedious, it is hypothesized that the critical load factor of the dome can be predicted by analyzing one of the critical beams. The curved beam located near the bottom of the dome sector is modeled as a Timoshenko beam using 2-element and 4-element meshes. The beam-decking connector elements are included to model the lateral restraint provided by the decking. Since the failure of the beam-decking connectors of the dome model is so dominant, material nonlinearity can be ignored in the analysis of the single curved beam model.

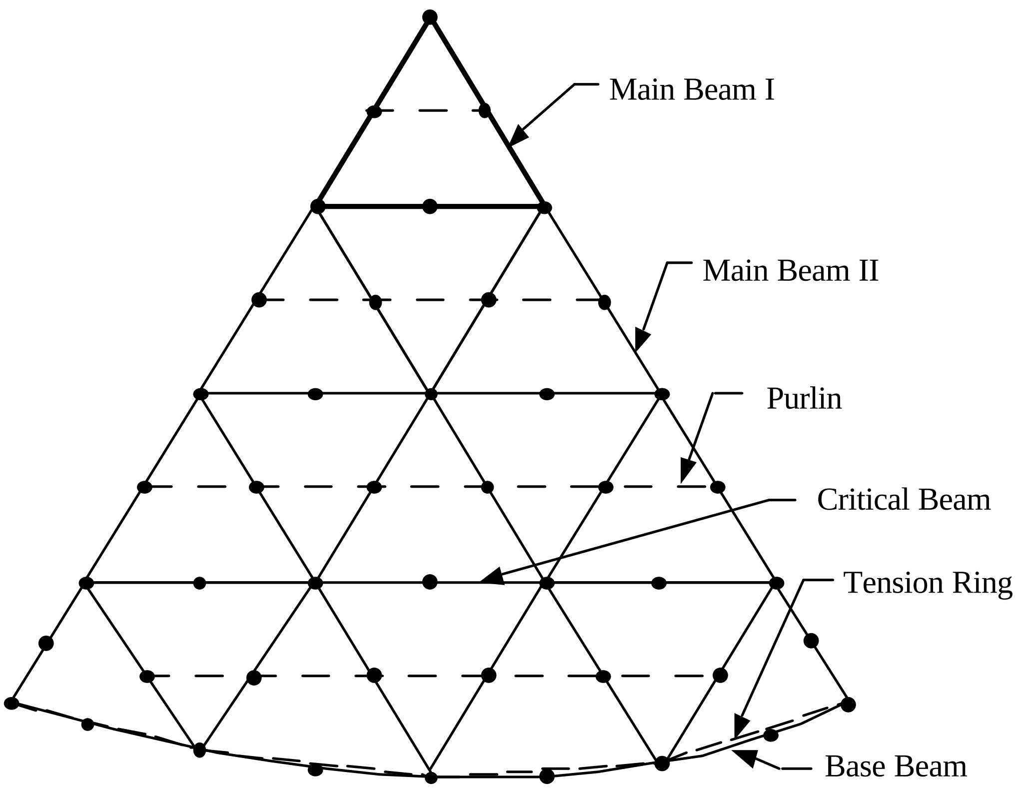

(a) Dome Sector

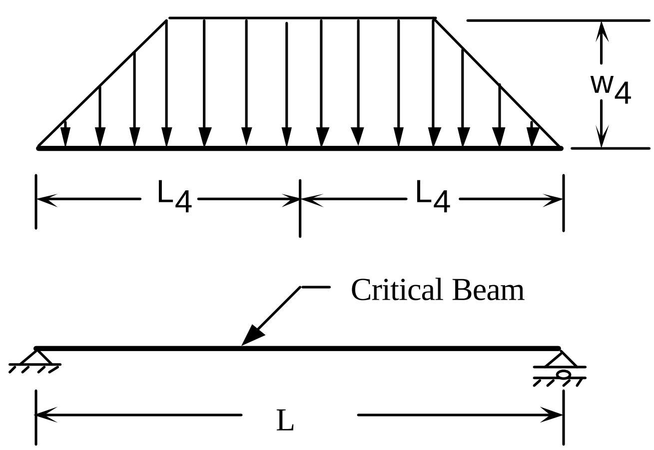

(b) Critical Beam with its Loading

Figure 6.1 Modeling of Dome with Single Curved Beam

6.2.1 Modeling of Single Curved Glulam Beam with ABAQUS

A 3-dimensional, isoparametric beam element, B32 in ABAQUS, is chosen to model the curved beam of the dome because the discretization of loads for Mindlin's (Timoshenko) beam theory produces no moments at each node which is consistent with the discretization of loads for the shell elements of the dome model. The longitudinal elastic modulus and the shear modulus are taken as $E = 1.8 \times 10^6$ psi and $G = 1.6 \times 10^5$ psi (Davalos, 1989).

6.2.2 Discretization of Loads

The concept of tributary areas (Figure 6.2) is used to compute distributed loads on the beams (Davalos, 1989). The distributed member loads are then discretized into nodal forces. The pressure loads used in the analyses are composed of the dead load pressure of 16 psf (766 Pa) and the live load pressure of 20 psf (958 Pa). The coordinates, displacements, and rotations for a 3-noded element (Figure 6.3) are interpolated in terms of the corresponding nodal values as (Bathe, 1982)

$$\mathbf{x} = \sum_{i=1}^{3} \mathbf{N}_i \mathbf{x}_i, \quad \mathbf{v} = \sum_{i=1}^{3} \mathbf{N}_i \mathbf{v}_i, \quad \boldsymbol{\theta} = \sum_{i=1}^{3} \mathbf{N}_i \boldsymbol{\theta}_i \qquad (6.1)$$

where
- x_i = x-coordinate of node i
- v_i = displacement of node i
- θ_i = rotation of node i
- N_i = interpolation function of node i

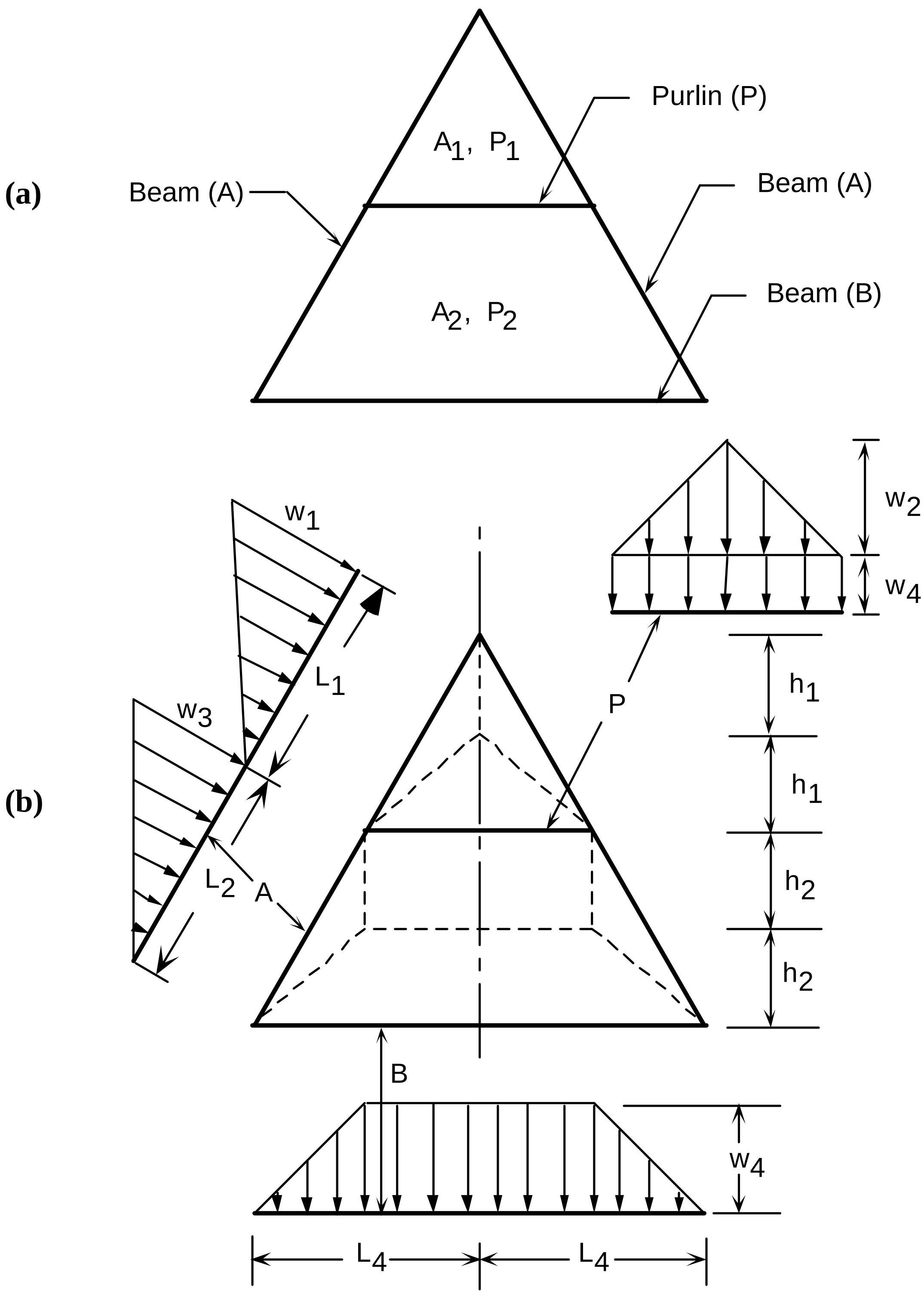

Figure 6.2 (a). Dome Panel; (b). Load Tributary Areas

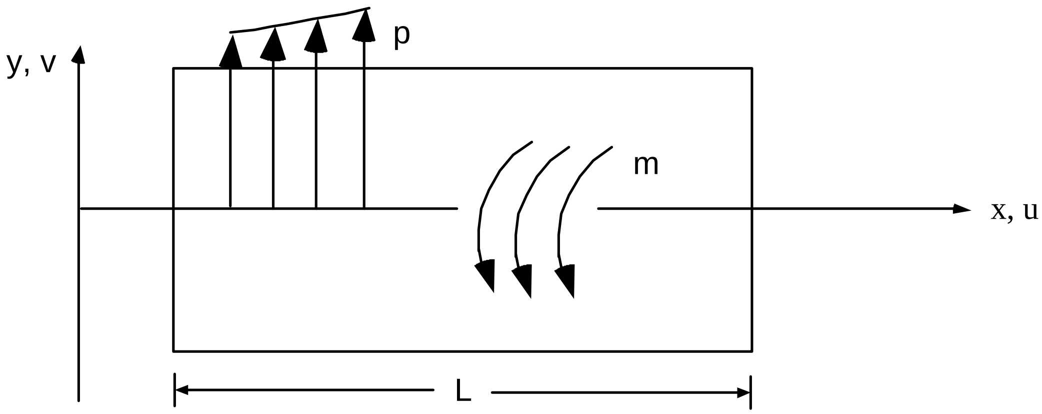

(a) Beam with Applied Loads

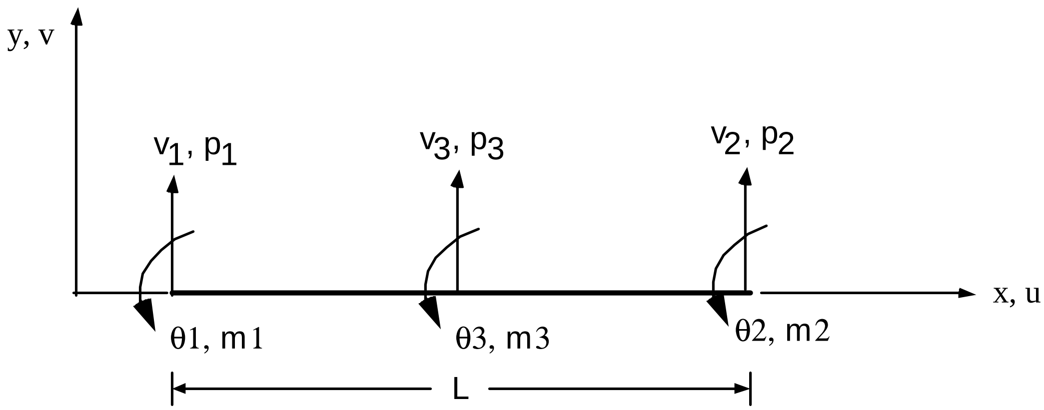

(b) 3-Node Beam Element

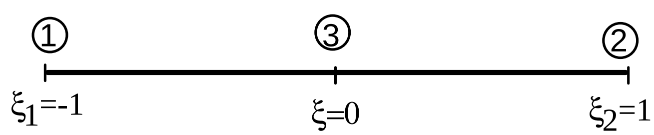

(c) Parent Element

Figure 6.3 Timoshenko Beam Element

The Lagrange quadratic interpolation functions for a 3-noded element are given as (Bathe, 1992)

$$
\begin{aligned}
N_1 &= -\frac{\xi}{2}(1-\xi) \\
N_2 &= \frac{\xi}{2}(1+\xi) \\
N_3 &= (1-\xi^2)
\end{aligned}
\tag{6.2}
$$

For the Mindlin-Timoshenko beam element , the displacements v and rotation θ are interpolated independently as shown in Eq. (6.1), but they are related to the shear strain by

$$\gamma(x,y) = \frac{dv}{dx} - \theta \tag{6.3}$$

The equivalent nodal forces and moments are also interpolated independently from distributed loads and moments as

$$f_{pi} = \int_{x_1}^{x_2} N_i\, p(x)\, dx \ , \quad i = 1,2,3 \tag{6.4}$$

$$f_{mi} = \int_{x_1}^{x_2} N_i\, m(x)\, dx\, , \quad i = 1,2,3 \tag{6.5}$$

For a straight beam element, the mid-node is given as

$$x_3 \quad = \quad \frac{1}{2}(x_1 + x_2) \tag{6.6}$$

The coordinates of the beam can be expressed from Eqs. (6.1), (6.2), and (6.6) as

$$\begin{aligned} x \quad &= \quad N_1 x_1 + N_2 x_2 + N_3 x_3 \\ &= \quad N_1 x_1 + N_2 x_2 + \frac{1}{2} N_3 (x_1 + x_2) \\ &= \quad \frac{1}{2}(1-\xi)x_1 + \frac{1}{2}(1+\xi)x_2 \end{aligned} \tag{6.7}$$

The derivative of x can be expressed from Eq. (6.7) as

$$dx \quad = \quad \frac{1}{2}(x_2 - x_1)d\xi \quad = \quad \frac{L}{2}d\xi \tag{6.8}$$

For a uniform distributed load p, the nodal forces can be computed from Eqs. (6.4) and (6.8) as

$$f_{pi} \quad = \quad \frac{L}{2} p \int_{-1}^{1} N_i \, d\xi \qquad , \quad i = 1,2,3 \tag{6.9}$$

The uniform distributed load p is discretized into the equivalent nodal forces as

$$
\begin{aligned}
f_{p1} &= \frac{1}{6}pL \\
f_{p2} &= \frac{1}{6}pL \\
f_{p3} &= \frac{2}{3}pL
\end{aligned}
\tag{6.10}
$$

as shown Figure 6.4a.

For a triangular load distribution as shown in Figure 6.4b, the load distribution is given as

$$
\begin{aligned}
p(x) &= \frac{p}{L}(x - x_1) \\
&= \frac{p}{L}.\frac{L}{2}(1+\xi) \\
&= \frac{p}{2}(1+\xi)
\end{aligned}
\tag{6.11}
$$

The equivalent nodal forces can be expressed from Eqs. (6.4), (6.8), and (6.11) as

$$
\begin{aligned}
f_{pi} &= \int_{-1}^{1} N_i \frac{p}{2}(1+\xi)\frac{L}{2}d\xi \\
&= \frac{pL}{4}\int_{-1}^{1} N_i (1+\xi)d\xi
\end{aligned}
\tag{6.12}
$$

where $i = 1,2,3$.

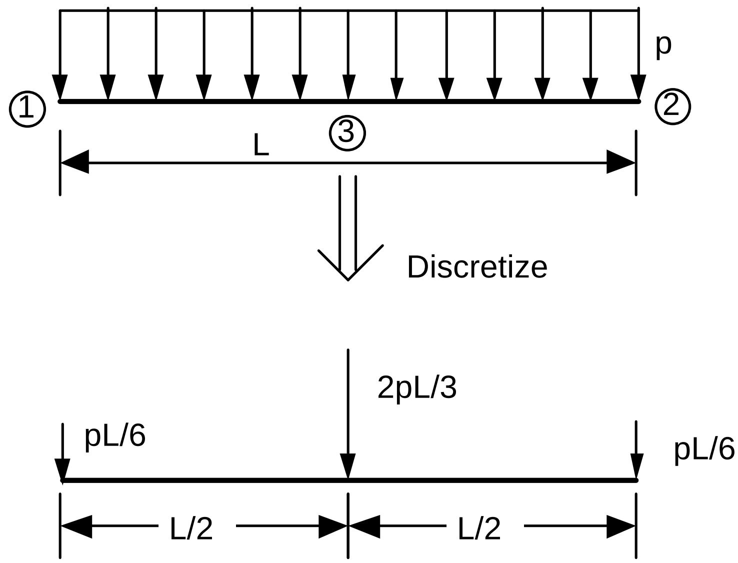

(a) Discretization of Uniform Distributed Load

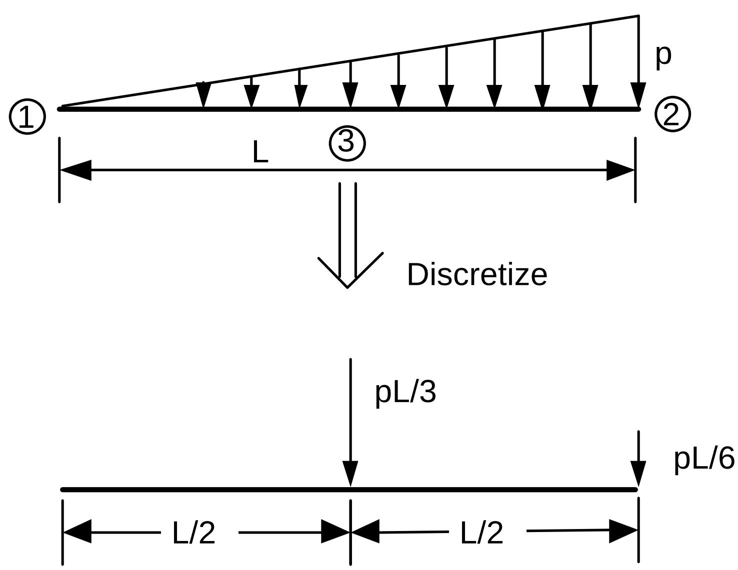

(b) Discretization of Triangular Distributed Load

Figure 6.4 Equivalent Nodal Forces.

The triangular load distribution is discretized into the equivalent nodal forces as

$$
\begin{aligned}
f_{p1} &= 0 \\
f_{p2} &= \frac{1}{6}pL \\
f_{p3} &= \frac{1}{3}pL
\end{aligned}
\tag{6.13}
$$

as shown Figure 6.4b.

6.2.3 Boundary Conditions

Since the Triax joint is a pin joint, the simply supported boundary condition was applied to the beam. Other boundary conditions such as fixed-fixed and fixed-pinned supports were also applied to the beam; however, only the simply supported boundary condition gave results close to the results from the entire dome analysis.

6.3 Results of Single Beam Model

A beam-decking connector element (nail) fails when its deflection reaches 1 in. A FORTRAN program was written to compute the nail deflections of the beam. There are 16 connector elements per finite element beam (Fig. 3.3). Based on the analyses of the dome model, the critical load of the beam is reached when about half of the nails have failed. The critical loads from the single beam model with 2-element and 4-element meshes are 10.8 and 8.8, respectively, compared to 9.0 from the nonlinear analysis of the entire dome model.

6.4 Summary

Analyzing large structures with the nonlinear finite element can be very time-consuming and expensive. The analysis of a single curved beam can be used to get a reasonable estimate of the critical load pressures of the dome. The critical beams are generally located near the bottom of each sector of the dome (Fig. 6.1a). Material nonlinearity can be ignored in the analysis of the single curved beam model. The beam is supported by simple supports. The critical load of the beam is reached when about half of the nails have failed.

Chapter 7

Conclusions and Recommendations

7.1 Conclusions

Finite element models based on the Crafts Pavilion dome (Triax) in Raleigh, North Carolina, and the Church of the Nazarene dome (Varax) in Corvallis, Oregon, were analyzed in this study. The analysis results presented focused on three issues: (1) the results of nonlinear stability analysis, (2) the effect of decking on the behavior of the dome, and (3) the effect of variations in the joint stiffness on the response of the dome model. Modeling considerations included 3-d beam finite elements, transverse isotropy, torsional warping, beam-decking connectors, beam-beam connectors, geometric and material nonlinearities, and the discretization of pressure loads.

The following conclusions can be drawn from this study:

1. The beam-decking connectors contribute significantly to the ultimate load capacity of the dome model. The failures of the beam-decking connectors (nails) seem to trigger failure of the dome model.

2. The effect of variations in the joint stiffness is significant for the dome models without decking. The critical load pressure decreases as the flexibility of the joints increases. For the dome model with beam-decking connectors, the critical load factors vary little with changes in the joint stiffness.

3. Material nonlinearity is not a factor for the dome models with snow load over the entire dome. The nonlinear material behavior is closely linked with the failure mode for the dome model with snow over half of the dome.

4. The unsymmetric load condition (uniform snow load over half of the dome) produces the most critical load pressures.

5. The analysis of a single curved beam can be used to get a rough estimate of the critical load pressures of the dome. The critical beams are generally located near the bottom of each sector of the dome (Fig. 6.1a). Material nonlinearity can be ignored in the analysis of the single curved beam model. The beam is supported by simply supports. The critical load of the beam is reached when about half of the nails have failed.

7.2 Recommendations

1. A 3-dimensional beam-decking connector element should be formulated to study the behavior in the parallel, perpendicular, and withdrawal directions with respect to the beam element.

2. Experimental tests should be conducted to obtain the nonlinear normal stress-strain relation for southern pine glued laminated timber.

3. Special load cases, such as snow concentrations and special hanging loads, should be investigated to determine the most critical load combination.

4. The effect of imperfections , such as material variability, support settlements, and fabrication errors should be studied.

5. It is possible that the effect of the decking has been overestimated in the analysis of the dome models. Therefore, experimental tests should be conducted on a scaled glulam dome model to verify the analytical results.

REFERENCES

American Institute of Timber Construction, *Timber Construction Manual*, 3rd edition, John Wiley & Sons, Inc., New York, 1985.

ASCE Standard, ASCE 7-93, *Minimum Designs Loads for Buildings and Other Structures*, American Society of Civil Engineers, New York, New York, 1994

ABAQUS, *General-Purpose Finite Element System*, Hibbitt, Karlsson and Sorensen, Inc., 1080 Main Street, Pawtucket, RI 02906, 1995.

Bathe,K.J., Finite Element Procedures in Engineering Analysis, Prentice-Hall, Inc., Englewood Cliffs, New Jersey, 1982.

Brendel, B., Zur Geometrisch Nichtlinearten Elastostabilität, Dissertation, Universitat Stuttgart, 1979.

Brendel, B., and Ramm, E., "Linear and Nonlinear Stability Analysis of Cylindrical Shells," *Computers and Structures*, Vol. 12, 1980, pp. 549-558.

Brendel, B. and Ramm, E., "Nichtlineare Stabilitätsuntersuchungen mit der methode der Finiten Elemente", Ingenieur-Archiv, Vol. 51, 1982, pp. 337-362

Broyles, D. L., *Triax Dome Modeling with I-DEAS 4.1*, M.S. thesis, Virginia Polytechnic Institute and State University, Blacksburg, VA, January 1990.

Conners, T. E., "Segmented Models for Stress-Strain Diagrams," *Wood Science and Technology*, Vol. 23, 1989, pp. 65-73.

Cook, R. D., Malkus, D. S., and Plesha, M. E., *Concepts and Applications of Finite Element Analysis*, 3rd edition, John Wiley and Sons, New York, 1989.

Davalos, J. F., *Geometrically Nonlinear Finite Element Analysis of a Glulam Timber Dome*, Ph.D. Dissertation, Virginia Polytechnic Institute and State University, Blacksburg, VA, July, 1989.

Davalos, J. F., Loferski, J. R., Holzer, S. M., and Yadama, V., "Transverse Isotropy Modeling of 3-d Glulam Timber Beams," *Journal of Materials in Civil Engineering*, ASCE, Vol. 3, No. 2, May 1991, pp. 125-139.

Dolan, J. D., *The Dynamic Response of Timber Shear Walls*, Ph.D. Dissertation, The University of British Columbia, Vancouver, Canada, October 1989.

Eshelby, R. W., *Private Communication*, Western Wood Structures, P.O. Box 130, Tualatin, OR, 97062, 1988.

Eshelby, R. W. and Evans, R. J., “Design Procedures for Reticulated Timber Domes,” *Proceedings of the 1988 International Conference on Timber Engineering*, Seattle, Washington, Vol. 1, 1988, pp. 283-287.

European Convention for Constructional Steelwork, *Recommendations for Calculating the Effects of Wind on Constructions*, ECCS - Technical Committee 12, Wind, Second edition, 1987.

Gutshall, S. T., *Monotonic and cyclic short-term performance of nailed and bolted timber connections*, M.S. thesis, Virginia Polytechnic Institute and State University, Blacksburg, VA, 1994.

Holzer, S. M., Watson, L. T., and Vu, P., “Stability Analyses of Lamella Domes”, Long Span Roof Structures, Proceedings of the ASCE 1981 Annual Convention and Exhibit, Committee on Spatial Structures, Structural Division, ASCE, October 1981, pp. 179-209.

Holzer, S. M. and Loferski, J. R., “Background for Research on Glulam Lattice Domes” Proceedings of the Sixth Annual Structures Congress, ASCE Structural Division, Olando, Florida, August 1987, pp. 305-318.

Holzer, S. M., Davalos, J. F., and Huang, C. Y., “A Review of Finite Element Stability Investigations of Spatial Wood Structures,” *Bulletin of the International Association for Shell and Spatial Structures (IASS)*, Vol. 31, No. 3, November 1990, pp. 161-171.

Holzer, S. M., Wu, C. H., and Tissaoui, J., “Finite Element Stability Analysis of a Glulam Dome,” *International Journal of Space Structures*, Vol. 7, No. 4, 1992, pp. 353-361.

Holzer, S. M., Kavi, S. A., Tongtoe, S., and Dolan, J. D. “What Controls the Ultimate Load of a Glulam Dome?,” *Proceedings of the IASS Symposium ’94*, Atlanta, GA, April 23-28, 1994, pp. 86-96.

Holzer, S. M. and Tongtoe, S., “Finite Element Analysis of a Glulam Dome,” *Proceedings of the IASS Symposium ‘95*, Milan, Italy, June 5-9, 1995, pp. 1365-1372.

I-DEAS, “Engineering Analysis, Model Solution and Optimization”, *Structural Dynamics Research Corporation*, 2000 Eastman Drive, Milford, OH 45150, 1995.

Kavi, S. A., *Nonlinear 3-D Beam/Connector Finite Element with Warping for a Glulam Dome*, M.S. thesis, Virginia Polytechnic Institute and State University, Blacksburg, VA, October 1993.

Medwadowski, S. J., “Modern Spatial Wood Structures in the United States,” *Bulletin of the IASS*, Vol. XXII-2 (76), 1981, pp. 13-25.

Melaragno, M., “An Introduction to Shell Structures: The Art and Science of Vaulting”, Van Nostrand Reinhold, New York, N.Y.,1991.

Natterer, J., Goehl, J., and Henn, G., “Large Halls and Roof Structures,” in Goetz, K-H. et al., *Timber Design and Construction Sourcebook*, McGraw-Hill Inc., New York, NY, USA, 1989, pp. 75-172.

NDS, “National Design Specification for Wood Construction”, *National Forest Products Association*, 1250 Connecticut Avenue, N.W.,Washington, D.C. 20036, 1991.

Neal, D. W., *The Triax Dome*, Culbertson, Noren, and Neal, Consulting Engineers, 1410 S. W. Morrison St., Portland, Oregon 97205, March, 1993.

Sakamoto, I., “Wooden Spatial Structures in Japan,” *Bulletin of the IASS,* Vol. 33(109), 1992, pp. 109-119.

Sedlak, V., “The Use of Lightweight Timber Structures in Architecture,” *Proceedings of Pacific Timber Engineering Conference*, Gold Coast, Australia, Vol. 1, 1994, pp. 102-110.

Telang, N. M., *Stability Analysis of a Glulam Dome with Nonlinear Material Law*, M.S. thesis, Virginia Polytechnic Institute and State University, Blacksburg, VA, January 1992.

Tissaoui, J., *Stability Analysis of Church of the Nazarene Varax Dome*, M.S. thesis, Virginia Polytechnic Institute and State University, Blacksburg, VA, January 1992.

Tsang, M. T., *3-D Finite Element Beam/Connector Model for a Glulam Dome Cap*, M.S. thesis, Virginia Polytechnic Institute and State University, Blacksburg, VA, January 1992.

Tsuboi, Y., et al., “Analysis, Design and Realization of Space Frames,” A State-of-the-Art Report by I.A.S.S. Working Group on Spatial Steel Structures, *Bulletin of the International Association for Shell and Spatial Structures*, Vol. XXV-1/2, April-August 1984.

Timoshenko, S. P. and Goodier, J. N., *Theory of Elasticity*, McGraw-Hill, New York, 1970.

Varax Domes, *Specifications, Section 13500 Varax Dome Structure and Roof Decking,* Western Wood Structures, Inc., Tualatin, Oregon, 1986.

Varax Engineering Company, *Church of the Nazarene, Corvallis, Oregon,* Western Wood Structures, Inc., Tualatin, Oregon, 1986.

Wu, C. H., *Modeling and Stability Investigation of a Glulam Dome*, M.S. Thesis, Virginia Polytechnic Institute and State University, Blacksburg, VA 24061, 1991.

Whitlow, J. C., Modeling Beam Decking Connectors Under Failure Conditions, M.S. thesis, Virginia Polytechnic Institute and State University, Blacksburg, VA 24061, 1995.

Zhou, Q., *Combined Linear/Nonlinear Stability Analysis of Plane and Space Frames,* M.S. thesis, Virginia Polytechnic Institute and State University, Blacksburg, VA, June 1993.

Appendix A

```
*HEADING
SDRC I-DEAS ABAQUS FILE TRANSLATOR  18-Jun-96   16:45:
** COMPUTE DEAD LOAD OF THE VARAX DOME USING SHELL ELEMENTS
*NODE, SYSTEM=R, NSET=ALL
          1, 7.6044293E+02,-1.7356670E+02, 1.0047803E+03
          2, 6.0982715E+02,-4.8632285E+02, 1.0047803E+03
          .
          .
          .
        273,-2.7091470E+02,-5.6263470E+02, 1.1081642E+03
        274,-4.3722296E+02,-5.4831354E+02, 1.0612103E+03
*NSET,NSET=PER
          1,          2,         48,         49,         87,         88
        133,        134,        165,        166,        204,        205
        243,        244,
*TRANSFORM,NSET=PER,TYPE=C
 0.0000E+00, 0.0000E+00, 0.0000E+00, 0.0000E+00, 0.0000E+00, 1.0000E+00
*ELEMENT,TYPE=STRI3   ,ELSET=ASHELL
     64,      3,     11,      9
     65,     11,     12,     39
     .
     .
     .
    608,     11,    196,     12
    609,    171,    167,    173
    504,    148,    149,    162
*SHELL SECTION,ELSET=ASHELL,MATERIAL=M0000001
 0.001    3
*MATERIAL,NAME=M0000001
*ELASTIC,TYPE=ISOTROPIC
 2.999E+07 2.900E-01
*DENSITY
 7.317E-04
*EXPANSION,TYPE=ISO,ZERO=71.33
 6.500E-06
*CONDUCTIVITY,TYPE=ISO
 5.620E+00
*BOUNDARY
ALL,1,6
*STEP
 LINEAR ANALYSIS
*STATIC
*DLOAD
ASHELL,BZ,104.1667
*NODE PRINT, NSET=ALL
RF3
*END STEP
```

Appendix B

```
*HEADING
COMPUTE SNOW LOAD OF THE VARAX DOME USING SHELL ELEMENTS
*NODE, SYSTEM=R, NSET=ALL
     1, 7.6044293E+02,-1.7356670E+02, 1.0047803E+03
     2, 6.0982715E+02,-4.8632285E+02, 1.0047803E+03
     .
     .
     .
   272,-4.8820590E+02,-3.8936826E+02, 1.0047803E+03
   273,-2.7091470E+02,-5.6263470E+02, 1.0047803E+03
   274,-4.3722296E+02,-5.4831354E+02, 1.0047803E+03
*NSET,NSET=PER
     1,      2,     48,     49,     87,     88
   133,    134,    165,    166,    204,    205
   243,    244,
*TRANSFORM,NSET=PER,TYPE=C
 0.0000E+00, 0.0000E+00, 0.0000E+00, 0.0000E+00, 0.0000E+00, 1.0000E+00
*ELEMENT,TYPE=STRI3   ,ELSET=ASHELL
   64,    3,   11,    9
   65,   11,   12,   39
   66,   11,   39,    9
   .
   .
   .
  609,  171,  167,  173
  504,  148,  149,  162
*SHELL SECTION,ELSET=ASHELL,MATERIAL=M0000001
 0.001   3
*MATERIAL,NAME=M0000001
*ELASTIC,TYPE=ISOTROPIC
 2.999E+07 2.900E-01
*DENSITY
 7.317E-04
*EXPANSION,TYPE=ISO,ZERO=71.33
 6.500E-06
*CONDUCTIVITY,TYPE=ISO
 5.620E+00
*BOUNDARY
ALL,1,6
*STEP
 LINEAR ANALYSIS
*STATIC
*DLOAD
ASHELL,BZ,173.6111
*NODE PRINT, NSET=ALL
RF3
*END STEP
```

Appendix C

```
C=====================================================================
C     PROGRAM TO DETERMINE THE DIRECTION COSINES OF THE BEAMS AND
C     PURLINS OF THE CHURCH OF THE NAZARENE VARAX DOME
C=====================================================================
C
      REAL XCOS(715),YCOS(715),ZCOS(715),XC(1700),YC(1700),ZC(1700),
     $      XCC(1700),YCC(1700),ZCC(1700), X(274),Y(274),Z(274)
      open(unit=55,file='allnodes.dat',status='old')
      open(unit=60,file='main.dat',status='old')
      open(unit=70,file='short.dat',status='old')
      open(unit=75,file='long.dat',status='old')
      open(unit=85,file='edge.dat',status='old')
      open(unit=88,file='el.out',status='unknown')
      open(unit=98,file='sec.out',status='unknown')
CC
      R = 1272.0
CC #################READ NODES
      DO 10 I=1,274
        READ (55,*) N, X(I), Y(I), Z(I)
10    CONTINUE
CC ################# READ MAIN BEAMS
      DO 20 J=1,231
        READ (60,*) NE, N1, N2
        XC(NE) =   Y(N1) * Z(N2) - Z(N1) * Y(N2)
        YC(NE) =  -X(N1) * Z(N2) + Z(N1) * X(N2)
        ZC(NE) =   X(N1) * Y(N2) - Y(N1) * X(N2)
        XNORM  = (XC(NE)**2+YC(NE)**2+ZC(NE)**2) ** 0.5
        XCC(NE) = XC(NE) / XNORM
        YCC(NE) = YC(NE) / XNORM
        ZCC(NE) = ZC(NE) / XNORM
        WRITE (88,200) NE
        WRITE (88,220) NE, N1, N2
        WRITE (98,230) NE
        WRITE (98,240)
        WRITE (98,250) XCC(NE),YCC(NE),ZCC(NE)
        WRITE (98,310)
        WRITE (98,320)
20    CONTINUE
CC ################# READ TOP PURLINS
      DO 30 II=1,56
        READ (70,*) NE, N1, N2
        XC(NE) =   Y(N1) * Z(N2) - Z(N1) * Y(N2)
        YC(NE) =  -X(N1) * Z(N2) + Z(N1) * X(N2)
        ZC(NE) =   X(N1) * Y(N2) - Y(N1) * X(N2)
        XNORM  = (XC(NE)**2+YC(NE)**2+ZC(NE)**2) ** 0.5
        XCC(NE) = XC(NE) / XNORM
        YCC(NE) = YC(NE) / XNORM
        ZCC(NE) = ZC(NE) / XNORM
```

```
      WRITE (88,200) NE
      WRITE (88,220) NE, N1, N2
      WRITE (98,230) NE
      WRITE (98,340)
      WRITE (98,250) XCC(NE),YCC(NE),ZCC(NE)
      WRITE (98,310)
      WRITE (98,320)
30    CONTINUE
CC ################# READ BOTTOM PURLINS
C
    DO 40 II=1,112
      READ (75,*) NE, N1, N2
      XC(NE) =   Y(N1) * Z(N2) - Z(N1) * Y(N2)
      YC(NE) =  -X(N1) * Z(N2) + Z(N1) * X(N2)
      ZC(NE) =   X(N1) * Y(N2) - Y(N1) * X(N2)
      XNORM  = (XC(NE)**2+YC(NE)**2+ZC(NE)**2) ** 0.5
      XCC(NE) = XC(NE) / XNORM
      YCC(NE) = YC(NE) / XNORM
      ZCC(NE) = ZC(NE) / XNORM
      WRITE (88,200) NE
      WRITE (88,220) NE, N1, N2
      WRITE (98,230) NE
      WRITE (98,440)
      WRITE (98,250) XCC(NE),YCC(NE),ZCC(NE)
      WRITE (98,310)
      WRITE (98,320)
40    CONTINUE
CC ################# READ EDGE   PURLINS
C
    DO 60 II=1,42
      READ (85,*) NE, N1, N2
      XC(NE) =   Y(N1) * Z(N2) - Z(N1) * Y(N2)
      YC(NE) =  -X(N1) * Z(N2) + Z(N1) * X(N2)
      ZC(NE) =   X(N1) * Y(N2) - Y(N1) * X(N2)
      XNORM  = (XC(NE)**2+YC(NE)**2+ZC(NE)**2) ** 0.5
      XCC(NE) = XC(NE) / XNORM
      YCC(NE) = YC(NE) / XNORM
      ZCC(NE) = ZC(NE) / XNORM
      WRITE (88,200) NE
      WRITE (88,220) NE, N1, N2
      WRITE (98,230) NE
      WRITE (98,540)
      WRITE (98,250) XCC(NE),YCC(NE),ZCC(NE)
      WRITE (98,310)
      WRITE (98,320)
60    CONTINUE
C
C
200   FORMAT (T1,'*ELEMENT,TYPE=B33,ELSET=E',T26,I3)
220   FORMAT (1X,I4,',',I4,',',I4)
230   FORMAT (T1,'*BEAM SECTION,SECTION=RECT,MATERIAL=WOOD,ELSET=E',T49,
```

```
     $        I3)
240   FORMAT (2X,'5.125,12.0')
250   FORMAT (1X,F9.4,',',F9.4,',',F9.4)
310   FORMAT ('*TRANSVERSE SHEAR STIFFNESS')
320   FORMAT (2X,'9972128.26, 9972128.26')
340   FORMAT (2X,'3.125,7.5')
440   FORMAT (2X,'5.125,7.5')
540   FORMAT (2X,'3.125,22.0')
      END
```

Appendix D

```
*HEADING
SDRC I-DEAS ABAQUS FILE TRANSLATOR  19-Jun-96   16:59:07
** VARAX DOME WITH FULL SNOW LOAD AND NONLINEAR MATERIAL LAW
*NODE, SYSTEM=R, NSET=ALL
         1, 7.6044293E+02,-1.7356670E+02, 1.0047803E+03
         2, 6.0982715E+02,-4.8632285E+02, 1.0047803E+03
         3, 0.0000000E+00, 0.0000000E+00, 1.2719993E+03
         .
         .
         .
       272,-4.8820590E+02,-3.8936826E+02, 1.1081630E+03
       273,-2.7091470E+02,-5.6263470E+02, 1.1081642E+03
       274,-4.3722296E+02,-5.4831354E+02, 1.0612103E+03
*NSET,NSET=PER
         1,          2,         48,         49,         87,         88
       133,        134,        165,        166,        204,        205
       243,        244,
*TRANSFORM,NSET=PER,TYPE=C
 0.0000E+00, 0.0000E+00, 0.0000E+00, 0.0000E+00, 0.0000E+00, 1.0000E+00
** -------------------------- TENSION RING
*ELEMENT,TYPE=C1D2    ,ELSET=RING
    455,     88,    205
    448,     49,    134
    444,      1,     48
    442,      2,      1
    453,    204,    243
    452,    244,    243
    451,    205,    204
    450,      2,    165
    449,    166,    165
    447,     87,    133
    446,    134,    133
    445,     88,     87
    443,     49,     48
    454,    166,    244
** ----------------------MAIN BEAMS
*ELEMENT,TYPE=B33,ELSET=E  1
    1,  21,  22
*ELEMENT,TYPE=B33,ELSET=E  2
    2,   6,  33
*ELEMENT,TYPE=B33,ELSET=E  3
    3,  33,  34
*ELEMENT,TYPE=B33,ELSET=E  4
    4,  34,   2
*ELEMENT,TYPE=B33,ELSET=E  5
    5,   3,   9
*ELEMENT,TYPE=B33,ELSET=E  6
    6,   9,  10
```

```
*ELEMENT,TYPE=B33,ELSET=E  7
    7,  10,   5
    .
    .
    .
    .
*ELEMENT,TYPE=B33,ELSET=E229
  229, 249, 245
*ELEMENT,TYPE=B33,ELSET=E230
  230, 248, 249
*ELEMENT,TYPE=B33,ELSET=E231
  231, 206, 248
** -------------------------- SHORT PURLINS
*ELEMENT,TYPE=B33,ELSET=E232
  232,  11,   9
*ELEMENT,TYPE=B33,ELSET=E233
  233,  21,  19
*ELEMENT,TYPE=B33,ELSET=E234
  234,  17,  15
    .
    .
    .
    .
*ELEMENT,TYPE=B33,ELSET=E285
  285, 223, 256
*ELEMENT,TYPE=B33,ELSET=E286
  286, 262, 190
*ELEMENT,TYPE=B33,ELSET=E287
  287, 118, 229
** -------------------------- LONG PURLINS
*ELEMENT,TYPE=B33,ELSET=E288
  288,  12,  39
*ELEMENT,TYPE=B33,ELSET=E289
  289,  39,  10
*ELEMENT,TYPE=B33,ELSET=E290
  290,  19,  40
    .
    .
    .
    .
*ELEMENT,TYPE=B33,ELSET=E397
  397, 259, 274
*ELEMENT,TYPE=B33,ELSET=E398
  398, 242, 257
*ELEMENT,TYPE=B33,ELSET=E399
  399, 263, 202
** ------------------------- EDGE BEAM
*ELEMENT,TYPE=B33,ELSET=E400
  400,  38,   2
*ELEMENT,TYPE=B33,ELSET=E401
  401,   2,  37
```

```
*ELEMENT,TYPE=B33,ELSET=E402
  402,  37,  36
    .
    .
    .
    .
*ELEMENT,TYPE=B33,ELSET=E439
  439, 231, 264
*ELEMENT,TYPE=B33,ELSET=E440
  440, 267, 195
*ELEMENT,TYPE=B33,ELSET=E441
  441, 123, 234
**-----------------------------------MAIN BEAM : B/C ELEMENTS
*USER ELEMENT,NODES=2,TYPE=U 1001,COORDINATES=3,PROPERTIES=7
1,2,3,4,5,6
*ELEMENT,TYPE=U 1001,ELSET=C 1001
 456,  21,  22
*UEL PROPERTY,ELSET=C 1001
16,6.000,13700.000,    1.000,0.0560,1.0000,768.00
*USER ELEMENT,NODES=2,TYPE=U 1002,COORDINATES=3,PROPERTIES=7
1,2,3,4,5,6
*ELEMENT,TYPE=U 1002,ELSET=C 1002
 457,   6,  33
*UEL PROPERTY,ELSET=C 1002
16,6.000,13700.000,    1.000,0.0560,1.0000,768.00
    .
    .
    .
    .
*USER ELEMENT,NODES=2,TYPE=U 1230,COORDINATES=3,PROPERTIES=7
1,2,3,4,5,6
*ELEMENT,TYPE=U 1230,ELSET=C 1230
 685, 248, 249
*UEL PROPERTY,ELSET=C 1230
16,6.000,13700.000,    1.000,0.0560,1.0000,768.00
*USER ELEMENT,NODES=2,TYPE=U 1231,COORDINATES=3,PROPERTIES=7
1,2,3,4,5,6
*ELEMENT,TYPE=U 1231,ELSET=C 1231
 686, 206, 248
*UEL PROPERTY,ELSET=C 1231
16,6.000,13700.000,    1.000,0.0560,1.0000,768.00
**-----------------------------------SHORT PURLINS:  B/C ELEMENTS
*USER ELEMENT,NODES=2,TYPE=U 1232,COORDINATES=3,PROPERTIES=7
1,2,3,4,5,6
*ELEMENT,TYPE=U 1232,ELSET=C 1232
 687,  11,   9
*UEL PROPERTY,ELSET=C 1232
16,3.750,13700.000,    1.000,0.0560,1.0000,768.00
*USER ELEMENT,NODES=2,TYPE=U 1233,COORDINATES=3,PROPERTIES=7
1,2,3,4,5,6
*ELEMENT,TYPE=U 1233,ELSET=C 1233
```

```
 688,  21,  19
*UEL PROPERTY,ELSET=C 1233
16,3.750,13700.000,    1.000,0.0560,1.0000,768.00
    .
    .
    .
    .
*USER ELEMENT,NODES=2,TYPE=U 1286,COORDINATES=3,PROPERTIES=7
1,2,3,4,5,6
*ELEMENT,TYPE=U 1286,ELSET=C 1286
 741, 262, 190
*UEL PROPERTY,ELSET=C 1286
16,3.750,13700.000,    1.000,0.0560,1.0000,768.00
*USER ELEMENT,NODES=2,TYPE=U 1287,COORDINATES=3,PROPERTIES=7
1,2,3,4,5,6
*ELEMENT,TYPE=U 1287,ELSET=C 1287
 742, 118, 229
*UEL PROPERTY,ELSET=C 1287
16,3.750,13700.000,    1.000,0.0560,1.0000,768.00
**-----------------------------------LONG PURLINS:  B/C ELEMENTS
*USER ELEMENT,NODES=2,TYPE=U 1288,COORDINATES=3,PROPERTIES=7
1,2,3,4,5,6
*ELEMENT,TYPE=U 1288,ELSET=C 1288
 743,  12,  39
*UEL PROPERTY,ELSET=C 1288
16,3.750,13700.000,    1.000,0.0560,1.0000,768.00
*USER ELEMENT,NODES=2,TYPE=U 1289,COORDINATES=3,PROPERTIES=7
1,2,3,4,5,6
*ELEMENT,TYPE=U 1289,ELSET=C 1289
 744,  39,  10
*UEL PROPERTY,ELSET=C 1289
16,3.750,13700.000,    1.000,0.0560,1.0000,768.00
    .
    .
    .
    .
*USER ELEMENT,NODES=2,TYPE=U 1398,COORDINATES=3,PROPERTIES=7
1,2,3,4,5,6
*ELEMENT,TYPE=U 1398,ELSET=C 1398
 853, 242, 257
*UEL PROPERTY,ELSET=C 1398
16,3.750,13700.000,    1.000,0.0560,1.0000,768.00
*USER ELEMENT,NODES=2,TYPE=U 1399,COORDINATES=3,PROPERTIES=7
1,2,3,4,5,6
*ELEMENT,TYPE=U 1399,ELSET=C 1399
 854, 263, 202
*UEL PROPERTY,ELSET=C 1399
16,3.750,13700.000,    1.000,0.0560,1.0000,768.00
**-----------------------------------BASE(EDGE) BEAMS : B/C ELEMENTS
*USER ELEMENT,NODES=2,TYPE=U 1400,COORDINATES=3,PROPERTIES=7
1,2,3,4,5,6
```

```
*ELEMENT,TYPE=U 1400,ELSET=C 1400
 855,  38,   2
*UEL PROPERTY,ELSET=C 1400
16,11.000,13700.000,    1.000,0.0560,1.0000,768.00
*USER ELEMENT,NODES=2,TYPE=U 1401,COORDINATES=3,PROPERTIES=7
1,2,3,4,5,6
*ELEMENT,TYPE=U 1401,ELSET=C 1401
 856,   2,  37
*UEL PROPERTY,ELSET=C 1401
16,11.000,13700.000,    1.000,0.0560,1.0000,768.00
     .
     .
     .
     .
*USER ELEMENT,NODES=2,TYPE=U 1440,COORDINATES=3,PROPERTIES=7
1,2,3,4,5,6
*ELEMENT,TYPE=U 1440,ELSET=C 1440
 895, 267, 195
*UEL PROPERTY,ELSET=C 1440
16,11.000,13700.000,    1.000,0.0560,1.0000,768.00
*USER ELEMENT,NODES=2,TYPE=U 1441,COORDINATES=3,PROPERTIES=7
1,2,3,4,5,6
*ELEMENT,TYPE=U 1441,ELSET=C 1441
 896, 123, 234
*UEL PROPERTY,ELSET=C 1441
16,11.000,13700.000,    1.000,0.0560,1.0000,768.00
************************** MAIN BEAMS
*BEAM SECTION,SECTION=RECT,MATERIAL=WOOD,ELSET=E  1
  5.125,12.0
    0.7818,   0.6235,   0.0000
*BEAM SECTION,SECTION=RECT,MATERIAL=WOOD,ELSET=E  2
  5.125,12.0
    0.3400,   0.9107,   0.2345
*BEAM SECTION,SECTION=RECT,MATERIAL=WOOD,ELSET=E  3
  5.125,12.0
    0.3399,   0.9107,   0.2345
    .
    .
    .
    .
*BEAM SECTION,SECTION=RECT,MATERIAL=WOOD,ELSET=E229
  5.125,12.0
    0.9468,  -0.2677,   0.1786
*BEAM SECTION,SECTION=RECT,MATERIAL=WOOD,ELSET=E230
  5.125,12.0
    0.9468,  -0.2677,   0.1786
*BEAM SECTION,SECTION=RECT,MATERIAL=WOOD,ELSET=E231
  5.125,12.0
    0.9468,  -0.2677,   0.1786
************************** SHORT PURLINS
*BEAM SECTION,SECTION=RECT,MATERIAL=WOOD,ELSET=E232
```

```
 3.125,7.5
  -0.8986,   0.4327,   0.0726
*BEAM SECTION,SECTION=RECT,MATERIAL=WOOD,ELSET=E233
 3.125,7.5
  -0.7468,   0.5955,   0.2960
*BEAM SECTION,SECTION=RECT,MATERIAL=WOOD,ELSET=E234
 3.125,7.5
  -0.9312,   0.2125,   0.2960
   .
   .
   .
   .
*BEAM SECTION,SECTION=RECT,MATERIAL=WOOD,ELSET=E284
 3.125,7.5
   0.6495,   0.5180,   0.5566
*BEAM SECTION,SECTION=RECT,MATERIAL=WOOD,ELSET=E285
 3.125,7.5
   0.7845,   0.3778,   0.4918
*BEAM SECTION,SECTION=RECT,MATERIAL=WOOD,ELSET=E286
 3.125,7.5
   0.1937,   0.8489,   0.4918
************************* LONG  PURLINS
*BEAM SECTION,SECTION=RECT,MATERIAL=WOOD,ELSET=E287
 3.125,7.5
   0.7845,  -0.3778,   0.4918
*BEAM SECTION,SECTION=RECT,MATERIAL=WOOD,ELSET=E288
 5.125,7.5
  -0.8916,   0.4294,   0.1441
*BEAM SECTION,SECTION=RECT,MATERIAL=WOOD,ELSET=E289
 5.125,7.5
  -0.8916,   0.4294,   0.1441
   .
   .
   .
   .
   .
*BEAM SECTION,SECTION=RECT,MATERIAL=WOOD,ELSET=E397
 5.125,7.5
   0.5201,   0.6523,   0.5513
*BEAM SECTION,SECTION=RECT,MATERIAL=WOOD,ELSET=E398
 5.125,7.5
   0.7516,   0.3620,   0.5513
*BEAM SECTION,SECTION=RECT,MATERIAL=WOOD,ELSET=E399
 5.125,7.5
   0.1856,   0.8134,   0.5513
************************* EDGE BEAMS
*BEAM SECTION,SECTION=RECT,MATERIAL=WOOD,ELSET=E400
 3.125,22.0
  -0.4972,   0.6234,   0.6035
*BEAM SECTION,SECTION=RECT,MATERIAL=WOOD,ELSET=E401
 3.125,22.0
```

```
   -0.7184,   0.3460,   0.6035
*BEAM SECTION,SECTION=RECT,MATERIAL=WOOD,ELSET=E402
  3.125,22.0
   -0.7184,   0.3460,   0.6035
    .
    .
    .
    .
*BEAM SECTION,SECTION=RECT,MATERIAL=WOOD,ELSET=E439
  3.125,22.0
    0.7184,   0.3460,   0.6035
*BEAM SECTION,SECTION=RECT,MATERIAL=WOOD,ELSET=E440
  3.125,22.0
    0.1774,   0.7774,   0.6035
*BEAM SECTION,SECTION=RECT,MATERIAL=WOOD,ELSET=E441
  3.125,22.0
    0.7184,  -0.3459,   0.6035
*SOLID SECTION, ELSET=RING , MATERIAL=STEEL
5.0
*MATERIAL, NAME=STEEL
*ELASTIC
 2.9E+07, 0.3
*MATERIAL, NAME=WOOD
*USER MATERIAL, CONSTANT=3
 12.00, 0.52, 0.33
*BOUNDARY
    PER , 2
    PER , 3
**--------------------------------------------------NEWTON RAP. STEP
*STEP, NLGEOM, INC=10
*STATIC
0.5, 1., 0.0
*CONTROLS, PARAMETER=FIELD, FIELD=DISPLACEMENT
1.,1.,,9.
*CONTROLS, PARAMETER=FIELD, FIELD=ROTATION
1.,1.,,2000.
*CLOAD,OP=NEW
       1     , 3, -438.2
       2     , 3, -438.2
       3       , 3, -998.3
       4       , 3, -821.9
       5       , 3, -822.0
       6       , 3, -731.0
       7       , 3, -861.4
       8       , 3, -731.2
       9       , 3, -847.0
      10       , 3, -822.3
      11       , 3, -847.0
      .
      .
      .
```

```
 .
 271      , 3, -699.7
 272      , 3, -823.3
 273      , 3, -823.3
 274      , 3, -1078.
*PRINT, RESIDUAL=NO
*NODE PRINT,SUMMARY=NO,FREQUENCY=30
U
*EL PRINT , SUMMARY=NO,POSITION=NODES  ,FREQUENCY=39
S
*EL PRINT ,SUMMARY=NO,FREQUENCY=100
SF
*NODE FILE,NSET=ALL,FREQUENCY=5
U
*END STEP
**   APPLY  SNOW LOAD(25 PSF)
**-------------------------------------------------------RIKS STEP
*STEP, NLGEOM,INC=30
*STATIC,RIKS
0.1, 1., 0.0, ,20.0
*CONTROLS, PARAMETER=FIELD, FIELD=DISPLACEMENT
1.,1.,,7.
*CONTROLS, PARAMETER=FIELD, FIELD=ROTATION
1.,1.,,2000.
**----------------------------------------DEAD LOAD + FULL SNOW LOAD
*CLOAD
   1    , 3, -438.2
   2    , 3, -438.2
   3      , 3, -998.3
   4      , 3, -821.9
   5      , 3, -822.0
   .
   .
   .
   .
 270      , 3, -699.7
 271      , 3, -699.7
 272      , 3, -823.3
 273      , 3, -823.3
 274      , 3, -1078.
 1  , 3, -588.8
 2  , 3, -588.8
 3  , 3, -1662.
 4  , 3, -1329.
 5  , 3, -1329.
 6  , 3, -1093.
 7  , 3, -1293.
 .
 .
 .
 .
```

```
  270  , 3, -1089.
  271  , 3, -1089.
  272  , 3, -1197.
  273  , 3, -1197.
  274  , 3, -1502.
**-------------------------------------NODE, ELEMENT SETS AND OUTPUTS
*NSET, NSET=APEX
3
*ELSET, ELSET=ESECTOR
35,36,37,38,39,40,77,78,79,80,81,82,107
108,109,110,111,112,113,114,115,116
117,118,119,120,121,122,123,124,125
126,127,128,129,130,131,132,133,254
255,256,257,258,259,260,336,337,338,
339,340,341,342,343,344,345,346,347,
348,349,417,418,419
*PRINT,RESIDUAL=NO
*NODE PRINT,FREQUENCY=38, SUMMARY=NO
U
*NODE FILE ,FREQUENCY=3
 U
*END STEP
*USER SUBROUTINE
*************************************************************************
******       SUBROUTINE TO TEST USER SUBROUTINE UMAT          ********
******                 NONLINEAR    MATERIAL   LAW                  ********
******                  NIKET M. TELANG                              ********
*************************************************************************
C
      SUBROUTINE UMAT(STRESS,STATEV,DDSDDE,SSE,SPD,SCD,
     1 RPL,DDSDDT,DRPLDE,DRPLDT,
     2 STRAN,DSTRAN,TIME,DTIME,TEMP,DTEMP,PREDEF,DPRED,CMNAME,
     3 NDI,NSHR,NTENS,NSTATV,PROPS,NPROPS,COORDS,DROT,PNEWDT,
     4 CELENT,DFGRD0,DFGRD1,NOEL,NPT,LAYER,KSPT,KSPTEP,KINC)
C
      INCLUDE 'ABA_PARAM.INC'
C
      CHARACTER*8 CMNAME
C
C
      DIMENSION STRESS(NTENS),STATEV(NSTATV),
     1 DDSDDE(NTENS,NTENS),DDSDDT(NTENS),DRPLDE(NTENS),
     2 STRAN(NTENS),DSTRAN(NTENS),TIME(2),PREDEF(1),DPRED(1),
     3 PROPS(NPROPS),COORDS(3),DROT(3,3),DFGRD0(3,3),DFGRD1(3,3)
C     DIMENSION DSTRES(2)
C
C
       DO 20 I=1,NTENS
         DO 10 J=1,NTENS
           DDSDDE(I,J)=0.0
10        CONTINUE
```

```
20    CONTINUE
C
C       SG=0.5200
C       WMC=12.0000
C
C       *LONGITUDINAL STRESS*
C
C
      TS=0.0
      TS=STRAN(1) + DSTRAN(1)
C
C      *TENSION ZONE*
C
      IF(TS .GT. 0.0)THEN
C
         BETA1=1805365.6
         BETA2=1934700.0
         BETA3=-45146768.0
         AK1=1.43237E-03
         AK2=0.02143
         ALFA1=-92.62689
         ALFA2=10496.5409
C
         IF(TS .LT. AK1)THEN
            DDSDDE(1,1)=BETA1
            STRESS(1)=BETA1*TS
         ELSEIF(TS .GE. AK1)THEN
            DDSDDE(1,1)= BETA2 + (2.*BETA3*TS)
            STRESS(1)=ALFA1 + BETA2*TS + BETA3*(TS**2)
         ENDIF
C
C      *COMPRESSION   ZONE*
C
      ELSEIF(TS .LE. 0.0)THEN
CC
         BETA1=2195036.0
         BETA2=3229460.0
         BETA3=-222916014.1
         AK1=2.3202E-03
         AK2=7.24367E-03
         ALFA2=10496.5409
         ALFA1=-1200.03
CC
         AK1C=-AK1
         AK2C=-AK2
CC       AK2C=-6.441551051E-03
         IF(TS .GE. AK1C)THEN
            DDSDDE(1,1)=BETA1
            STRESS(1)=-BETA1*ABS(TS)
         ELSEIF(TS .LT. AK1C  .AND. TS .GE. AK2C)THEN
            DDSDDE(1,1)=BETA2 + 2.*BETA3*ABS(TS)
```

```
          STRESS(1)=-(ALFA1 + BETA2*ABS(TS) +
     1            BETA3*((ABS(TS))**2))
        ELSEIF(TS .LT. AK2C)THEN
          DDSDDE(1,1)=0.0
          STRESS(1)=-ALFA2
        ENDIF
      ENDIF
C
C       *TORSIONAL SHEAR STRESS*
C
       TT=0.0
       TT=STRAN(2) + DSTRAN(2)
C
        DDSDDE(2,2)=(1.6000E+05)
        STRESS(2)=DDSDDE(2,2)*TT
C
      RETURN
      END
*************************************************************************
****  USER SUBROUTINE TO DEFINE *3D* NONLINEAR BEAM/CONNECTOR ELEMENT
****               SANDEEP KAVI AND SAMRUAM TONGTOE
*************************************************************************
      SUBROUTINE UEL(RHS,AMATRX,SVARS,ENERGY,
     1 NDOFEL,NRHS,NSVARS,PROPS,NPROPS,COORDS,MCRD,NNODE,
     2 U,DU,V,A,JTYPE,TIME,DTIME,KSTEP,KINC,JELEM,PARAMS,
     3 NDLOAD,JDLTYP,ADLMAG,PREDEF,NPREDF,LFLAGS,MLVARX,DDLMAG,MDLOAD,
     4 PNEWDT,JPROPS,NJPROP,PERIOD)
C
      INCLUDE 'ABA_PARAM.INC'
C
      DIMENSION RHS(MLVARX,*),AMATRX(NDOFEL,NDOFEL),PROPS(*),
     1 SVARS(*),ENERGY(8),COORDS(MCRD,NNODE),U(NDOFEL),
     2 DU(MLVARX,*),V(NDOFEL),A(NDOFEL),TIME(2),PARAMS(*),
     3 JDLTYP(MDLOAD,*),ADLMAG(MDLOAD,*),DDLMAG(MDLOAD,*),
     4 PREDEF(2,NPREDF,NNODE),LFLAGS(*),JPROPS(*)
      DIMENSION R(12,12),TR(12,12),DM(12),R1(6,6),GDM1(6),GDM2(6),
     1 DM1(6),DM2(6),DM3(6),S(6),DISP(16),RH(12,2)
C
CC INITIALIZATION OF MATRICES
C
      DO 5 I=1,NDOFEL
       DO 10 J=1,NDOFEL
         AMATRX(I,J)=0.0
10    CONTINUE
5     CONTINUE
C
      DO 15 I=1,NDOFEL
       DO 20 J=1,NRHS
         RHS(I,J)=0.0
20     CONTINUE
15    CONTINUE
```

```
C
      DO 25 I=1,12
       DO 30 J=1,12
          R(I,J)=0.0
          TR(I,J)=0.0
          DM(I)=0.0
30     CONTINUE
25    CONTINUE
C
      DO 35 I=1,6
       DO 40 J=1,6
          R1(I,J)=0.0
          GDM1(I)=0.0
          GDM2(I)=0.0
          DM1(I)=0.0
          DM2(I)=0.0
          DM3(I)=0.0
          S(I)=0.0
40     CONTINUE
35    CONTINUE
C
CC DEFINING THE ROTATION MATRIX
C  NODAL COORDINATES
C
         XCOS1 = COORDS(1,1)
         YCOS1 = COORDS(2,1)
         XCOS2 = COORDS(1,2)
         YCOS2 = COORDS(2,2)
CC MAIN BEAMS >>
       IF(JTYPE.LT.2000)THEN
         ZCOS1 = COORDS(3,1)
         ZCOS2 = COORDS(3,2)
CC EDGE BEAMS >>
       ELSE
         ZCOS1 = COORDS(3,1)
         ZCOS2 = COORDS(3,2)
       ENDIF
C
         T1 = XCOS2 - XCOS1
         T2 = YCOS2 - YCOS1
         T3 = ZCOS2 - ZCOS1
         TNORM = (T1**2+T2**2+T3**2)**0.5
C
         R11 = YCOS1*ZCOS2 - ZCOS1*YCOS2
         R12 = -(XCOS1*ZCOS2 - ZCOS1*XCOS2)
         R13 = XCOS1*YCOS2 - YCOS1*XCOS2
         R1NORM = (R11**2+R12**2+R13**2)**0.5
C
         R21 = T2*R13-T3*R12
         R22 = T3*R11-T1*R13
         R23 = T1*R12-T2*R11
```

```
      R2NORM = (R21**2+R22**2+R23**2)**0.5
C
CC ROTATION MATRIX FOR STIFFNESS CALCULATION (R).
C
      DO 45 I=1,10,3
        R(I,I) = T1/TNORM
        R(I,I+1)=T2/TNORM
        R(I,I+2)=T3/TNORM
        R(I+1,I)=R11/R1NORM
        R(I+1,I+1)=R12/R1NORM
        R(I+1,I+2)=R13/R1NORM
        R(I+2,I)=R21/R2NORM
        R(I+2,I+1)=R22/R2NORM
        R(I+2,I+2)=R23/R2NORM
C ALTERNATIVELY >>
C        R(I+2,I)=R(1,2)*R(2,3)-R(2,2)*R(1,3)
C        R(I+2,I+1)=R(2,1)*R(1,3)-R(1,1)*R(2,3)
C        R(I+2,I+2)=R(1,1)*R(2,2)-R(1,2)*R(2,1)
45    CONTINUE
C
CC TRANSPOSE OF ROTATION MATRIX
C
      DO 50 I=1,12
        DO 55 J=1,12
          TR(I,J) = R(J,I)
55      CONTINUE
50    CONTINUE
C
CC ROTATION MATRIX FOR DISPLACEMENT CALCULATION (R1).
C
      DO 60 I=1,4,3
        R1(I,I) = T1/TNORM
        R1(I,I+1)=T2/TNORM
        R1(I,I+2)=T3/TNORM
        R1(I+1,I)=R11/R1NORM
        R1(I+1,I+1)=R12/R1NORM
        R1(I+1,I+2)=R13/R1NORM
        R1(I+2,I)=R21/R2NORM
        R1(I+2,I+1)=R22/R2NORM
        R1(I+2,I+2)=R23/R2NORM
60    CONTINUE
C
CC PUT GLOBAL NODAL DISPLACEMENT OF NODE #1 INTO GDM1
C
      DO 65 I = 1,6
        GDM1(I)=U(I)
65    CONTINUE
C
CC PUT GLOBAL NODAL DISPLACEMENT OF NODE #2 INTO GDM2
C
      DO 70 I = 7,12
```

```
      GDM2(I-6)=U(I)
70    CONTINUE
C
CC TRANSFORM NODAL DISPLACEMENTS FROM GLOBAL TO LOCAL FOR
CC NODE #1 AND #2, AND PUT THE LOCAL DISPLACEMENT INTO
CC DM1 AND DM2
C
      DO 75 I=1,6
        DO 80 J=1,6
          DM1(I)=DM1(I)+R1(I,J)*GDM1(J)
          DM2(I)=DM2(I)+R1(I,J)*GDM2(J)
80      CONTINUE
75    CONTINUE
C
CC PUT THE NODE DISPLACEMENTS OF THE BEAM THAT ACTIVATE THE
CC NAIL DISPLACEMENT INTO DM3, ACCORDING TO ORIENTATION OF THE
CC LOCAL AXES OF THE BEAMS (REFER TO MCODE OF BEAMS)
C
CC MAIN BEAMS >>
      IF(JTYPE.LT.2000)THEN
        DM3(1)=DM1(2)
        DM3(2)=DM1(4)
        DM3(3)=DM1(6)
        DM3(4)=DM2(2)
        DM3(5)=DM2(4)
        DM3(6)=DM2(6)
CC EDGE BEAMS >>
      ELSE
        DM3(1)=DM1(3)
        DM3(2)=DM1(4)
        DM3(3)=DM1(5)
        DM3(4)=DM2(3)
        DM3(5)=DM2(4)
        DM3(6)=DM2(5)
      ENDIF
C
CC LOCAL DISPLACEMENTS OF THE TWO NODES CONNECTING THE ELEMENT
CC MAIN BEAMS >>
      IF(JTYPE.LT.2000)THEN
        DM(2) = DM1(2)
        DM(4) = DM1(4)
        DM(6) = DM1(6)
        DM(8) = DM2(2)
        DM(10) = DM2(4)
        DM(12) = DM2(6)
CC EDGE BEAMS >>
      ELSE
        DM(3) = DM1(3)
        DM(4) = DM1(4)
        DM(5) = DM1(5)
        DM(9) = DM2(3)
```

```
         DM(10) = DM2(4)
         DM(11) = DM2(5)
       ENDIF
C
CC ***** FIND EACH NAIL DISPLACEMENT ACCORDING TO ITS LOCATION ON *****
CC *****  THE BEAM AND DEFINE THE CONNECTOR ELEMENT ACCORDINGLY   *****
C
      NS = IDINT(PROPS(1))
      SPACE = TNORM/PROPS(1)
C
      DO 85 L=1,NS
C
        DO 90 I=1,NDOFEL
         DO 95 J=1,NRHS
          RH(I,J) = 0.0
95        CONTINUE
90       CONTINUE
C
CC INTERPOLATION FUNCTIONS
C
        XI=SPACE*L/TNORM
C
        H = PROPS(2)
C
CC MAIN BEAMS >>
       IF(JTYPE.LT.2000)THEN
        S(1)=1.-3.*XI**2.+2.*XI**3.
        S(2)=-(1.-XI)*H
        S(3)=(XI-2.*XI**2.+XI**3.)*TNORM
        S(4)=3.*XI**2.-2.*XI**3.
        S(5)=-XI*H
        S(6)=(XI**3.-XI**2.)*TNORM
CC EDGE BEAMS >>
       ELSE
        S(1)=1.-3.*XI**2.+2.*XI**3.
        S(2)=(1.-XI)*H
        S(3)=-(XI-2.*XI**2.+XI**3.)*TNORM
        S(4)=3.*XI**2.-2.*XI**3.
        S(5)=XI*H
        S(6)=-(XI**3.-XI**2.)*TNORM
       ENDIF
C
      DISP(L) = 0.0
      D = 0.0
      C = 0.0
C
CC COMPUTE THE NAIL DISPLACEMENT BY INTERPOLATION FUNCTIONS
CC MULTIPLY S WITH DM3
C
        DO 100 J=1,6
         D=D+S(J)*DM3(J)
```

```
100       CONTINUE
      DISP(L) = ABS(D)
C
CC ************** TO DEFINE THE CONNECTOR F.E. MODEL ************
C
CC THE GLOBAL STIFFNESS MATRIX OF THE CONNECTORS
C
C  THE CONNECTOR STIFFNESS MATRIX IS IN THE LOCAL FRAME OF REFERENCE.
C  WE NEED TO FIND THE GLOBAL STIFFNESS MATRIX. THE ROTATION MATRIX
C  FOR THE BEAMS AND ITS TRANSPOSE IS USED FOR THIS PURPOSE.
C  THE TRANSFORMATION FROM THE LOCAL TO THE GLOBAL IS OBTAINED BY
C  PRE-MULTIPLYING THE LOCAL STIFFNESS MATRIX (SM) BY THE TRANSPOSE
C  OF ROTATION MATRIX (TR) AND THEN POST-MULTIPLYING THE PRODUCT BY
C  THE ROTATION MATRIX (R).
C
CC ASSIGN VALUES TO UPPER TRIANGLE MATRIX ENTRIES
C
        G1=S(1)*S(1)
        G2=S(1)*S(2)
        G3=S(2)*S(2)
        G4=S(1)*S(3)
        G5=S(2)*S(3)
        G6=S(3)*S(3)
        G7=S(1)*S(4)
        G8=S(2)*S(4)
        G9=S(3)*S(4)
        G10=S(4)*S(4)
        G11=S(1)*S(5)
        G12=S(2)*S(5)
        G13=S(3)*S(5)
        G14=S(4)*S(5)
        G15=S(5)*S(5)
        G16=S(1)*S(6)
        G17=S(2)*S(6)
        G18=S(3)*S(6)
        G19=S(4)*S(6)
        G20=S(5)*S(6)
        G21=S(6)*S(6)
C
      IF (DISP(L).LT.PROPS(5)) THEN
C
        C = PROPS(3)
C
      CALL AMATRH(R,TR,AMATRX,DM,RH,G1,G2,G3,G4,G5,G6,G7,G8,G9,G10,
     1 G11,G12,G13,G14,G15,G16,G17,G18,G19,G20,G21,C,NDOFEL,JTYPE)
C
      ELSEIF (DISP(L).GE.PROPS(5)) THEN
C
        C = PROPS(4)
C
      CALL AMATRH (R,TR,AMATRX,DM,RH,G1,G2,G3,G4,G5,G6,G7,G8,G9,G10,
```

```
     1 G11,G12,G13,G14,G15,G16,G17,G18,G19,G20,G21,C,NDOFEL,JTYPE)
C
CC MAIN BEAMS >>
C
       IF(JTYPE.LT.2000)THEN
         IF(D.GT.0.0)THEN
           RH(2,1) = RH(2,1) - PROPS(7)*S(1)
           RH(4,1) = RH(4,1) - PROPS(7)*S(2)
           RH(6,1) = RH(6,1) - PROPS(7)*S(3)
           RH(8,1) = RH(8,1) - PROPS(7)*S(4)
           RH(10,1) = RH(10,1) - PROPS(7)*S(5)
           RH(12,1) = RH(12,1) - PROPS(7)*S(6)
         ELSE
           RH(2,1) = RH(2,1) + PROPS(7)*S(1)
           RH(4,1) = RH(4,1) + PROPS(7)*S(2)
           RH(6,1) = RH(6,1) + PROPS(7)*S(3)
           RH(8,1) = RH(8,1) + PROPS(7)*S(4)
           RH(10,1) = RH(10,1) + PROPS(7)*S(5)
           RH(12,1) = RH(12,1) + PROPS(7)*S(6)
         ENDIF
C
CC EDGE BEAMS >>
C
       ELSE
         IF(D.GT.0.0)THEN
           RH(3,1) = RH(3,1) - PROPS(7)*S(1)
           RH(4,1) = RH(4,1) - PROPS(7)*S(2)
           RH(5,1) = RH(5,1) - PROPS(7)*S(3)
           RH(9,1) = RH(9,1) - PROPS(7)*S(4)
           RH(10,1) = RH(10,1) - PROPS(7)*S(5)
           RH(11,1) = RH(11,1) - PROPS(7)*S(6)
         ELSE
           RH(3,1) = RH(3,1) + PROPS(7)*S(1)
           RH(4,1) = RH(4,1) + PROPS(7)*S(2)
           RH(5,1) = RH(5,1) + PROPS(7)*S(3)
           RH(9,1) = RH(9,1) + PROPS(7)*S(4)
           RH(10,1) = RH(10,1) + PROPS(7)*S(5)
           RH(11,1) = RH(11,1) + PROPS(7)*S(6)
         ENDIF
       ENDIF
      ENDIF
C
CC **THE RIGHT-HAND-SIDE VECTOR
C
CC CONTRIBUTION OF ELEMENT IN GLOBAL FRAME OF REFERENCE (RHS)
CC PRE-MULTIPLY (RH) BY THE TRANSPOSE OF ROTATION MATRIX (TR).
C
       DO 105 I=1,12
         DO 110 J=1,12
            RHS(I,1) = RHS(I,1) + TR(I,J)*RH(J,1)
110     CONTINUE
```

```
105    CONTINUE
C
85    CONTINUE
C
      RETURN
      END
***************************************************************************
      SUBROUTINE AMATRH (R,TR,AMATRX,DM,RH,G1,G2,G3,G4,G5,G6,G7,G8,G9,
     1 G10,G11,G12,G13,G14,G15,G16,G17,G18,G19,G20,G21,C,NDOFEL,JTYPE)
C
      IMPLICIT REAL*8(A-H,O-Z)
C
      DIMENSION R(12,12),TR(12,12),AMATRX(NDOFEL,NDOFEL),DM(12),
     1 RH(12,2)
      DIMENSION DSM1(12,12),DSM(12,12)
C
      DO 5 I=1,12
       DO 10 J=1,12
           DSM(I,J) = 0.0
           DSM1(I,J) = 0.0
10     CONTINUE
5     CONTINUE
C
CC MAIN BEAMS >>
C
       IF(JTYPE.LT.2000)THEN
C
CC STIFFNESS MATRIX (LOCAL) OF L(TH) NAIL.
C
         DSM(2,2)=C*G1
         DSM(2,4)=C*G2
         DSM(4,4)=C*G3
         DSM(2,6)=C*G4
         DSM(4,6)=C*G5
         DSM(6,6)=C*G6
         DSM(2,8)=C*G7
         DSM(4,8)=C*G8
         DSM(6,8)=C*G9
         DSM(8,8)=C*G10
         DSM(2,10)=C*G11
         DSM(4,10)=C*G12
         DSM(6,10)=C*G13
         DSM(8,10)=C*G14
         DSM(10,10)=C*G15
         DSM(2,12)=C*G16
         DSM(4,12)=C*G17
         DSM(6,12)=C*G18
         DSM(8,12)=C*G19
         DSM(10,12)=C*G20
         DSM(12,12)=C*G21
C
```

```
CC EDGE BEAMS >>
C
      ELSE
C
CC STIFFNESS MATRIX (LOCAL) OF L(TH) NAIL.
C
        DSM(3,3)=C*G1
        DSM(3,4)=C*G2
        DSM(4,4)=C*G3
        DSM(3,5)=C*G4
        DSM(4,5)=C*G5
        DSM(5,5)=C*G6
        DSM(3,9)=C*G7
        DSM(4,9)=C*G8
        DSM(5,9)=C*G9
        DSM(9,9)=C*G10
        DSM(3,10)=C*G11
        DSM(4,10)=C*G12
        DSM(5,10)=C*G13
        DSM(9,10)=C*G14
        DSM(10,10)=C*G15
        DSM(3,11)=C*G16
        DSM(4,11)=C*G17
        DSM(5,11)=C*G18
        DSM(9,11)=C*G19
        DSM(10,11)=C*G20
        DSM(11,11)=C*G21
C
      ENDIF
C
CC ASSIGN VALUES TO THE LOWER TRIANGLE ENTRIES IN MATRIX
C
        DO 15 I=1,12
          DO 20 J=1,12
           IF(I.GT.J) DSM(I,J) = DSM(J,I)
20         CONTINUE
15       CONTINUE
C
CC PRE-MULTIPLYING STIFFNESS MATRIX FOR THE USER ELEMENT BY THE
CC TRANSPOSE OF THE ROTATION MATRIX.(TR X SM = SM1)
C
      DO 25 I=1,12
       DO 30 J=1,12
        DO 35 K=1,12
           DSM1(I,J) = DSM1(I,J) + TR(I,K)*DSM(K,J)
35       CONTINUE
30     CONTINUE
25    CONTINUE
C
CC **THE TANGENT (JACOBIAN) STIFFNESS MATRIX**
CC POST-MULTIPLYING THE ABOVE OBTAINED MATRIX BY
```

```
CC THE ROTATION MATRIX.(SM1 X R = AMATRX).
C
       DO 40 I=1,12
         DO 45 J=1,12
          DO 50 K=1,12
            AMATRX(I,J) = AMATRX(I,J) + DSM1(I,K)*R(K,J)
50         CONTINUE
45       CONTINUE
40      CONTINUE
C
CC CONTRIBUTION OF ELEMENT IN BEAM LOCAL FRAME OF REFERENCE (RH).
C
         DO 55 I=1,NDOFEL
          DO 60 J=1,NDOFEL
            RH(I,1) =  RH(I,1) - DSM(I,J)*DM(J)
60         CONTINUE
55        CONTINUE
      RETURN
      END
```

Appendix E

```
C
C PROGRAM TO COMPUTE NAIL DEFLECTIONS :
C COMPLETE VARAX DOME
C
C THE PROGRAM REQUIRES jbeams.dat, jbeam2.dat,
C and jdome.dat FILES
C THE COMPLETE OUTPUT IS WRITTEN TO SECTOR.OUT FILE
C A SUMMARY OF OUTPUT IS WRITTEN TO SECTOR.SUM FILE
C
      IMPLICIT REAL*8(A-H,O-Z)
      REAL DMAX, ELDMAX
      INTEGER ELMAX,ELNUM,MAXNODE,MAXEL,FAIL,ELFAIL
      DIMENSION U1(274),U2(274),U3(274),RM1(274),RM2(274),RM3(274),
     1 DM(6),S(6),DISP(16),X(274),Y(274),Z(274),N1(441),
     1 N2(441),ELDMAX(441),ELNUM(441),FAIL(441)
C
C     DESCRIPTION OF VARIABLES
C
C     DMAX   :   THE MAXIMUM NAIL DISPLACEMENT IN SECTOR
C     ELMAX  :   THE ELEMENT CONTAINING DMAX
C     ELDMAX :   THE LARGEST NAIL DISPLACEMENT IN AN ELEMENT
C     MAXNODE:   THE LARGEST NODE NUMBER
C     MAXEL  :   THE NUMBER OF ELEMENTS
C     FAIL   :   THE NUMBER OF CONNECTORS FAILED IN AN ELEMENT
C     ELFAIL :   THE NUMBER OF ELEMENTS WITH FAILED NAILS
C
C     INITIALIZATION OF VARIABLES
C
      DMAX=0.0
      ELMAX=0
      MAXNODE=274
      MAXEL=441
      ELFAIL=0
C
      OPEN(UNIT=10,FILE='jbeams.dat',STATUS='OLD')
      OPEN(UNIT=20,FILE='jdome.dat',STATUS='OLD')
      OPEN(UNIT=30,FILE='jbeam2.dat',STATUS='OLD')
      OPEN(UNIT=40,FILE='jdome.out',STATUS='UNKNOWN')
      OPEN(UNIT=50,FILE='jdome.sum',STATUS='UNKNOWN')
C
CC ######### READ FROM JBEAM1.DAT
      DO 5 I=1,MAXEL,1
        READ (10,*) ELNUM(I),N1(I),N2(I)
        ELDMAX(I)=0.0
        FAIL(I)=0
5     CONTINUE
      NS=16
CC      H=6.0
```

```
CC
CC    ELNUM(L)= ELEMENT NUMBER
CC    N1(L) = NODE #1
CC    N2(L) = NODE #2
CC    NS = NUMBER OF SPRINGS
CC    H = RIGID LINK LENGTH
CC
C
CC ######### READ FROM JBEAM2.DAT
      DO 20 I=1,MAXNODE,1
        READ (30,*) N,D1,D2,D3,D4,D5,D6
          U1(I)=D1
          U2(I)=D2
          U3(I)=D3
          RM1(I)=D4
          RM2(I)=D5
          RM3(I)=D6
20    CONTINUE
C
CC ######### READ FROM JDOME DAT
      DO 10 I=1,MAXNODE,1
        READ (20,*) N,X(I),Y(I),Z(I)
10    CONTINUE
C
      DO 15 L=1,MAXEL,1
         M=ELNUM(L)
         M1=N1(L)
         M2=N2(L)
         IF (M .LE. 231) THEN
            H=6.0
         ELSE IF (M .GT. 231 .AND. M .LE. 287) THEN
            H=3.75
         ELSE IF (M .GT. 287 .AND. M .LE. 399) THEN
            H=3.75
         ELSE IF (M .GT. 399 .AND. M .LE. 441) THEN
            H=11.0
        END IF
C
         T1 = X(M2) - X(M1)
         T2 = Y(M2) - Y(M1)
         T3 = Z(M2) - Z(M1)
         TNORM = (T1**2+T2**2+T3**2)**0.5
C
CC    TNORM = LENGTH OF BEAM
C
      DO 30 I=1,6
          DM(I)=0.0
          S(I)=0.0
30    CONTINUE
C
         DM(1)=U2(M1)
```

```
      DM(2)=RM1(M1)
      DM(3)=RM3(M1)
      DM(4)=U2(M2)
      DM(5)=RM1(M2)
      DM(6)=RM3(M2)
C
     WRITE(40,60) M
     WRITE(40,65) TNORM
C
     SPACE = TNORM/16.0
     DO 40 K=1,(NS-1)
       XI=SPACE*K/TNORM
        S(1)=1.-3.*XI**2.+2.*XI**3.
        S(2)=-(1.-XI)*H
        S(3)=(XI-2.*XI**2.+XI**3.)*TNORM
        S(4)=3.*XI**2.-2.*XI**3.
        S(5)=-XI*H
        S(6)=(XI**3.-XI**2.)*TNORM
       DISP(K)=0.0
       D=0.0
     DO 50 I=1,6
        D=D+S(I)*DM(I)
50   CONTINUE
        IF (M.EQ.35) THEN
         WRITE(40,66) XI,S(1),S(2),S(3),S(4),S(5),S(6)
         WRITE(40,67) SPACE,DM(1),DM(2),DM(3),DM(4),DM(5),DM(6)
        END IF
        DISP(K)=ABS(D)
        IF (DISP(K) .GT. DMAX) THEN
           DMAX=DISP(K)
           ELMAX=ELNUM(L)
        END IF
        IF (DISP(K) .GT. ELDMAX(L)) THEN
           ELDMAX(L)=DISP(K)
        END IF
        IF (DISP(K) .GE. 1.0) THEN
           FAIL(L)=FAIL(L)+1
        END IF
     WRITE(40,70) K,SPACE*K,DISP(K)
40   CONTINUE
15   CONTINUE
     DO 55 I=1,MAXEL
     IF (FAIL(I) .GT. 0) THEN
        ELFAIL=ELFAIL+1
     END IF
55   CONTINUE
60   FORMAT('**BEAM NUMBER #',I3,' >>>>>>>>>>')
65   FORMAT('**LENGTH #',F8.2,' >>>>>>>>>>')
66   FORMAT(F8.2,F8.2,F8.2,F8.2,F8.2,F8.2,F8.2)
67   FORMAT(F8.2,F8.2,F8.2,F8.2,F8.2,F8.2,F8.2)
70   FORMAT('**DISPL. OF NAIL #',I2,'  LOCATED AT',
```

```
     1F6.2,'IN. FROM LEFT END ==>',F8.4,' IN.')
      WRITE(50,*) '****SUMMARY INFORMATION****'
      WRITE(50,*) ' '
      WRITE(50,80) DMAX,ELMAX
      WRITE(50,*) ' '
80    FORMAT('THE MAXIMUM NAIL DEFLECTION=',F8.4,
     1' IN. OCCURS IN ELEMENT ',I3)
      WRITE(50,120) ELFAIL
      WRITE(50,*) 'NAILS HAVE FAILED IN THE FOLLOWING ELEMENTS'
      DO 85 K=1,MAXEL
         IF (FAIL(K) .GE. 1) THEN
            WRITE (50,*) ELNUM(K)
         END IF
85    CONTINUE
      DO 90 K=1,MAXEL
         WRITE(50,100) ELNUM(K),ELDMAX(K)
         WRITE(50,110) FAIL(K), ELNUM(K)
         WRITE(50,*) ' '
90    CONTINUE
100   FORMAT('ELEMENT #',I3,': MAX NAIL DEFLECTION =',F8.4,
     1' IN.')
110   FORMAT(I2,' NAILS HAVE FAILED IN ELEMENT #',I4)
120   FORMAT(I3,' ELEMENTS HAVE FAILED CONNECTORS')
      END
```

Appendix F

Varax dome nail deflections at critical pressures: Full Snow

Element number	Number of failed nails	Maximum nail deflection (in.)
2	4	1.50
3	14	1.88
23	2	1.01
24	6	1.14
25	5	1.13
27	5	1.07
41	9	1.26
57	15	1.19
58	4	1.12
74	5	1.09
83	5	1.56
84	16	2.09
93	6	1.11
96	15	1.11
101	7	1.43
102	16	1.56
103	10	1.58
107	10	1.45
108	1	1.04
110	4	1.45
111	13	1.80
113	1	1.01
114	16	1.05
115	2	1.04
122	6	1.41
123	16	1.58
124	8	1.46
128	8	1.59
129	16	1.70
130	10	1.68
145	5	1.62
146	14	2.01
148	11	1.49
149	1	1.11
151	2	1.05
152	16	1.06
160	9	1.58
161	16	1.71

Varax dome nail deflections at critical pressures: Full Snow (continued)

Element number	**Number of failed nails**	**Maximum nail deflection (in.)**
162	10	1.69
164	3	1.04
166	6	1.43
167	16	1.59
168	7	1.45
172	7	1.22
205	2	1.19
206	13	1.66
220	7	1.44
221	16	1.55
222	11	1.56
227	15	1.11
243	3	1.04
251	10	1.46
253	3	1.04
258	8	1.30
261	16	2.28
262	16	1.79
270	4	1.43
275	9	1.39
282	6	1.16
286	5	1.59
287	15	1.59
290	9	1.14
291	4	1.11
292	2	1.04
293	3	1.04
296	16	2.48
297	11	2.31
300	8	1.51
301	8	1.51
303	14	4.39
306	3	1.12
307	3	1.12
308	2	1.03
309	2	1.03
312	9	1.94
313	7	1.99
316	1	1.04

Varax dome nail deflections at critical pressures: Full Snow (continued)

Element number	Number of failed nails	Maximum nail deflection (in.)
317	3	1.08
319	10	4.12
322	7	1.99
323	9	2.03
326	6	1.41
327	7	1.45
328	9	2.13
329	9	2.20
330	9	3.19
331	16	3.19
332	8	2.45
333	9	2.51
334	12	5.29
335	9	2.60
338	10	2.54
339	9	2.51
340	7	1.39
341	6	1.36
342	9	1.57
343	7	1.57
344	16	2.84
345	8	2.84
346	10	3.36
347	16	3.28
348	9	2.85
349	8	2.79
350	12	5.38
351	10	4.04
354	13	2.54
355	12	2.52
356	7	1.58
357	9	1.58
358	9	1.39
359	5	1.35
360	16	3.37
361	11	3.25
362	13	3.08
363	16	3.08
364	10	2.96

Varax dome nail deflections at critical pressures: Full Snow (continued)

Element number	Number of failed nails	Maximum nail deflection (in.)
365	10	2.94
366	15	4.42
367	15	5.25
376	3	1.13
377	3	1.16
382	11	2.14
383	8	2.54
386	12	2.02
387	11	2.03
388	5	1.40
389	9	1.45
392	16	2.97
393	12	2.96
394	8	1.71
395	13	1.82
396	9	2.17
397	8	2.18
398	12	2.15
399	14	5.28

Appendix G

Varax dome nail deflections at critical pressures: Half Snow

Element number	Number of failed nails	Maximum nail deflection (in.)
36	10	1.33
37	10	1.38
41	10	1.84
42	6	1.72
45	14	1.37
54	15	1.52
55	1	1.06
59	9	1.44
60	3	1.30
74	8	2.09
75	16	1.96
76	10	1.94
78	11	1.50
79	14	1.52
83	9	2.07
84	16	2.45
85	5	1.59
89	4	1.14
90	16	1.43
91	12	1.49
92	15	2.04
93	16	2.32
94	3	1.28
95	14	1.18
96	12	1.18
98	15	1.87
99	16	1.64
100	9	1.77
101	7	1.04
102	11	1.03
106	6	1.03
107	10	1.55
108	16	1.47
109	7	1.56
110	9	1.91
111	16	2.31
112	5	1.71
119	4	1.11

Varax dome nail deflections at critical pressures: Half Snow (continued)

Element number	Number of failed nails	Maximum nail deflection (in.)
120	3	1.10
125	6	1.18
126	16	1.46
127	2	1.13
128	3	1.05
129	16	1.08
130	1	1.02
133	9	1.11
243	16	1.70
244	13	1.24
245	5	1.03
246	6	1.15
247	4	1.01
248	5	1.21
250	9	1.44
251	16	2.44
252	16	1.90
253	16	1.92
254	1	1.00
258	16	1.22
259	8	1.42
260	16	1.86
261	16	2.58
262	16	2.07
287	9	2.23
304	15	1.35
312	16	1.67
313	13	1.67
314	14	1.18
315	3	1.14
316	8	1.74
317	8	1.75
320	4	1.05
321	16	1.46
322	16	1.19
323	5	1.17
324	4	1.15
325	16	1.40
328	16	

Varax dome nail deflections at critical pressures: Half Snow (continued)

Element number	Number of failed nails	Maximum nail deflection (in.)
329	16	2.25
330	16	2.33
331	16	2.35
332	16	2.21
333	16	3.24
334	4	1.59
335	6	1.60
336	8	1.34
337	10	1.47
338	7	1.30
339	7	1.29
342	7	1.09
343	3	1.09
344	5	1.42
345	3	1.06
346	8	1.14
347	9	1.92
348	10	5.55
349	12	5.44
350	9	1.62
351	4	1.36
368	9	1.08
383	6	1.32

VITA

Samruam Tongtoe was born in Chonburi, Thailand, on September 15, 1961. He received a full scholarship from the Royal Thai Air Force for attendance at The Citadel, The Military College of South Carolina. He graduated from The Citadel in May 1985, with a Bachelor of Science degree in Civil Engineering. After graduating in 1985, he attended Virginia Tech where he obtained a Master of Science degree in Civil Engineering in 1987. After graduation, he worked as an airport designer with Talbert Cox and Associates in Charlotte, NC, for one year. He then returned to his homeland and was commissioned as First Lieutenant in The Royal Air Force. He was assigned to teach at The Royal Thai Air Force Academy. In 1992, he received another scholarship from The Air Force to pursue his Ph.D. in Civil Engineering. He plans to return to Thailand to continue serving in The Royal Thai Air Force.